Cellular stress in vitro and longevity in vivo

Dekker, P.

Cellular stress *in vitro* and longevity *in vivo*

Pim Dekker

Financial support for the publication of this thesis by the Nederlandse Vereniging voor Gerontologie (Dutch Society for Gerontology) and by Unilever PLC is gratefully acknowledged.

ISBN: 978-94-6182-063-1

This research was funded by the Netherlands Genomics Initiative (NCHA 050-060-810), the Innovation Oriented research Program on Genomics (SenterNovem; IGE01014 and IGE5007), the Netherlands Genomics Initiative/Netherlands Organization for scientific research (NGI/NWO; 05040202 and 050-060-810), EU funded Network of Excellence Lifespan (FP6 036894) and Unilever PLC.

Cover design and layout: Gijs Grob
With courtesy of AMPELMANN GmbH. The design company specializes in emotional lifestyle products with high utility value. More information under: www.ampelmann.de
Printed by: Off Page, Amsterdam

Cellular stress *in vitro* and longevity *in vivo*

Proefschrift

ter verkrijging van
de graad van Doctor aan de Universiteit Leiden,
op gezag van Rector Magnificus prof. mr. P.F. van der Heijden,
volgens besluit van het College voor Promoties
te verdedigen op dinsdag 28 februari 2012
klokke 16.15 uur

door

Pim Dekker
geboren te Rotterdam
in 1973

Promotie commissie

Promotores:	Prof. Dr. R.G.J. Westendorp
	Prof. Dr. H.J. Tanke
Co-promotores:	Dr. A.B. Maier
	Dr. D. van Heemst
Referenten:	Prof. Dr. P.D. Adams (Glasgow University, UK)
	Prof. Dr. P.E. Slagboom
	Prof. Dr. A.M. Deelder

A very popular error:
having the courage of one's convictions;
rather it is a matter of having the courage
for an attack on one's convictions

F. Nietzsche

Contents

Chapter 1.	General introduction	9
Chapter 2.	Rapid flow cytometric method for measuring Senescence Associated-β-galactosidase activity in human fibroblasts	19
Chapter 3.	Stress-induced responses of human skin fibroblasts *in vitro* reflect human longevity	39
Chapter 4.	Relation between maximum replicative capacity and oxidative stress-induced responses in human skin fibroblasts *in vitro*	61
Chapter 5.	Chronic inhibition of the respiratory chain in human fibroblast cultures: Differential responses related to subject chronological and biological age	79
Chapter 6.	Microarray-based identification of age-dependent differences in gene expression of human dermal fibroblasts	103
Chapter 7.	Human *in vivo* longevity is reflected *in vitro* by differential metabolism as measured by ^{1}H-NMR profiling of cell culture supernatants	137
Chapter 8.	General discussion	165
Nederlandse samenvatting		175
List of publications		179
Dankwoord		180
Curriculum Vitae		181

Chapter 1

General introduction

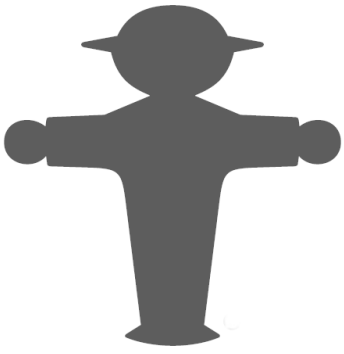

Aging theories

As we age, the organs that make up our bodies progressively lose their functionality, resulting in age-related diseases and ultimately death. Various theories have been put forward to explain why the process of aging should occur (1). Initially it was proposed that aging is programmed to prevent populations from becoming too large, but in the wild mortality is much more likely to occur as a result of extrinsic mortality (predation, infection, starvation, environmental conditions). According to the 'mutation accumulation theory', germ-line mutations which act late in life are not selected for by evolution since in the wild, organisms will be removed from the population before the mutations have any effect. This selection shadow is also important in the theory of 'antagonistic pleiotropy', proposing that genes with beneficial effects early in life can be deleterious later in life. In our modern world we can live up to and into the selection shadow, allowing pleiotropic genes to affect our bodies. In the 'disposable soma theory' the organism is thought to distribute a finite amount of energy between maintenance of the body and reproduction. The 'disposable soma theory' implicates that organisms are subject to damage. One of the first theories to explain this damage is the 'oxygen radical theory of aging' (2).

Sources and types of damage

The sources of cellular damage can be both extrinsic and intrinsic and mostly consist of or result in free radical molecules. Examples of extrinsic sources are sunlight (UV-A and UV-B), ionizing radiation (radioactivity), polluted air (NO-radicals), food (fat, charred products) and environmental chemicals (pesticides) (3). Whereas common sense can protect us from many extrinsic stressors, this is more difficult for intrinsic sources of stress. The very process that keeps us alive, that of cellular energy production, also results in the production of damaging reactive oxygen species (ROS)(4). Additionally, the fuel used to produce energy in the mitochondria, glucose, acts as a damaging agent, either directly damaging proteins by binding to them (nonenzymatic glycation or NEG) or by inducing ROS (5). The damaging nature of ROS has even been harnessed by evolution: leukocytes produce ROS and use them to attack infectious pathogens and there is increasing evidence that ROS serve as signaling molecules (6). When these processes are not regulated properly, excess ROS will

lead to damage, for example in chronic inflammations. Indeed, with increasing age the immune system gets progressively deregulated (7).

Cellular responses to stress-induced damage

Multicellular organisms have become increasingly complex during evolution and many have renewable tissues. The skin and gut are examples of organs which are continuously renewed by proliferative progenitor cells, but damage to tissues is also repaired by cells which have become proliferative temporarily. In a healthy organism, the loss of cells is balanced by the new formation of cells, a situation also known as 'proliferative homeostasis'. As described above, damage on the cellular level can deregulate vital cellular processes, resulting in cell death or the opposite: uncontrolled proliferation or cancer. Both will clearly disturb the proliferative homeostasis and affect organs and the body. Current thinking dictates that evolution has devised proteins to both protect cells (caretakers) and remove damaged cells from the pool of proliferative cells (gatekeepers) (8).

When cells contract damage, various mechanisms come into action to first arrest the cell cycle, and then gauge the extent of the damage and to finally react accordingly. If the damage is repairable, the cell will do so and continue proliferating afterwards. Autophagy, the process in which the cell degrades its own organelles in the lysosomes, is an important process for repair and the turnover of damaged cellular constituents and affects longevity (9).

If the damage is irreversible, cells can die in an orchestrated and controlled manner, a process called apoptosis, or stay alive in a permanent state of arrest termed cellular senescence. In case of extensive damage the regulation of apoptosis and senescence might also be compromised and cells will die in an uncontrolled fashion, a phenomenon called necrosis.

Apoptosis

Apoptosis is currently relatively well-understood. Though apoptosis is an important anti-cancer mechanism, it is not only essential for the removal of damaged cells but also plays an important role in the development and maintenance of the healthy organism (10). Morphological hallmarks of apoptosis are condensed chromatin, nuclear fragmentation, shrinkage of the cell and plasma membrane blebbing. The process can be initiated

intracellularly, in case of cellular damage, or by external signal molecules (e.g. TNF-family proteins). When stress has led to DNA damage, the tumor suppressor proteins p53 and Rb are activated and will activate a pathway leading to mitochondrial membrane permeabilization and release of cytochrome c which activates a number of proteases from the caspase-family. Despite being fragmented, the degradation of all cellular constituents happens in vesicles, preventing surrounding cells from being damaged by degrading enzymes.

Senescence

Already in 1956, Hayflick observed that human fibroblasts, though growing very well *in vitro*, had a limited lifespan of about 50±10 population doublings (PDs), the so-called Hayflick limit (11), after which fibroblasts stopped proliferating but could be kept alive for months and displayed an abnormal morphology when compared with proliferating fibroblasts. This state was called replicative senescence (RS). Later studies described more morphological and biochemical properties that are different in senescent cells: they contain higher levels of ROS and of ROS-induced damage products like lipofuscin and changed mass and functionality of mitochondria and lysosomes. Indeed, one of the most widely used markers, Senescence Associated-β-galactosidase (SA-β-gal) activity (12) is of lysosomal origin.

It was suggested that the aging of an organism was the result of proliferative cells having a maximum replicative capacity (13), implying the existence of a 'cellular clock'. When proliferating, cells are not capable to replicate their DNA all the way to the end of linear chromosomes. Non-coding G-rich repeats, called telomeres, function as buffer zones and shorten after every division. This led to the 'telomere-length mitotic clock hypothesis', but it soon became obvious that the maximum replicative capacity of cells was not only a matter of shortening telomeres. Some cells can actively elongate their telomeres with the enzyme telomerase. Indeed, artificial expression of telomerase dramatically extends replicative capacity of cells *in vitro*, even if the telomeres are shorter than those of control cells which do not express telomerase, suggesting that there is no simple relation between telomere length and maximum replicative capacity (14;15).

Replicative exhaustion is not the only cause of cellular senescence. It can also be induced prematurely by various types of stressors like signaling molecules (e.g. cytokines), ROS and

oncogenes (stress induced premature senescence or SIPS) (16;17). In most cases, senescent cells display upregulated activity of the tumor suppressor proteins p53 and Rb, which also play an important role in the DNA damage response (DDR) which has been shown to be an important initiator of cellular senescence. Telomeres are bound to a complex of proteins forming a protective 'cap'. Shortening of telomeres or damage-inducing factors like ROS can lead to 'uncapping' after which the exposed telomeres are considered as DNA damage by cells.

The cyclin-inhibitor p16 plays an important role in senescence. It is thought to activate Rb in a p53-independent manner, thus creating an extra level of protection against cancer. Indeed, in many human tumors p16 is inactivated. Not all senescent fibroblasts express p16 and those that do, generally do not express p21 or display the typical DNA damage foci at the telomeres. These findings suggest that there is a DNA damage induced route to senescence and a route activated by other stressors, leading to senescence via p16.

The involvement of p53 and Rb in both apoptosis and senescence indicates an interaction between the two pathways, but it is not well understood which factors determine if a cell goes into apoptosis or into senescence (8;10).

Models for studying aging

Animal models

Our knowledge of the mechanisms of aging is to a large extent the result of studying short-lived species (18). Much has been learned from knocking out or overexpressing single genes in these model organisms, but most age-related processes and diseases involve many genes in multiple signaling pathways and complex interactions on the systemic, tissue, cellular and genetic level. Although species ranging from worms to mammals seem to share many mechanisms, translation of results from experiments with these animal model systems to the human situation is very precarious (19). In Drosophila and C. Elegans, the p53 and Rb homologues also regulate apoptosis and senescence but not as an anti-cancer mechanism (8). Between mammals significant differences in signaling can be found. In mouse cells, either p53 or Rb inactivation prevents senescence, whereas in human cells inactivation of both p53 and Rb is required. In mouse cells, p16 inactivation in senescent cells does not

delay the onset of senescence, whereas it does in human cells (17). There are also many differences in signaling between the different tissues within an organism. Thus, cellular responses to stress and damage will be dependent on species, cell type and the type and extent of stress or damage (16).

In vivo versus in vitro

As already alluded to, manipulation of single genes in model organisms has given much insight in to the pathways governing the mechanisms of aging. Evidently, this genetic manipulation is not possible in humans for ethical reasons. It is, however, possible to experiment with cells isolated from humans. Analogous to the translation of results from animal models to humans, the translation of *in vitro* results to the *in vivo* situation is difficult for two main reasons. First, *in vitro* characteristics of cells depend on culture conditions like the type of medium, batch and concentration of added serum, oxygen concentration and the number of PDs undergone *in vitro*, making it difficult to compare studies (20). Second, cells *in vitro* have been removed from their natural environment, being deprived of many factors in the blood (e.g. cytokines and growth factors) and cell-cell and cell-matrix interactions (19). Despite these caveats, cells cultured *in vitro* reflect differences between the organisms they were derived from. Skin fibroblasts derived from longer living species are more resistant to toxic stress when compared with shorter living species (21). Even within species, skin fibroblasts from longer living mutant mice were more resistant to stress (22).

Aim of this thesis

Earlier we showed that nonagenarian siblings from families with the propensity for longevity displayed a 41% lower risk of mortality compared with sporadic nonagenarians (23) and that the offspring of these nonagenarian siblings displayed a significantly lower prevalence of myocardial infarction, hypertension and diabetes mellitus when compared with their partners (23). The general objective of this thesis is to study cellular processes responsible for the increased longevity in the offspring, using human dermal fibroblast strains. We aimed to first show differences in *in vitro* cellular phenotypes, comparing fibroblast strains from offspring and partners under non-stressed conditions and after oxidative stress. As a proof-of-principle we also compared fibroblast strains from chronologically young and old subjects. We

focussed on apoptosis and senescence since they are thought to play a major role in stress responses. Second, we were interested in the signaling pathways driving the differences in cellular phenotypes.

Study populations

The Leiden Longevity Study

This study was set up to investigate the contribution of genetic factors to healthy longevity by establishing a cohort enriched for familial longevity (24). From July 2002 to May 2006, 420 families were recruited consisting of 991 long-lived Caucasian siblings together with 1705 of their offspring and 760 of the partners thereof. There were no selection criteria on health or demographic characteristics. Compared with their partners, the offspring were shown to have a 30% lower mortality rate and a lower prevalence of cardio-metabolic diseases (23;24). A biobank was established from fibroblasts cultivated from skin biopsies from a subset of offspring-partner pairs.

The Leiden 85-plus Study

This study is a prospective population-based follow up study in which 599 inhabitants of Leiden, the Netherlands, aged 85 years took part (25). The study was set up to assess common chronic diseases and general impairments in the general oldest-old population. Information on common chronic diseases was obtained from records of subjects' general practitioners and pharmacies while general impairments were assessed with functional tests and standardized questions during face-to-face interviews. A biobank was established from fibroblasts cultivated from skin biopsies of surviving 90-year-old participants and from biopsies taken from 27 young subjects, serving as a control group.

References

(1) Kirkwood TB, Austad SN. Why do we age? Nature 2000;408:233-238.

(2) Harman D. Aging: a theory based on free radical and radiation chemistry. J Gerontol 1956;11:298-300.

(3) Schroeder P, Krutmann J. Environmental Oxidative Stress - Environmental Sources of ROS. *The Handbook of Environmental Chemistry*. Heidelberg: Springer Berlin, 2005: 19-31.

(4) Passos JF, von Zglinicki T. Mitochondria, telomeres and cell senescence. Exp Gerontol 2005;40:466-472.

(5) Suji G, Sivakami S. Glucose, glycation and aging. Biogerontology 2004;5:365-373.

(6) Fialkow L, Wang Y, Downey GP. Reactive oxygen and nitrogen species as signaling molecules regulating neutrophil function. Free Radical Biol Med 2007;42:153-164.

(7) Bruunsgaard H, Pedersen M, Pedersen BK. Aging and proinflammatory cytokines. Curr Opin Hematol 2001;8:131-136.

(8) Campisi J. Cancer and ageing: rival demons? Nat Rev Cancer 2003;3:339-349.

(9) Madeo F, Tavernarakis N, Kroemer G. Can autophagy promote longevity? Nat Cell Biol 2010;12:842-846.

(10) Vicencio JM, Galluzzi L, Tajeddine N, Ortiz C, Criollo A, Tasdemir E, Morselli E, Ben Younes A, Maiuri MC, Lavandero S, Kroemer G. Senescence, apoptosis or autophagy? When a damaged cell must decide its path--a mini-review. Gerontology 2008;54:92-99.

(11) Hayflick L, Moorhead PS. Serial Cultivation of Human Diploid Cell Strains. Experimental Cell Research 1961;25:585-621.

(12) Dimri GP, Lee XH, Basile G, Acosta M, Scott C, Roskelley C, Medrano EE, Linskens M, Rubelj I, Pereirasmith O, Peacocke M, Campisi J. A Biomarker That Identifies Senescent Human-Cells in Culture and in Aging Skin In-Vivo. P Natl Acad Sci USA 1995;92:9363-9367.

(13) Rubin H. The disparity between human cell senescence in vitro and lifelong replication in vivo. Nat Biotechnol 2002;20:675-681.

(14) Blackburn EH. Telomere states and cell fates. Nature 2000;408:53-56.

(15) Karlseder J, Smogorzewska A, de LT. Senescence induced by altered telomere state, not telomere loss. Science 2002;295:2446-2449.

(16) Campisi J, d'Adda di Fagagna F. Cellular senescence: when bad things happen to good cells. Nat Rev Mol Cell Biol 2007;8:729-740.

(17) Ben-Porath I, Weinberg RA. The signals and pathways activating cellular senescence. Int J Biochem Cell Biol 2005;37:961-976.

(18) Austad SN. Methusaleh's Zoo: how nature provides us with clues for extending human health span. J Comp Pathol 2010;142 Suppl 1:S10-21.

(19) Horrobin DF. Modern biomedical research: an internally self-consistent universe with little contact with medical reality? Nat Rev Drug Discov 2003;2:151-154.

(20) Macieira-Coelho A. Relevance of in vitro studies for aging of the organism. A review. Z Gerontol Geriatr 2001;34:429-436.

(21) Harper JM, Salmon AB, Leiser SF, Galecki AT, Miller RA. Skin-derived fibroblasts from long-lived species are resistant to some, but not all, lethal stresses and to the mitochondrial inhibitor rotenone. Aging Cell 2007;6:1-13.

(22) Salmon AB, Murakami S, Bartke A, Kopchick J, Yasumura K, Miller RA. Fibroblast cell lines from young adult mice of long-lived mutant strains are resistant to multiple forms of stress. Am J Physiol Endocrinol Metab 2005;289:E23-E29.

(23) Westendorp RG, van Heemst D, Rozing MP, Frolich M, Mooijaart SP, Blauw GJ, Beekman M, Heijmans BT, de Craen AJ, Slagboom PE. Nonagenarian siblings and their offspring display lower risk of mortality and morbidity than sporadic nonagenarians: The Leiden Longevity Study. J Am Geriatr Soc 2009;57:1634-1637.

(24) Schoenmaker M, de Craen AJ, de Meijer PH, Beekman M, Blauw GJ, Slagboom PE, Westendorp RG. Evidence of genetic enrichment for exceptional survival using a family approach: the Leiden Longevity Study. Eur J Hum Genet 2006;14:79-84.

(25) Bootsma-van der Wiel A, Gussekloo J, de Craen AJM, van Exel E, Bloem BR, Westendorp RGJ. Common chronic diseases and general impairments as determinants of walking disability in the oldest-old population. J Am Geriatr Soc 2002;50:1405-1410.

Chapter 2

Rapid flow cytometric method for measuring Senescence Associated-β-galactosidase activity in human fibroblasts

Gerard Noppe*, Pim Dekker*, Corine de Koning-Treurniet, Joke Blom, Diana van Heemst, Roeland W. Dirks, Hans J. Tanke, Rudi G.J. Westendorp, Andrea B. Maier

Cytometry A 2009; 75(11), 910-916

*: Both authors contributed equally to this work

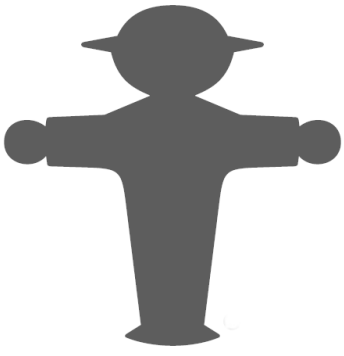

Summary

Senescence Associated-β-galactosidase (SA-β-gal) activity is a widely used marker for cellular senenescence. SA-β-gal activity is routinely detected cytochemically, manually discriminating negative from positive cells. This method is time-consuming, subjective and therefore prone to operator-error. We aimed to optimize a flow cytometric method described by other workers using endothelial cells to better differentiate between populations of fibroblasts in degrees of SA-β-gal activity. Skin fibroblasts were isolated from young (mean±SD age: 25.5±1.8) and very old (age 90.2±0.3) subjects. Different pH modulators were tested for toxicity. To induce stress-induced senescence, fibroblasts were exposed to rotenone. Senescence was assessed measuring SA-β-gal activity by cytochemistry (X-gal) and by flow cytometry (C_{12}FDG). The pH modulator Bafilomycin A1 (Baf A1) was found to be least toxic for fibroblasts and to differentiate best between non-stressed and stressed fibroblast populations. Under non-stressed conditions, fibroblasts from very old subjects showed higher SA-β-gal activity than fibroblasts from young subjects. This difference was found for both the flow cytometric and cytochemical methods ($p=0.013$ and $p=0.056$ respectively). Under stress-induced conditions the flow cytometric method but not the cytochemical method revealed significant higher SA-β-gal activity in fibroblasts from very old compared with young subjects ($p=0.004$ and $p=0.635$ respectively). We found the modified flow cytometric method measuring SA-β-gal activity superior in discriminating between degrees of senescence in different populations of fibroblasts.

Introduction

Cellular senescence can be induced by exhaustion of replicative capacity (1) or exposure to cellular stress (2). A variety of cellular markers of senescence have thus far been identified, amongst which there are cellular morphology (3), telomere length (4) and Senescence Associated-β-galactosidase (SA-β-gal) activity (5-8). β-Galactosidase is a collective name for enzymes which cleave non-reducing β-D-galactose residues from glycoproteins, sphingolipids and keratan sulfate in β-D-galactosides (9). These enzymes function optimally at pH 4. In senescent cells, β-galactosidase activity can also be detected at pH 6, although the function of SA-β-gal at this pH remains unknown (6).

SA-β-Gal activity can be cytochemically detected using 5-bromo-4-chloro-3-indolyl-β-D-galactoside (X-gal) as a substrate. Fibroblasts are stained, digitally recorded and SA-β-gal positive fibroblasts are manually counted and expressed as a percentage of total fibroblasts (6-8). Subjectivity, i.e. a low inter-rater reproducibility, is the main disadvantage of the method, and the procedure is highly time consuming. Kurz *et al.* (10) used a method based on flow cytometry to quantify SA-β-gal activity in endothelial cells (HUVEC). The flow cytometric method is not subjective and has a high throughput when compared with the cytochemical method. Kurz *et al.* (10) found the flow cytometric method to correlate well with the cytochemical method when using HUVECs.

Although the use of human fibroblasts was also exemplified in the paper by Kurz *et al*. (10), here we further extend the applications of the flow cytometric method in fibroblasts by performing the experiments under conditions of lysosomal alkalinisation and measuring stress induced premature senescence (SIPS). In this manuscript, we describe the optimization of the flow cytometric procedure, for use in human diploid fibroblasts and its comparison to the conventional cytochemical method. To investigate if the two methods are equally able to discriminate SA-β-gal activity between subpopulations of fibroblasts, we have compared fibroblast strains derived from young and very old subjects, both under non-stressed and stressed conditions.

Materials & methods

Fibroblast Cultures

Fibroblast strains were obtained from participants of the Leiden 85-plus Study, a population-based follow up study in which 599 inhabitants of Leiden, the Netherlands, aged 85 years took part (11). Skin biopsies were taken as described earlier (12) at the age of 89 or 90 years. In order to have a contrast in chronological age, skin biopsies were also obtained from young subjects (mean±SD age: 25.5±1.8 years).

Biopsies were taken from the sun unexposed medial side of the upper arm and cultured under standardized conditions (12) at 37℃, 5%CO_2 and 100% humidity in D-MEM:F-12 supplemented with 10% fetal calf serum (FCS, Gibco, batch no. 40G4932F), 1 mM MEM sodium pyruvate, 10 mM HEPES, 2 mM Glutamax and antibiotics (100 Units/ml penicillin, 100 µg/ml streptomycin, 2.5 µg/ml amphotericin B). This medium will be referred to as growth medium. All reagents were obtained from GIBCO, Breda, the Netherlands. When cultures reached 80% to 90% confluence, fibroblasts were subcultured using a 1:4 split ratio.

Experiments for optimization of the sample preparation were performed with two fibroblast strains from young subjects. Immunohistochemical double staining for p16 and SA-β-gal was performed using three randomly chosen strains under non-stressed and stressed conditions as well as one high passage strain that had undergone 79 population doublings. After optimization, fibroblast strains from ten young and ten very old subjects, which were randomly selected from the Leiden 85-plus Study, were compared.

Induction of cellular stress

Fibroblasts were seeded at a density of $2.6x10^4$ fibroblasts per 25-cm^2 flask and in Permanox 2-chamber slides (Nunc, VWR, Amsterdam, the Netherlands) at $1.0x10^4$ fibroblasts per chamber (4.2 cm^2/chamber). In pilot experiments, fibroblasts were stressed with 0.2 µM - 1 µM rotenone for three days (data not shown). Exposure to 0.6 µM rotenone induced considerable senescence after three days and this concentration was subsequently used to stress fibroblast strains from young and very old subjects.

Four hours after seeding, medium was replaced by growth medium supplemented with 0.6 µM rotenone. Fibroblasts were incubated for 72 hours in rotenone-supplemented medium, after which they were analyzed. All experiments were repeated.

Lysosomal pH adjustment

Lysosomal pH was increased to pH 6 by adding bafilomycin A1 (baf A1) or chloroquine (10;13) to the growth medium. Nigericin in a buffered solution was used to change the pH of all intracellular compartments (10;14;15).

Baf A1: Fibroblasts were incubated for one hour in growth medium supplemented with 100 nM baf A1 at 37℃, 5% CO_2, and one hour in growth medium with 100 nM baf A1 and 33 µM 5-Dodecanoylaminofluorescein-di-β-D-galactopyranoside (C_{12}FDG) prior to analysis.

Chloroquine: Fibroblast were incubated for two hours in growth medium containing 100 or 300 µM chloroquine at 37℃, 5% CO_2, and one hour in growth medium with 100 or 300 µM chloroquine and 33 µM C_{12}FDG.

Nigericin (10 µM) was added to the culture in the presence of a potassium-rich 2-(N-morpholino) ethanesulfonic acid (MES) buffer (150 mM KCl, 10 mM NaCl, 1 mM $MgCl_2$, 0.1 mM $CaCl_2$, 10 mM Glucose, 10 mM MES buffer), pH 6, and incubated for 15 minutes at 37℃, not CO_2 enriched, after which C_{12}FDG was added (33 µM) followed by one hour incubation at 37℃, not CO_2-enriched.

Measurement of toxicity pH-modulators

Toxicity of pH modulators was determined by measuring apoptosis and necrosis using the TACS Annexin V-FITC kit (R&D Systems, Abingdon, United Kingdom) and a FACSCalibur flow cytometer (BD, Oxford, United Kingdom). Events were gated into quadrants and Annexin V positive/propidium iodide (PI) negative (Annexin V+/PI-) and Annexin V positive/propidium iodide (PI) positive (Annexin V+/PI+) fibroblasts were analyzed as percentages of the total fibroblast population.

Immunohistochemical double staining for p16 and senescence-associated β-galactosidase

To show that rotenone induces senescence, double staining for p16 and SA-β-gal was performed as previously described by Itahana *et al*. (16). Fibroblasts were seeded in Permanox 4-chamber slides at 4000 cells/chamber and allowed to attach for four hours. After treatment with 600 nM rotenone for three days, fibroblasts were fixed with 4% paraformaldehyde in PBS for 4 minutes and stained for SA-β-gal activity as described in the subsequent paragraph. After permeabilization for 20 minutes in 0.2% Triton (Sigma, St Louis, MO, USA) in PBS, samples were blocked with blocking buffer (3% BSA in PBS) for one hour at room temperature and incubated for two hours with anti-p16 (JC8) antibody (Santa Cruz Biotechnology Inc., Santa Cruz, USA), diluted 1/100 in blocking buffer. After three washes with PBS, coverslips were incubated with Alexa Fluor® 488 labeled anti-mouse antibody (Invitrogen, Breda, The Netherlands) diluted 1:1000 in blocking buffer for one hour. Slides were mounted with Vectashield Fluorescent Mounting Medium (Vector laboraties, Burlingame, CA, USA) and photographed with a Leica fluorescence microscope (Leica Microsystems, Rijswijk, the Netherlands). Per sample, 100 randomly chosen cells were assessed for SA-β-gal positivity and for p16 positivity.

Flow cytometric measurement of SA-β-gal activity

C_{12}FDG is a substrate which, when hydrolyzed by SA-β-gal, becomes fluorescent and membrane impermeable (10,17). C_{12}FDG was added to the pH modulation medium/buffer. Fibroblasts were incubated with this solution for one hour at 37℃, 5% CO_2 (nigericin-buffer incubation not CO_2 enriched). After incubation, fibroblasts were trypsinized with trypsin EDTA (Sigma, St Louis, MO, USA), washed with PBS, resuspended in 200 µl PBS, and analyzed immediately using a FACSCalibur flow cytometer. Data were analyzed using FACSDiva software (BD, Oxford, United Kingdom). Cell debris was excluded on basis of light scatter parameters. C_{12}FDG was measured on the FL1 detector (500-510 nm wavelength). SA-β-gal activity was expressed as the FL1 median fluorescence intensity (MdFI, in arbitrary units) of the fibroblast population.

Cytochemical staining for SA-β-gal activity

The cytochemical method was conducted as described by Dimri *et al.* (6). A Senescence Cells Histochemical Staining Kit was used (Sigma, St Louis, MO, USA) and fibroblasts were processed according to the manufacturer's guidelines. Slides were washed twice with PBS, counterstained with Mayers-Hematoxylin staining solution (Sigma, St Louis, MO, USA) for 5 minutes at room temperature and washed twice again with PBS. Fibroblasts were then viewed by phase contrast on a Leica microscope (Leica Microsystems, Rijswijk, the Netherlands) and recorded at a 100x magnification by a digital color camera. Per sample, 500 randomly selected fibroblasts were photographed and counted. The number of positive, blue fibroblasts was divided by the total number of counted fibroblasts, resulting in the percentage of SA-β-gal positive fibroblasts.

Statistical analysis

All analyses were performed with the software package SPSS 14.0 (SPSS Inc., Chicago, IL). Differences between pH modulators were analyzed by one-tailed Student's *t* test. Differences between non-stressed and stressed fibroblasts as well as differences between fibroblast strains from young and very old subjects were analyzed by two-tailed Student's *t* test. Results of cytochemical SA-β-gal measurements were divided into tertiles and related to the flow cytometric results. Differences between tertiles were analyzed by ANOVA. Co-localization of p16 and SA-β-gal was described by calculating the specificity (p16-negative fibroblasts as percentage of SA-β-gal-negative fibroblasts) and sensitivity (p16-positive fibroblasts as percentage of SA-β-gal-positive fibroblasts). To determine the correlation between the flow cytometric and the cytochemical methods, we used Pearson correlation analysis.

Results

Toxicity

Unlike the cytochemical assay, in which cells are fixed with formalin, the flow cytometric method measures SA-β-gal activity in living cells. Therefore, the toxicity of the pH modulating agents was examined. Compared with fibroblasts without pH modification, the percentage of

annexin V+/PI- fibroblasts, reflecting early apoptotic cells, was only significantly increased after treatment with 300 µM chloroquine (Figure 1A). Rotenone treatment was used as a positive control for induction of apoptosis, and yielded a significant increase in percentage of early apoptotic cells (3.2±0.61%). Of the four pH modulating conditions tested, the increases in percentage of annexin V+/PI- fibroblasts compared with no pH modulation were smallest

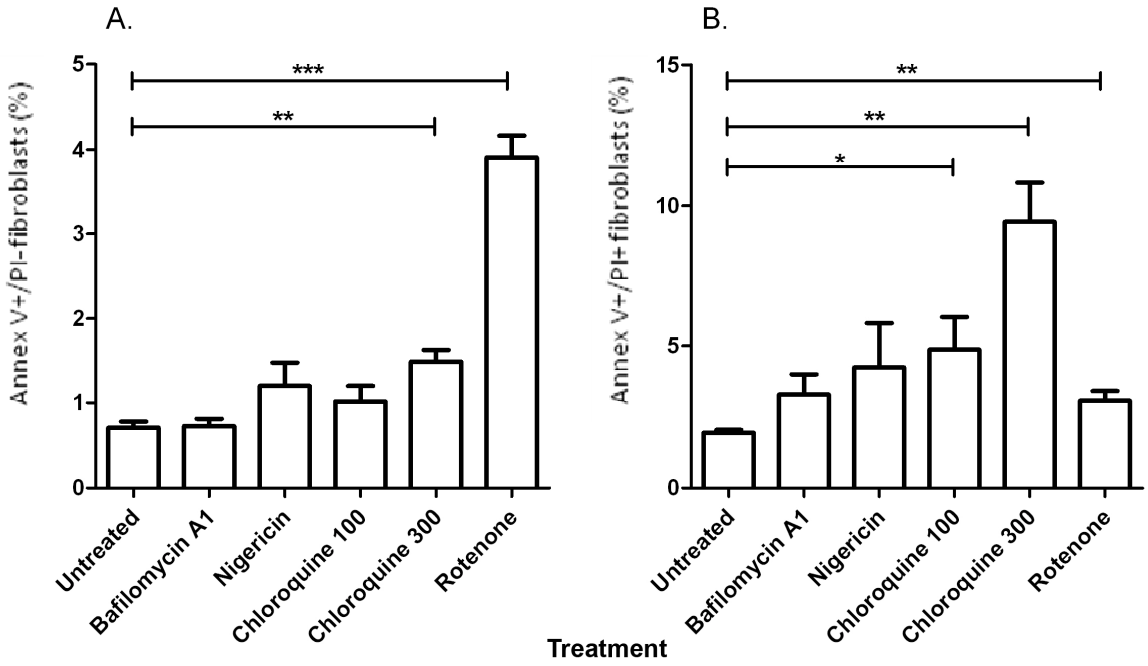

Figure 1. Apoptosis and cell death induced by pH modulation. A, Mean percentage of annexin V+/PI- fibroblasts, reflecting early apoptotic cells. B, Mean percentage of Annexin-V positive/PI positive fibroblasts, reflecting cell death. Mean ± SEM of repeated experiments in two strains. *p≤0.05 **p≤0.01 ***p≤0.001"

for bafilomycin A1 (mean increase ± SD: 0.02±0.27%) compared with treatment with nigericin (0.49±0.63%), 100 µM chloroquine (0.31±0.47%) and 300 µM chloroquine (0.77±0.47%). In Figure 1B, increases in the percentage of annexin V+/PI+ fibroblasts, followed a similar trend as shown in Figure 1A. All pH-modulating agents yielded an increase in the percentage of annexin V+/PI+ fibroblasts. This increase was not significant for bafilomycin A1 and nigericin (1.34±1.35% and 2.29±3.2% respectively). Chloroquine treatment induced a significant

increase in percentage of annexin V-positive/ PI-positive fibroblasts (100 µM: 2.92±2.37%, 300 µM: 7.48±2.88%) as did rotenone treatment (1.13±0.87%).

C_{12}FDG conversion

To determine if the pH modulators would affect the ability to discriminate between degrees of SA-β-gal activity, senescence was induced with rotenone and SA-β-gal activity was assessed using C_{12}FDG. Figure 2 shows representative histograms of both non-stressed and rotenone-stressed fibroblast strains. Discrimination between non-stressed and stressed fibroblasts was best when the pH was modulated using Baf A1 (Median Fluorescence Intensity [MdFI] in arbitrary units, non-stressed: 1475±154, stressed: 2405±260, p=0.008). Other pH modulators also showed changes in MdFI (nigericin: non-stressed: 502±16, stressed: 698±7, p=0.0001; 300 µM chloroquine: 350±48 vs. 482±28, p=0.012), except for 100 µM chloroquine (997±68 AU vs. 866±74, p=0.29).

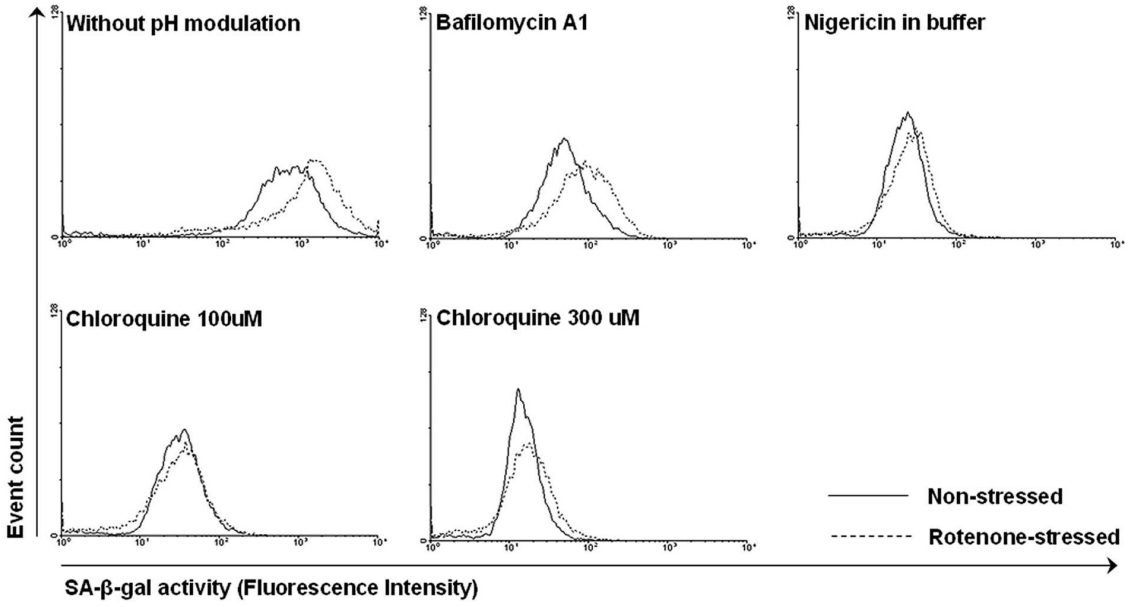

Figure 2. Change in SA-β-gal activity measured by the flow cytometric method in fibroblast strains after induction of stress-induced premature senescence. Histograms are representative examples of SA-β-gal activity in non-stressed and rotenone-stressed fibroblast strains (n=2, duplicate experiments). Samples were treated with pH modulating agents prior to analysis. Scales are equal.

Even though pH modulation appeared not to be essential to SA-β-gal activity quantification with the flow cytometric method as shown in Figure 2, it is a necessary step for the cytochemical method. When no pH modulation is applied all cells would stain blue, making it impossible to distinguish senescent from non-senescent cells. Modulation of the lysosomal pH was thus applied in further experiments, to better compare the flow cytometric method with the cytochemical method. Based on toxicity and SA-β-gal activity, we concluded that Baf A1 was the agent of choice for pH modulation and was thus used in all subsequent experiments.

Rotenone induced senescence increases SA-β-gal activity and p16 expression

Figure 3 displays a representative photograph of fibroblasts positive for both SA-β-gal activity and p16. The absence and presence of SA-β-gal activity and p16 expression were assessed for three fibroblast strains, both under non-stressed and stressed conditions.

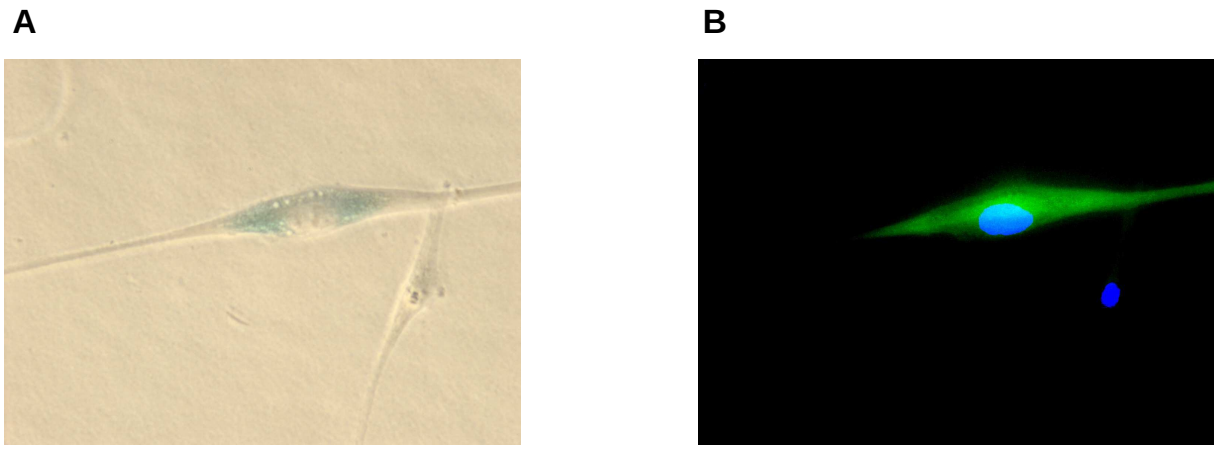

Figure 3. SA-β-gal activity and p16 expression at 3 days after rotenone treatment. A, Phase-contrast photograph showing a SA-β-gal positive (blue) and a SA-β-gal negative fibroblast. B, Immunofluorescent photograph showing a p16 positive (green) and a p16 negative fibroblast. Blue: DAPI.

The combined results for these three strains are presented in Table 1. Under non-stressed conditions, 54% of the fibroblasts were double-negative for SA-β-gal activity and p16 expression (66%, 47% and 50% for the three strains respectively) whereas under rotenone-stressed conditions, 43% of the fibroblasts were double-positive (33%, 40% and 55%). High passage fibroblasts were included in the experiment as positive control (47%). Despite the

considerable concordance, discordance remained present. Specificity and sensitivity were calculated to be 78% and 37% respectively for non-stressed fibroblasts and 62% and 73% respectively for stressed fibroblasts.

Table 1. SA-β-gal activity and p16 expression of three fibroblast strains, under non-stressed and rotenone stressed conditions and in one strain at high passage.

	SA-β-gal negative # cells (%)	SA-β-gal positive # cells (%)	Total # cells (%)
Low passage, non-stressed,			
p16 negative	163 (54)	57 (19)	220 (73)
p16 positive	47 (16)	33 (11)	80 (27)
Total	210 (70)	90 (30)	300 (100)
Low passage, rotenone-stressed			
p16 negative	79 (26)	45 (15)	124 (41)
p16 positive	48 (16)	128 (43)	176 (59)
Total	127 (42)	173 (58)	300 (100)
High passage			
p16 negative	23 (23)	10 (10)	33 (33)
p16 positive	20 (20)	47 (47)	67 (67)
Total	43 (43)	57 (57)	100 (100)

For each strain, 100 cells were counted. High passage strain was stained after 79 population doublings.

Comparison of flow cytometric- and cytochemical method

Twenty fibroblast strains, ten fibroblast strains from young and ten from very old subjects, were used to determine the relation between the flow cytometric and the cytochemical method. The two methods were performed simultaneously for each fibroblast strain, both under non-stressed and stressed conditions. Rotenone induced a significant increase in SA-β-gal activity for both methods as shown in Figure 4A and B. Figure 4C and D show the three tertiles of percentages of SA-β-gal positive fibroblasts detected by the cytochemical method

plotted against the corresponding SA-β-gal MdFI values determined by the flow cytometric method.

Under non-stressed conditions (Figure 4C), significant increases in flow cytometric SA-β-gal activity between tertiles of the cytochemical method were found (trend: p=0.01). When analyzed continuously, the MdFI correlated significantly with the percentages of SA-β-gal positive fibroblasts (r^2=0.31, p=0.014). Under stressed conditions (Figure 4D) no relation was found between the flow cytometric method and cytochemical method (trend p=0.82). Even though both methods detect a significant increase of SA-β-gal activity upon rotenone treatment, we found no relation between the two methods under stressed conditions.

To clarify which of the two methods is the method of choice, both methods measuring SA-β-gal activity were used to discriminate fibroblasts from young and old donors. Figure 5A shows the significant difference in SA-β-gal activity that was found in fibroblasts from young and very old subjects under non-stressed conditions using the flow cytometric method (MdFI in arbitrary units, young: 2161±643, old: 3125±903, p=0.013). When analyzed with the cytochemical method (Figure 5B), the same difference in SA-β-gal activity in young and very old subjects was found, though this difference was not statistically significant (young: 18.7±5.84%, old: 28.3±13.65%, p=0.056). Upon induction of senescence with rotenone, the difference in SA-β-gal activity between young and very old subjects remained by using the flow cytometric method (MdFI in arbitrary units, 3438±689 vs. 4617±880, p=0.004), but was absent when the cytochemical method was performed (44.3±10.7% vs. 47.3±16.1%, p=0.634).

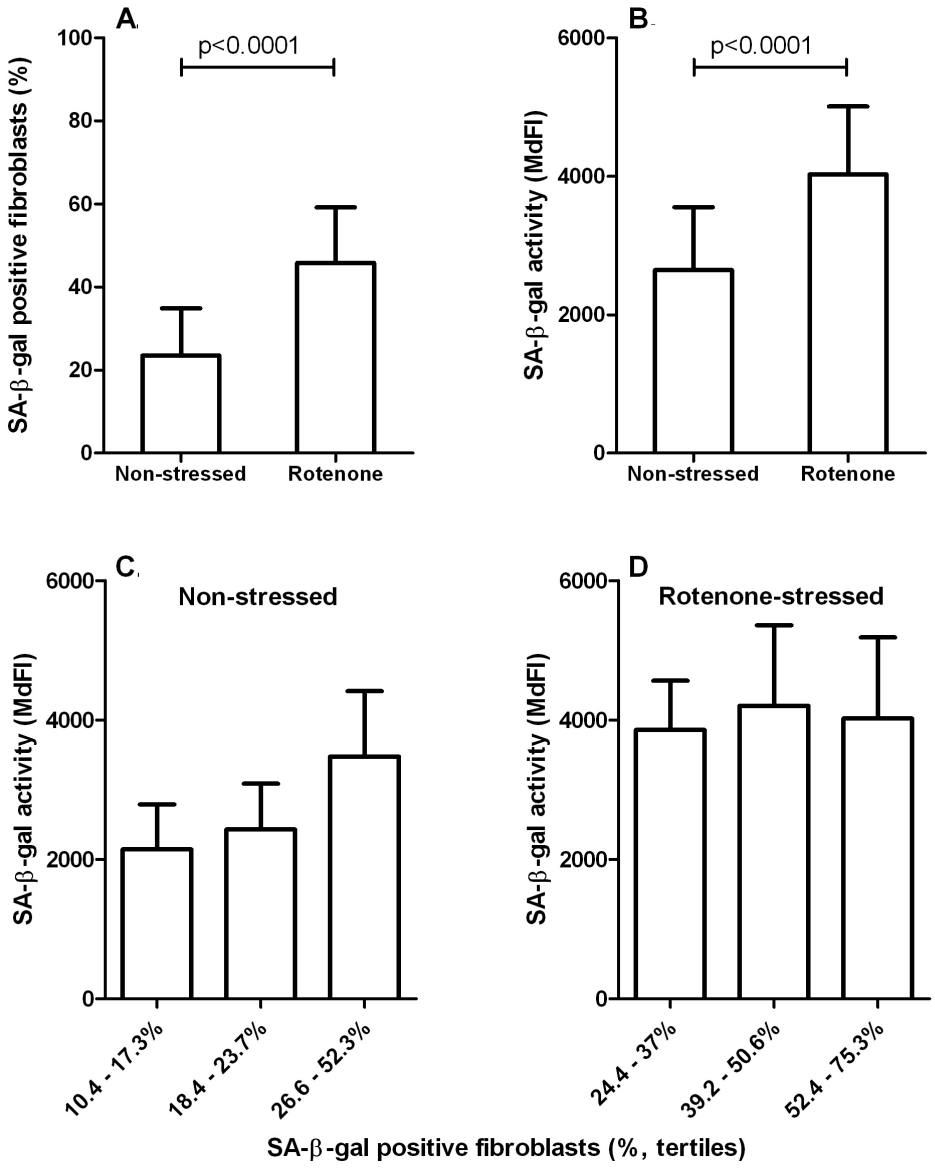

Figure 4. A/B, SA-β-gal activity measured with the cytochemical and flow cytometric methods under non-stressed conditions and after stress with rotenone. A, cytochemical method. B, flow cytometric method. C/D, correlation between SA-β-gal activity measured by the flow cytometric method and cytochemical method. C, Non-stressed fibroblasts, ANOVA for trend p=0.01. D, rotenone-stressed fibroblasts, ANOVA for trend p=0.82. N=20 fibroblast strains. MdFI: Median Fluorescence Intensity, bars: mean±SD.

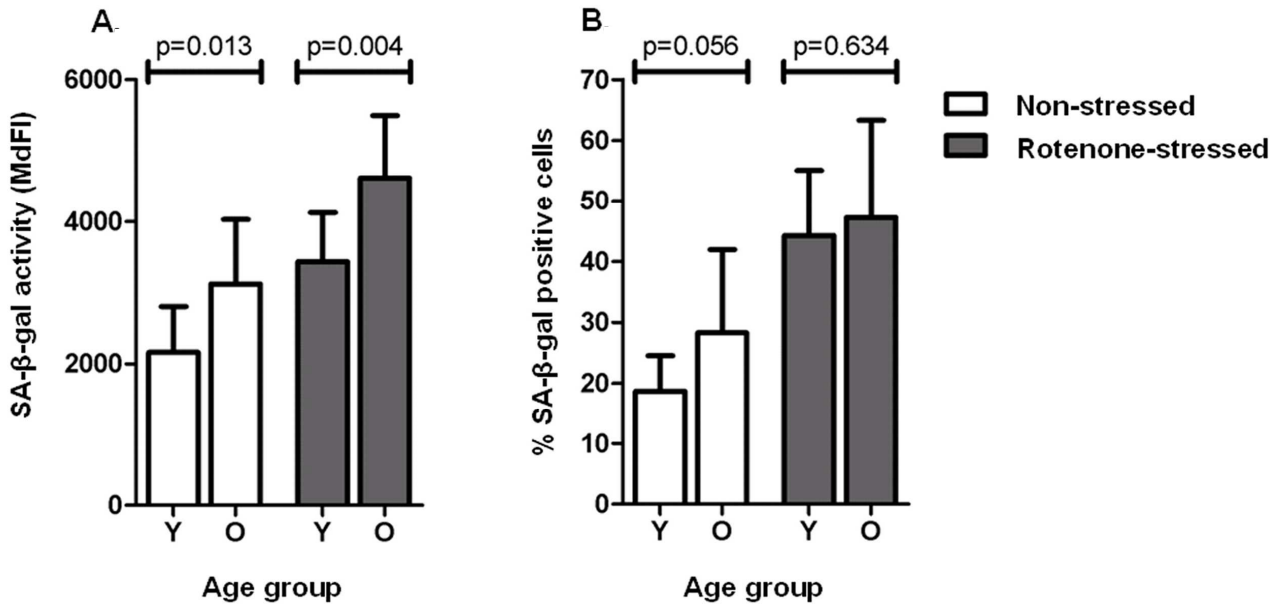

Figure 5. SA-β-gal activity of fibroblast strains from young and very old subjects measured by: A, the flow cytometric method and B, the cytochemical method. Bar-charts display SA-β-gal activity of fibroblast strains from young (Y, n=10) and very old (O, n=10) subjects, in non-stressed and rotenone-stressed conditions. MdFI: Median Fluorescence Intensity, bars: mean±SD.

Discussion

The cytochemical detection of SA-β-gal activity is a widely used marker for cellular senescence and was firstly described by Dimri *et al.* (6). Although the cytochemical method is widely used, it is subjective, prone to inter-rater variability and time-consuming. Kurz *et al.* (10) described a method to measure SA-β-gal activity in HUVECs by flow cytometry, using a fluorogenic substrate. Using this method, cells are neither strictly negative nor positive for SA-β-gal activity but each cell in a population is quantified separately, resulting in more accurate evaluation of differences in SA-β-gal activity within and between populations of cells. This method was validated with the conventional cytochemical method as described by Dimri *et al.* (6). Because cellular senescence is widely studied in human diploid fibroblasts, we aimed to optimize the flow cytometric method using this cell type.

Rotenone was chosen as senescence-inducing agent because it acts on mitochondrial complex I, leading to increased levels of intracellular Reactive Oxygen Species (ROS) (17), which is supposed to mimic the physiological process of ROS induced damage that underlies the aging process (18). Armstong *et al.* showed the apoptotic effect of rotenone when applied in high concentrations (19). When used in lower concentrations, we found that rotenone induces senescence as measured by colocalisation of increased p16 expression and increased SA-β-gal activity. As a positive control, we also observed colocalisation of increased p16 expression coinciding with increased SA-β-gal activity in high passage fibroblasts as was previously observed by Itahana *et al*. (16). In line with these results, Duan *et al*. (20) showed that antisense p16 postponed senescence and decreased SA-β-gal activity, indicating that SA-β-gal activity is indeed a good marker of senescence. However, the discordance in SA-β-gal activity and p16 expression as described in Table 1 shows that increased p16 expression is not a prerequisite for an increase in SA-β-gal activity and that SA-β-gal activity does not always depend on p16 expression. Although various markers have been described that identify senescent cells, the current consensus is that none of these markers is specific for senescence only (21). One of the hallmarks of senescence is growth arrest, which can be mediated by two main pathways: the p53/p21 and the p16/pRB pathways. Although p16 is expressed by many senescent cells, it is not exclusive for senescence (16;22), which is a possible explanation for the SA-β-gal negative/p16 positive fibroblasts observed in our experiments. The SA-β-gal positive/p16 negative fibroblasts could well be the result of senescence induced by pathways other than p16, for example p53. Additionally, examples of senescence have been described that are independent of p16 and p53 (23;24).

Both the flow cytometric and the cytochemical method showed significant increases in SA-β-gal activity after exposure to stress. Under non-stressed conditions, both methods were able to detect a difference between fibroblast strains derived from young subjects compared with strains from very old subjects. When these fibroblast strains were exposed to stress, only the flow cytometric method was able to identify differences in SA-β-gal activity between fibroblasts from young and very old subjects. This could be due to the marked differences between the two methods, the most notable being that, using the cytochemical method, SA-

β-gal activity of individual fibroblasts is assessed dichotomously, whereas the flow cytometric method measures SA-β-gal activity in the fibroblasts on a continuous fluorescence scale. It may thus be well conceivable that two samples measured cytochemically might yield similar percentages of SA-β-gal positive fibroblasts while the intensity of the stained fibroblasts is different between the samples. This difference between samples would be detected by the flow cytometric method since every fibroblast is measured on a continuous scale. Another important difference is that the cytochemical method is performed on fixed fibroblasts whereas flow cytometry is applied to living fibroblasts. Enzyme activity depends on a proper configuration of the protein involved. It is likely that in fixed fibroblasts, enzyme activity will be affected by protein cross-linking and it may thus be hypothesized that measuring SA-β-gal activity with the flow cytometric method in living fibroblasts may better reflect biology.

Since the flow cytometric method described relies on living fibroblasts, we tested the pH modulators for toxicity. We found that Baf A1 was not toxic for fibroblasts whereas chloroquine and nigericin were. Kurz *et al.* (10) show that the SA-β-activity is indeed lysosomal, so we preferred to selectively change lysosomal pH (Baf A1 and chloroquine), as opposed to cytosolic pH (nigericin buffer). Since Baf A1 was virtually non-toxic, whereas chloroquine was not, Baf A1 was our pH-modulator of choice.

Our results suggest that under most conditions, both methods show changes in SA-β-gal activity, but we found the flow cytometric method superior to discriminate between populations of fibroblasts, showing different levels of induced SA-β-gal activity being associated with senescence. Taking into account that the flow cytometric is also less labor-intensive and more time- and cost-effective than the cytochemical method, we strongly recommend flow cytometry for measuring SA-β-gal activity in cultured fibroblasts.

References

(1) Hayflick L, Moorhead PS. Serial Cultivation of Human Diploid Cell Strains. Exp Cell Res 1961;25(3):585-621.

(2) Toussaint O, Dumont P, Remacle J, Dierick JF, Pascal T, Frippiat C *et al*. Stress-induced premature senescence or stress-induced senescence-like phenotype: one in vivo reality, two possible definitions? ScientificWorldJournal 2002;2:230-47.:230-247.

(3) Toussaint O, Medrano EE, von Zglinicki T. Cellular and molecular mechanisms of stress-induced premature senescence (SIPS) of human diploid fibroblasts and melanocytes. Exp Gerontol 2000;35(8):927-945.

(4) von Zglinicki T, Saretzki G, Ladhoff J, d'Adda di Fagagna F, Jackson SP. Human cell senescence as a DNA damage response. Mech Ageing Dev 2005;126(1):111-117.

(5) Bassaneze V, Miyakawa AA, Krieger JE. A quantitative chemiluminescent method for studying replicative and stress-induced premature senescence in cell cultures. Anal Biochem 2008;372(2):198-203.

(6) Dimri GP, Lee XH, Basile G, Acosta M, Scott C, Roskelley C *et al*. A Biomarker That Identifies Senescent Human-Cells in Culture and in Aging Skin In-Vivo. P Natl Acad Sci USA 1995;92(20):9363-9367.

(7) Maier AB, Westendorp RG, van Heemst D. Beta-galactosidase activity as a biomarker of replicative senescence during the course of human fibroblast cultures. Ann N Y Acad Sci 2007;1100:323-332.

(8) Severino J, Allen RG, Balin S, Balin A, Cristofalo VJ. Is beta-galactosidase staining a marker of senescence in vitro and in vivo? Exp Cell Res 2000;257(1):162-171.

(9) Gossrau RZ, Lojda Z, Stoward PJ. Glycosidase. In: Pearse AGE, Stoward PJ, editors. Histochemistry: theoretical and Applied. Edinburgh: Churcill Livingstone; 1991.

(10) Kurz DJ, Decary S, Hong Y, Erusalimsky JD. Senescence-associated beta-galactosidase reflects an increase in lysosomal mass during replicative ageing of human endothelial cells. J Cell Sci 2000;113(20):3613-3622.

(11) von Faber M, Bootsma-van der Wiel A, van Exel E, Gussekloo J, Lagaay AM, van Dongen E *et al*. Successful aging in the oldest old: Who can be characterized as successfully aged? Arch Intern Med 2001;161(22):2694-2700.

(12) Maier AB, le Cessie S, Koning-Treurniet C, Blom J, Westendorp RG, van Heemst D. Persistence of high-replicative capacity in cultured fibroblasts from nonagenarians. Aging Cell 2007;6(1):27-33.

(13) Yoshimori T, Yamamoto A, Moriyama Y, Futai M, Tashiro Y. Bafilomycin A1, a specific inhibitor of vacuolar-type H(+)-ATPase, inhibits acidification and protein degradation in lysosomes of cultured cells. J Biol Chem 1991;266(26):17707-17712.

(14) Escobales N, Longo E, Cragoe EJ, Jr., Danthuluri NR, Brock TA. Osmotic activation of Na(+)-H+ exchange in human endothelial cells. Am J Physiol 1990;259(4 Pt 1):C640-C646.

(15) Negulescu PA, Machen TE. Intracellular ion activities and membrane transport in parietal cells measured with fluorescent dyes. Methods Enzymol 1990;192:38-81.

(16) Itahana K, Zou Y, Itahana Y, Martinez JL, Beausejour C, Jacobs JJ *et al*. Control of the replicative life span of human fibroblasts by p16 and the polycomb protein Bmi-1. Mol Cell Biol 2003;23(1):389-401.

(17) Li N, Ragheb K, Lawler G, Sturgis J, Rajwa B, Melendez JA *et al*. Mitochondrial complex I inhibitor rotenone induces apoptosis through enhancing mitochondrial reactive oxygen species production. J Biol Chem 2003;278(10):8516-8525.

(18) Harman D. Aging: a theory based on free radical and radiation chemistry. J Gerontol 1956;11(3):298-300.

(19) Armstrong JS, Hornung B, Lecane P, Jones DP, Knox SJ. Rotenone-induced G2/M cell cycle arrest and apoptosis in a human B lymphoma cell line PW. Biochem Biophys Res Commun 2001;289(5):973-978.

(20) Duan J, Zhang Z, Tong T. Senescence delay of human diploid fibroblast induced by anti-sense p16INK4a expression. J Biol Chem 2001;276(51):48325-48331.

(21) Campisi J, d'Adda di Fagagna F. Cellular senescence: when bad things happen to good cells. Nat Rev Mol Cell Biol 2007;8(9):729-740.

(22) Beausejour CM, Krtolica A, Galimi F, Narita M, Lowe SW, Yaswen P *et al*. Reversal of human cellular senescence: roles of the p53 and p16 pathways. EMBO J 2003;22(16):4212-4222.

(23) Michaloglou C, Vredeveld LC, Soengas MS, Denoyelle C, Kuilman T, van der Horst CM *et al*. BRAFE600-associated senescence-like cell cycle arrest of human naevi. Nature 2005;436(7051):720-724.

(24) Olsen CL, Gardie B, Yaswen P, Stampfer MR. Raf-1-induced growth arrest in human mammary epithelial cells is p16-independent and is overcome in immortal cells during conversion. Oncogene 2002;21(41):6328-6339.

Chapter 3

Stress-induced responses of human skin fibroblasts *in vitro* reflect human longevity

Pim Dekker, Andrea B. Maier, Diana van Heemst, Corine de Koning-Treurniet, Joke Blom, Roeland W. Dirks, Hans J. Tanke, Rudi G.J. Westendorp

Aging Cell 2009; 8(5), 595-603

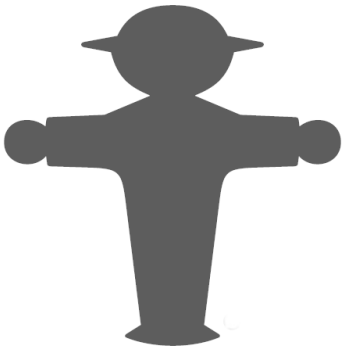

Summary

Unlike various model organisms, cellular responses to stress have not been related to human longevity. We investigated cellular responses to stress in skin fibroblasts that were isolated from young and very old subjects, and from offspring of nonagenarian siblings and their partners, representatives of the general population. Fibroblast strains were exposed to rotenone and hyperglycemia and assessed for Senescence Associated-β-galactosidase (SA-β-gal) activity by flow cytometry. Apoptosis/cell death was measured with the Annexin-V/PI assay and cell-cycle analysis (Sub-G1 content) and growth potential was determined by the colony formation assay. Compared with fibroblast strains from young subjects, baseline SA-β-gal activity was higher in fibroblast strains from old subjects ($p=0.004$) as were stress-induced increases (rotenone: $p<0.001$, hyperglycemia: $p=0.027$). For measures of apoptosis/cell death, fibroblast strains from old subjects showed higher baseline levels (AnnexinV+/PI+ cells: $p=0.040$, Sub-G1: $p=0.014$) and smaller stress-induced increases (Sub-G1: $p=0.018$) than fibroblast strains from young subjects. Numbers and total size of colonies under non-stressed conditions were higher for fibroblast strains from young subjects ($p=0.017$ and $p=0.006$ respectively). Baseline levels of SA-β-gal activity and apoptosis/cell death were not different between fibroblast strains from offspring and partner. For fibroblast strains from offspring, stress-induced greater were smaller for SA-β-gal activity (rotenone: $p=0.064$, hyperglycemia: $p<0.001$) and greater for apoptosis/cell death (Annexin V+/PI- cells: $p=0.041$, AnnexinV+/PI+ cells: $p=0.008$). Numbers and total size of colonies under non-stressed conditions were higher for fibroblast strains from offspring ($p=0.001$ and $p=0.024$ respectively) whereas rotenone-induced decreases were smaller ($p=0.008$ and $p=0.004$ respectively). These data provide strong support for the hypothesis that *in vitro* cellular responses to stress reflect the propensity for human longevity.

Introduction

Organisms are continuously exposed to intrinsic and environmental stressors. Many of these stressors result in the formation of Reactive Oxygen Species (ROS) that are thought to play an important role in aging and age-related diseases (1). Low levels of ROS may be essential to maintain` homeostasis, but excess ROS will cause damage to important macromolecules, including DNA, proteins and lipids (2). Organisms with self-renewable tissues can replace damaged cells, rejuvenating tissues to maintain body homeostasis, depending on the balance between cell proliferation and cell death. However, as proliferating cells can transform into cancer cells as a result of genomic damage, several protective mechanisms have evolved to prevent cells from becoming neoplastic (3;4). Faced with damage, a proliferating cell can take several routes, depending on the cell type, and the type and extent of damage that has occurred. First, it can arrest the cell cycle, repair the damage and continue to proliferate. Second, it can permanently stop proliferating and become senescent (5;6). Third, it can be removed in a controlled manner by apoptosis or in an uncontrolled manner by necrosis (7).

Though ROS-induced damage can cause cells to go into apoptosis or senescence, little is known about the relative contributions of these cellular fates in response to stressors and how these change with age. Conversely, mechanisms that determine cellular repair and cell turnover may directly influence the rate of aging. Amongst others, these may include (epi-) genetic factors that determine cellular responses to stressors. So far, evidence for a direct link between cellular stress responses and the rate of aging has come only from model organisms. Between species, fibroblasts from longer living animals (i.e. different genetic background) have a higher resistance to stress *in vitro* (8;9), and within species, fibroblasts from various mutant, long-lived mice were found to be more stress-resistant than their wild-type counterparts (10). Conversely, mutant mice having an enhanced p53 response, associated with excessive induction of apoptosis and senescence, were shown to have a higher cancer resistance but a shortened longevity (11).

In humans, *in vitro* cellular stress responses have not been related to longevity so far. To study how cellular responses to stress may change during aging, we compared stress-induced increases in markers of senescence and apoptosis in fibroblast strains derived from

young and very old subjects. We also studied fibroblast strains from offspring of nonagenarian siblings and their partners with a similar chronological age but who represent the average of the general population. We hypothesized that fibroblasts from old subjects would be more prone to go into senescence and into apoptosis when compared with fibroblasts from young subjects and that fibroblasts from subjects with the propensity for longevity (i.e. biologically younger) would show more resistance to go into senescence and apoptosis compared with fibroblasts of their partners.

Materials and Methods

Study design

The Leiden 85-Plus Study (12) is a prospective population-based study in which all inhabitants aged 85 year or older of the city of Leiden, the Netherlands, were invited to take part. Between September 1997 and September 1999, 599 out of 705 eligible subjects (85%) were enrolled. All participants were followed for mortality and 275 subjects survived to the age of 90 years. During the period December 2003 up to May 2004, a biobank was established from fibroblasts cultivated from skin biopsies from 68 of the 275 surviving 90-year-old participants. During the period August to November 2006, we also established a biobank from biopsies taken from 27 young subjects (23-29 years old). Given the extreme age difference of almost 65 years between the groups of old and young subjects, a relatively small sample size of 10 subjects per age group was chosen, consisting of 5 fibroblast strains from the 42 nonagenarian females, 5 strains from the 26 nonagenarian males, 7 strains 24 young females and the 3 available strains of young males (Table 2).

The Leiden Longevity Study (13) was set up to investigate the contribution of genetic factors to healthy longevity by establishing a cohort enriched for familial longevity. From July 2002 to May 2006, 420 families were recruited consisting of 991 long-lived Caucasian siblings together with their 1705 of their offspring and 760 of the partners thereof. There were no selection criteria on health or demographic characteristics. Compared with their partners, the offspring were shown to have a 30% lower mortality rate and a lower prevalence of cardio-

metabolic diseases (13;14). During the period November 2006 and May 2008, a biobank was established from fibroblasts cultivated from skin biopsies from 150 offspring-partner pairs. Because it was expected that the difference in biological age between the offspring and partner groups would be much smaller than the extreme difference in chronological age between the groups of old and young subjects, a relatively large sample size of 80 strains from 40 couples was chosen, consisting of 20 fibroblast strains from the 65 female offspring, 20 strains from the 86 male offspring, as well as 20 strains from the 86 female partners and 20 strains from the 63 male partners (Table 2).

Fibroblast Cultures

Three-mm (Leiden 85-plus Study) and 4-mm skin biopsies (LLS) were taken from the sun unexposed medial side of the upper arm. Fibroblasts were grown in D-MEM:F-12 (1:1) medium supplemented with 10% fetal calf serum (FCS), 1 mM MEM sodium pyruvate, 10 mM HEPES, 2 mM glutamax I, and antibiotics (100 Units/mL penicillin, 100 µg/mL streptomycin, and 0.25–2.5 µg/mL amphotericin B), all obtained from Gibco, Breda, the Netherlands. Different FCS batches were used for fibroblasts from the Leiden 85-plus Study (Gibco, batch no. 40G4932F) and for fibroblasts from the LLS (Bodinco, Alkmaar, the Netherlands, batch no. 162229). This medium will be referred to as standard medium. Fibroblasts were incubated at 37℃ with 5% CO_2 and 100% humidity. All cultures that are used in the present study were grown under predefined, highly standardized conditions as published earlier (15) and frozen at low passage.

Experimental setup

Experiments were set up in batches of maximally 10 fibroblast strains which were thawed from frozen stocks on day zero. On day one, the medium was changed and on day four fibroblasts were passaged 1:4 and passaged further in equal numbers on days six and eight to have similar confluences for experiments. On day 11, fibroblasts were seeded for experiments.

To induce stress we used rotenone and hyperglycemia. Rotenone is known to induce ROS at the mitochondrial level (16) and increased ROS can induce senescence (17). Hyperglycemia has also been shown to induce increased ROS at the cellular level (18) as well as premature

senescence in human skin fibroblasts (19). In pilot experiments, fibroblasts were stressed with 0.2 µM and 1 µM rotenone and with 111 mM glucose for three days and seven days. Senescence was measured by SA-β-gal activity and apoptosis by sub-G1 cell debris and by Annexin V/PI assay. Exposure to 1 µM rotenone induced apoptosis after three days and most fibroblasts had died after seven days. Exposure to 0.2 µM rotenone and 111 mM glucose did not induce appreciable apoptosis after three or seven days, but did induce senescence after seven days, more so than after three days. Based on these results, it was decided to measure apoptosis at three days and senescence at seven days after exposure to stress.

Stock solutions of rotenone were prepared in DMSO (both from Sigma, St Louis, MO, USA) at a concentration of 100 µM and stored at -40^{o}C in aliquots. Initial tests showed that DMSO (0.2%) did not affect the results. Hyperglycemic medium was prepared by adding 17 g/L D-glucose (Sigma, St Louis, MO, USA) to standard medium, resulting in a final concentration of 20 g/L (111 mM) glucose. For the seven-day time point, medium was replaced with freshly supplemented medium after three days.
Experiments were repeated for each fibroblast strain and each condition. The experimental conditions and measured parameters are summarized in Table 1.

Table 1. Experimental conditions and measured parameters.

	Stressor	
	3 days	7 days
Sub-G1 (%) Annexin V+/PI- cells (%) Annexin V+/PI+ cells (%)	1 µM rotenone	nd
FACS SA-β-gal activity (MdFI)	nd	0.2 µM rotenone 111 mM glucose
Colony Formation assay (# colonies & total area in mm^2)		

nd: not done.

Senescence

To determine cellular senescence we used the widely described marker SA-β-gal activity. Earlier we demonstrated the validity and superiority of the flow cytometric method over the cytochemical method measuring SA-β-gal activity in human fibroblasts (20). In short, fibroblasts were seeded at 130 cells/cm^2 in 75-cm^2 flasks and were prepared as described by Kurz *et al.* (21). To change the lysosomal pH to pH 6, fibroblasts were incubated with medium containing 100 nM bafilomycin A1 (VWR, Amsterdam, the Netherlands) for one hour and then incubated with 33 µM of the β-gal substrate C_{12}FDG (Invitrogen, Breda, The Netherlands) in the presence of 100 nM bafilomycin A1. After trypsinisation, fibroblasts were washed once and resuspended in 200 µl ice cold phosphate buffered saline (PBS) and measured in the FITC-channel. Analysis was performed on the median fluorescence intensity (MdFI) values.

Apoptosis/cell death

Fibroblasts were seeded at 1000 cells/cm^2 in 75-cm^2 flasks. Sample preparation was performed on ice. Aspirated medium and washes were collected to include any floating cells and cell debris indicating cell death in the analysis. Fibroblasts were trypsinized and washed with PBS. The suspension was divided over two tubes, one for Annexin V/propidium iodide (PI) analysis and one for cell cycle analysis.

For the flow cytometric Annexin V/PI analysis, the TACS Annexin V-FITC kit was used (R&D Systems, Abingdon, United Kingdom). Fibroblasts were processed according to the manufacturer's guidelines. Analysis was performed on a LSRII flow cytometer (Becton Dickinson, Franklin Lakes, USA). The Annexin V-FITC signal was measured in the FITC-channel and the PI signal in the PE-Texas Red channel. Events were gated into quadrants and Annexin V positive/PI negative (Annexin V+/PI-) and Annexin V positive/PI positive (Annexin V+/PI+) fibroblasts were analyzed as percentages of the total cell population.

For the flow cytometric cell cycle analysis, fibroblasts were centrifuged at 1000 rpm for 5 minutes, washed by resuspending in PBS, centrifuged again and resuspended in 200 µl 70% ethanol. Samples were kept at -40℃ at least overnight. After adding 1 mL PBS, fibroblasts were centrifuged at 2000 rpm for 5 minutes and resuspended in 200 µl PBS containing 50 µg/mL PI and 20 µg/mL RNAse (Sigma, St Louis, MO, USA). Fibroblasts were stored

overnight at 4℃ and measured in the PE-Texas Red channel. In the resulting histograms, Sub-G1 events (dead cells and cell debris) were gated and analyzed as percentages of the total cell population.

Colony formation assay

After having been exposed to the stressors for seven days and allowed to grow in standard medium for another week, medium was removed from the dishes, fibroblasts were washed with PBS and fixed with 0.25% gluteraldehyde for 30 minutes. Fibroblasts were washed with water and stained with 0.6 mg/ml Coomassie in 1:6 methanol/water overnight, washed again with water and air dried. Dishes were then scanned with a high resolution Agfa XY-15 flatbed scanner (Agfa Gevaert, Mortsel, Belgium) and colonies were manually scored with the freely available image analysis software package ImageJ 1.37v.

Statistics

All analyses were performed with the software package SPSS 14.00 (SPSS Inc., Chicago, IL). Differences in cellular characteristics between non-stressed and stressed fibroblast strains were compared by Student's *t*-test and were represented as mean±SD. Stress-induced increases were calculated by subtracting the values from non-stressed fibroblasts from those of stressed fibroblasts for each strain separately. Non-stressed levels and stress-induced increases were then compared between fibroblast strains from young and old subjects (Leiden 85-plus Study, SA-β-gal activity: n=20, apoptosis/cell death: n=20) and between fibroblast strains from offspring and partners (LLS, SA-β-gal activity: n=40, apoptosis/cell death: n=80). Stress-induced increases were represented as mean ±SE.

Since experiments were performed in batches of maximally ten fibroblast strains simultaneously, group differences were also compared using linear mixed-effect models (LMMs) to account for repeat experiments and batch effects. Cumulative frequency plots were made for flow cytometry results of SA-β-gal activity to inspect possible changes in distributions of MdFI values of SA-β-gal activity resulting from exposure to stress and from differences between young and old subjects, offspring and partners.

Results

Table 2 shows characteristics for the randomly selected subset of subjects from whom fibroblast strains were tested. Partners and offspring were of similar age, height and weight. As observed in the whole cohort, the prevalences of cardio-metabolic disease were lower in the offspring group as compared with the partners group (14), perhaps illustrating the lower rate of aging among the long-lived families.

Table 2. Comparison of clinical characteristics in young and old subjects from the Leiden 85-plus Study and in offspring and partners from the Leiden Longevity Study.

	Leiden 85-plus Study		Leiden Longevity Study	
	Young	Old	Offspring	Partners
Demographic data				
N (female)	10 (7)	10 (5)	40 (20)	40 (20)
Age (years, mean±SD)	25.5 (1.8)	90.2 (0.3)	58.2 (7.4)	57.1 (8.5)
Anthropometric data				
Height (cm, mean±SD)	177 (10)	164 (7)	171 (8)	173 (8)
Weight (kg, mean±SD)	69.9 (11.1)	67.5 (9.8)	77 (11)	78 (13)
Current smoking– no.	1/8	3/10	3/40	8/39
Diseases				
Myocardial infarction – no./total known	0/10	3/9	0/35 (0)	1/37
Stroke – no./total known	0/10	1/9	1/37 (2.9)	1/35
Hypertension – no./total known.	0/10	7/9	6/35 (17.1)	10/37
Diabetes mellitus – no./total known.	0/10	1/9	1/34 (2.9)	2/36
Malignancies – no./total known	0/10	0/9	1/33 (3.0)	1/35
Chronic obstructive pulmonary disease – no./total known	0/10	1/10	1/34 (2.9)	1/37
Rheumatoid arthritis – no./total known	0/10	0/10	0/72 (0)	0/72

Stress induced changes in markers of senescence, apoptosis/cell death and colony formation

There were significant increases in the distributions of MdFI values (i.e. SA-β-gal activity) in fibroblast strains from young and old subjects after seven days of exposure to stress (non-stressed: 272±90 [mean±SD] MdFI, 0.2 µM rotenone: 544±262 MdFI, 111 mM glucose: 375±261 MdFI, Figure 1A). Similar significant increases were observed in fibroblast strains from offspring and partners (non-stressed: 263±78 MdFI, 0.2 µM rotenone: 400±112 MdFI, 111 mM glucose: 323±94 MdFI, Figure 2A). For fibroblasts from young and old subjects and from offspring and partners, exposure to 1 µM rotenone for three days resulted in significant increases of sub-G1 cell debris (young/old, non-stressed: 14.8±6.4%, 1 µM rotenone 47.3±5.0%; offspring/partners, non-stressed: 18.9±5.6%, 1 µM rotenone: 44.8±6.5%), Annexin V+/PI- fibroblasts (young/old, non-stressed: 0.13±0.10%, 1 µM rotenone 7.33±2.7%; offspring/partners, non-stressed: 0.43±0.31%, 1 µM rotenone: 8.40±3.06%) and Annexin V+/PI+ fibroblasts (young/old, non-stressed: 0.19±0.13, 1 µM rotenone 2.77±0.88%; offspring/partners, non-stressed: 0.43±0.20 %, 1 µM rotenone: 1.99±0.85%).

There were significant decreases in colony number for fibroblast strains from young and old subjects after seven days of exposure to stress (non-stressed: 115±78, 0.2 µM rotenone: 80±56, mean±SD) and for fibroblast strains from offspring and partners (non-stressed: 164±44, 0.2 µM rotenone: 72±43, 111 mM glucose: 83±47 MdFI, mean±SD). All stress induced changes mentioned above were highly significant ($p<0.0001$) for all parameters measured and showed considerable interindividual variation.

Markers of senescence, apoptosis/cell death and colony formation dependent on differences in chronological and biological age

Under non-stressed conditions, fibroblast strains from old subjects showed significantly higher levels of SA-β-gal activity when compared with fibroblast strains of young subjects (Table 3, Figure 1B). Under non-stressed conditions, there were significantly lower levels of Sub-G1 cell debris for fibroblast strains from young subjects compared with strains from old subjects (Table 3). After exposure to 0.2 µM rotenone or 111 mM glucose, fibroblast strains from old subjects showed greater increases in SA-β-gal activity than fibroblast strains from young subjects (Table 3, Figure 1C and 1D). After exposure to 1 µM rotenone, there were

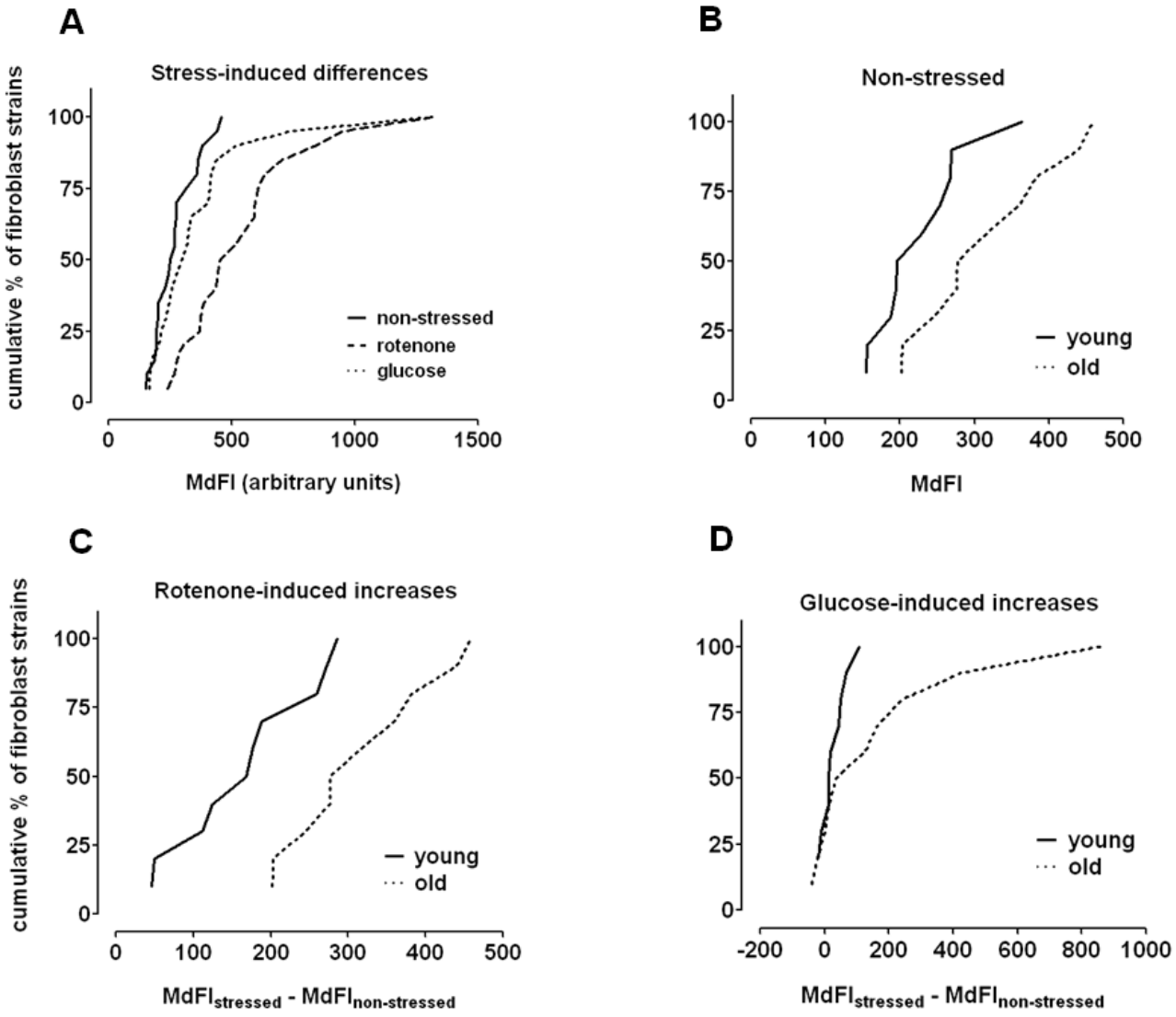

Figure 1 Cumulative frequency plots of SA-β-gal activity in fibroblast strains. A, activity in fibroblast strains under non-stressed conditions, treated with 0.2 μM rotenone and with 111 mM glucose for three days (young and old subjects from the Leiden 85-plus study combined, n=20). B, activity under non-stressed condition in strains from young (n=10) and old (n=10) subjects. C, rotenone-induced increases of activity (stressed minus non-stressed) in young and old subjects. D, hyperglycemia -induced increases of activity in young and old subjects. MdFI: median fluorescence intensity.

Table 3. Markers of senescence and apoptosis/cell death in fibroblast strains from young and old subjects (Leiden 85-plus Study) under non-stressed levels and stress-induced conditions.

	mean (SE)			
	Young (n=10)	Old (n=10)	Δ^a (SE)	P
Non-stressed				
7d				
SA-β-gal FACS (MdFI)	227 (21)	316 (21)	-89 (29)	**0.004**
3d				
Sub-G1 (%)	12.4 (1.4)	17.2 (1.5)	-4.8 (1.9)	**0.014**
Annexin V+ / PI- cells (%)	0.14 (0.04)	0.11 (0.04)	+0.03 (0.05)	0.57
Annexin V+ / PI+ cells (%)	0.14 (0.03)	0.23 (0.03)	-0.09 (0.04)	**0.040**
Stress-induced increase				
0.2 µM rotenone, 7d				
SA-β-gal FACS (MdFI)	+ 168 (36)	+ 377 (36)	-209 (51)	**<0.001**
111 mM glucose, 7d				
SA-β-gal FACS (MdFI)	+ 26 (47)	+ 180 (47)	-154 (67)	**0.027**
1 µM rotenone, 3d				
Sub-G1 (%)	+35.8 (2.6)	+29.2 (2.6)	+6.6 (2.6)	**0.018**
Annexin V+/PI- cells (%)	+7.32 (1.51)	+7.10 (1.51)	+0.22 (1.00)	0.83
Annexin V+/PI+ cells (%)	+2.78 (0.27)	+2.39 (0.27)	+0.39 (0.38)	0.30

Fibroblast strains from young subjects (mean±SD age: 25.5±1.8) were compared with fibroblast strains from very old subjects (mean±SD age: 90.3±2.1). Stress-induced increases: stressed minus non-stressed, MdFI: median fluorescence intensity, a: difference between young and old (young minus old).

significantly greater increases in levels of Sub-G1 cell debris for fibroblast strains from young subjects compared with fibroblast strains from old subjects (Table 3). Under non-stressed conditions, no differences in tested parameters were found between fibroblast strains from offspring and fibroblast strains from partners (Table 4, Figure 2B). After both rotenone- and hyperglycemia-treatment, fibroblast strains from offspring showed smaller increases in SA-β-gal activity than fibroblast strains from partners (Table 4, Figure 2C and 2D), being statistically significant for hyperglycemia-stressed fibroblasts. When stress-induced increases in apoptotic parameters were compared between offspring and partners, increases were

consistently greater in fibroblast strains from offspring (Table 4), being statistically significant for Annexin V+/PI- fibroblasts and Annexin V+/PI+ fibroblasts. Under non-stressed conditions, significantly more colonies were formed in fibroblast strains from young subjects compared with strains from old subjects (Table 5).

Table 4. Markers of senescence and apoptosis/cell death in fibroblast strains from offspring and their partners (Leiden Longevity Study) under non-stressed and stress-induced conditions.

		mean (SE)			
	n_{offspr}/ $n_{partner}$	Offspring	Partner	Δ^a (SE)	p
Non-stressed					
7d					
SA-β-gal FACS (MdFI)	20/20	269 (23)	266 (23)	3 (16)	0.85
3d					
Sub-G1 (%)	40/39	17.4 (0.8)	16.9 (0.8)	+ 0.5 (1.0)	0.64
Annexin V+/PI- cells (%)	40/40	0.43 (0.05)	0.41 (0.05)	+ 0.02 (0.07)	0.68
Annexin V+ PI+ cells (%)	40/40	0.42 (0.03)	0.43 (0.03)	+ 0.01 (0.03)	0.89
Stress-induced increase					
0.2 µM rotenone, 7d					
SA-β-gal FACS (MdFI)	20/20	+ 121 (19)	+ 156 (19)	- 35 (19)	0.064
111 mM glucose, 7d					
SA-β-gal FACS (MdFI)	20/20	+ 30 (13)	+ 88 (13)	- 55 (15)	**<0.001**
1 µM rotenone, 3d					
Sub-G1 (%)	40/39	+ 26.1 (1.2)	+ 23.8 (1.2)	+ 2.3 (1.3)	0.115
Annexin V+/PI- cells (%)	40/40	+ 8.69 (0.59)	+ 7.77 (0.59)	+ 0.92 (0.45)	**0.041**
Annexin V+/PI+ cells (%)	40/40	+ 1.83 (0.15)	+ 1.51 (0.15)	+ 0.32 (0.12)	**0.008**

Fibroblast strains from offspring (mean±SD age: 58.2±7.4years) were compared with fibroblast strains from partners (mean±SD age: 57.1±8.5 years). Stress-induced increases: stressed minus non-stressed, MdFI: median fluorescence intensity, a: difference between young and old (offspring minus partner).

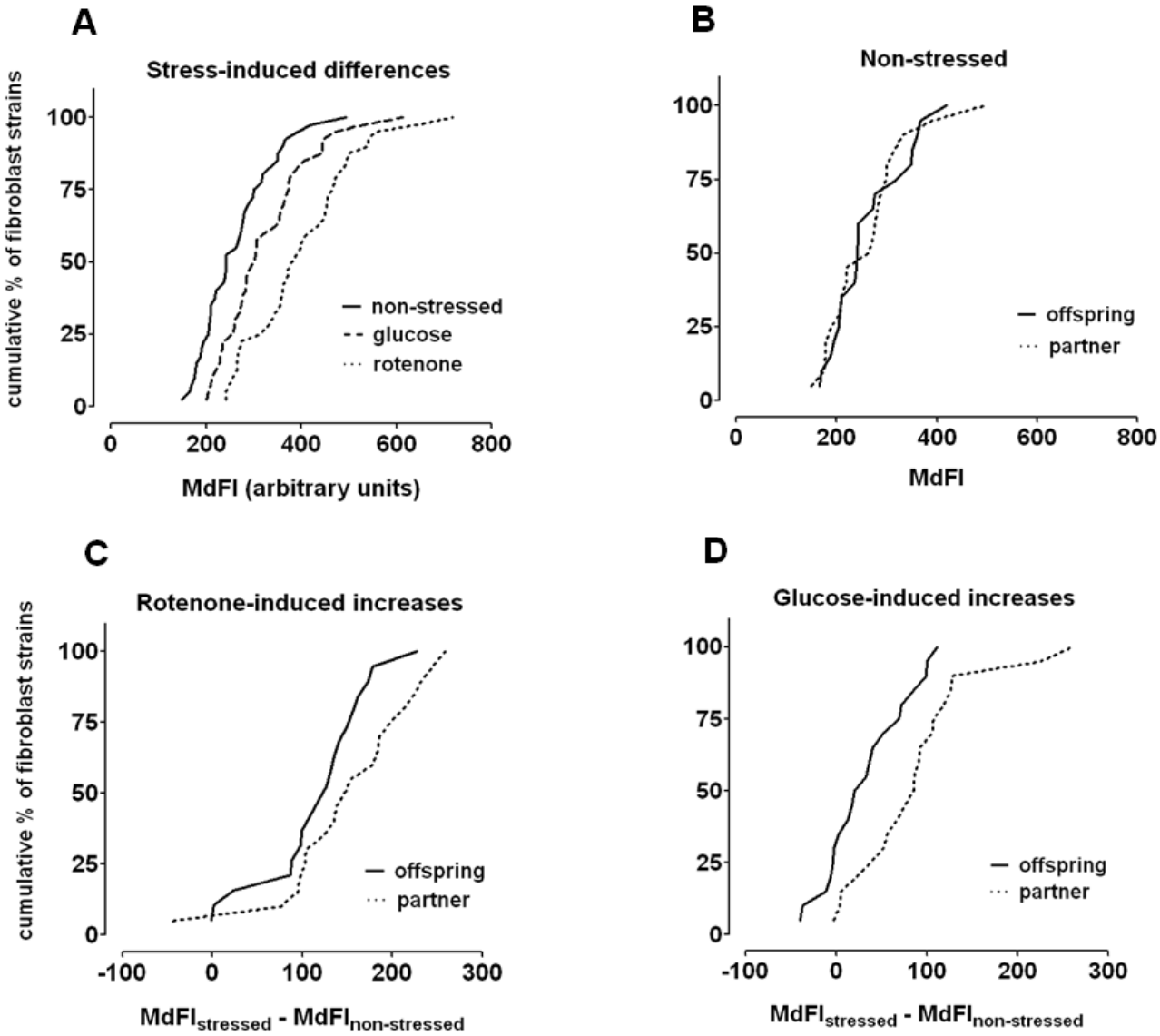

Figure 2. Cumulative frequency plots of SA-β-gal activity in fibroblast strains. A, activity in fibroblast strains under non-stressed conditions, treated with 0.2 μM rotenone and with 111 mM glucose for three days (offspring and partners from the Leiden Longevity Study combined, n=40). B, activity under non-stressed conditions in strains from offspring (n=20) and partners (n=20). C, rotenone-induced increases of activity (stressed minus non-stressed) in offspring and partners. D, hyperglycemia-induced increases of activity in offspring and partners. MdFI: median fluorescence intensity

Total colony size was also greater. After rotenone treatment, although not significant, a higher fraction of surviving colonies and a higher fraction of total colony size were observed for strains from young subjects compared with old subjects. Considering the contrast in biological age, the number and total size of colonies were significantly higher for fibroblast strains from offspring when compared with partners under non-stressed conditions (Table 5). After treatment with rotenone or hyperglycemia, significantly higher fractions of surviving colonies and bigger total colony sizes were observed in strains from offspring when compared with partners (Table 5).

Table 5. Differences in non-stressed levels and stress-induced decreases in growth potential observed with the colony formation assay dependent on differences in chronological (Leiden 85-plus Study) and biological age (Leiden Longevity Study).

	Leiden 85-plus Study			Leiden Longevity Study		
	Young (n=10)	Old (n=9)	p	Offspring (n=37)	Partner (n=37)	P
Number of colonies						
Non-stressed, 7d (# colonies/plate)	142 (16)	96 (16)	**0.017**	171 (7)	149 (7)	**0.001**
Surviving fraction (%)						
0.2 µM rotenone, 7d	66 (5)	56 (5)	0.12	44 (3)	37 (3)	**0.008**
111 mM glucose, 7d	nd	nd		50 (3)	45 (3)	0.056
Total colony size						
Non-stressed, 7d (Total colony size in mm^2/plate)	1535 (167)	918 (167)	**0.006**	1980 (95)	1734 (95)	**0.024**
Fraction remaining (%)						
0.2 µM rotenone, 7d	59 (5)	50 (5)	0.21	40 (2)	33 (2)	**0.004**
111 mM glucose, 7d	nd	nd		44 (3)	40 (3)	0.16

'Fraction remaining': total area of colonies per plate under stressed conditions divided by total area of colonies per plate under non-stresses conditions. nd: not done.

Discussion

In this study, we addressed the questions whether *in vitro* cellular responses to stress change with chronological age and whether *in vitro* cellular responses to stress depend on the propensity for longevity. To address these questions, we used fibroblast strains derived from young and old subjects, and from middle-aged offspring from nonagenarian siblings and their partners. Subjects of the last two groups were of similar chronological age and had equal distributions of men and women, thus any observed difference in cellular stress responses might be attributable to the biological age of the subjects, i.e. the propensity for longevity in the offspring.

The main findings of our studies are as follows. First, under non-stressed conditions, we observed that, compared with fibroblast strains obtained from the very old, fibroblast strains from young subjects show lower levels of senescence, as observed with SA-β-gal activity, higher growth potential, and also lower levels of cell debris. In line with our findings, it has been shown in primates that the proportion of senescent skin fibroblasts increases with age *in vivo*, supporting the biological relevance of cellular senescence for this cell type (22-25). Both findings are consistent with the notion that cellular senescence and apoptosis increase with chronological age and play an important role in age-related pathology (7;26;27).
Second, after induction of stress, either by rotenone or hyperglycemia, fibroblast strains from old subjects showed a higher increase in levels of senescence when compared with fibroblast strains from young subjects as observed with SA-β-gal activity and lower growth potential as measured with the colony formation assay. These results are in line with the findings of Ressler *et al*. who showed *in vivo* that with increasing age, an increasing number of human skin cells (dermal and epidermal) become positive for p16, a protein involved in the regulation of stress induced premature senescence (25).
Third, after stress, fibroblast strains from offspring of long-lived families showed lower increases in levels of senescence compared with fibroblasts from partners as observed with SA-β-gal activity and growth potential. Such a stress-resistant phenotype of fibroblasts has been reported for long-lived dwarf mice when compared with wild type mice (10), but, to the best of our knowledge, not for humans with different aging trajectories.

Rotenone was chosen as senescence-inducing agent because it acts on mitochondrial complex I, leading to increased levels of intracellular Reactive Oxygen Species (ROS) (16), which would mimic the physiological process of ROS induced damage that is hypothesized to underlie the aging process. When used in lower concentrations, we have found earlier that rotenone induces senescence as measured by colocalisation of increased p16 expression and increased SA-β-gal activity (20). As a positive control, we have also observed colocalisation of increased p16 expression coinciding with increased SA-β-gal activity in high passage fibroblasts (20), as was previously observed by Itahana *et al*. (28). Various cellular stressors have also been reported by others to induce SA-β-gal activity coinciding with increased p16 expression (29-35). In addition it was shown that p16 inhibition by means of antisense p16 resulted in delayed expression of SA-β-gal activity (36).
Glucose was chosen as an alternative stressor as it has been implicated to interfere in aging processes for a relatively long period of time. Many of the age-related disorders and diseases occur earlier in life in diabetics than in healthy people (37) and in various model organisms, glucose handling (insulin/IGF-signaling) has been shown to affect longevity (38). Furthermore, hyperglycemia has been shown to induce increased ROS at the cellular level (18) as well as premature senescence in human skin fibroblasts (19). Recently it was shown within the Leiden Longevity Study that the prevalence of diabetes was higher in partners compared with offspring (4.4% vs. 7.6%, p=0.004) and similar percentages are present in the randomly chosen set of subjects from whom fibroblast strains were tested (14).

Contrary to our hypothesis we found arguments for stress-induced apoptosis to be more present in fibroblast strains from fibroblast strains from offspring compared their partners. The fact that fibroblast strains from biologically younger subjects are more prone to go into apoptosis than to become senescent, could be advantageous to the organism to prevent damaged cells from becoming neoplastic. Although both apoptosis and senescence will prevent damaged cells from becoming neoplastic, apoptosis is thought to lead to greater loss of cells that would need to be replaced by new cells from a pool of mitotically active cells or stem cells. In aging organisms, stem cells loose the ability to replace cells lost by apoptosis, partially explaining age-related decline of cellularity in tissues (39). Though the number of fibroblasts in the dermis is markedly reduced during aging (40;41), skin fibroblasts from very

old subjects still show a high replicative capacity *in vitro* (15), making it unlikely that loss of cellularity in skin can be solely explained by exhaustion of replicative capacity. There is recent evidence that loss of cellularity in skin is more likely the result of the accumulation of senescent cells, which are capable to change the micro-environment. For instance, senescent cells have a secretory phenotype that promotes the invasiveness of premalignant epithelial cells (42).

An important strength of our study is the large number of fibroblast strains obtained from subjects of various chronological and biological ages, collected and stored in a highly standardized manner. Another strength is the fact that we studied stress-induced senescence rather than replicative senescence, since it has been shown that the maximum number of population doublings does not reflect human life history trajectories (43). This suggests that replicative senescence *in vitro* may be significantly influenced by cell culture conditions and that stress-induced senescence might better differentiate between cellular phenotypes. During the lifetime of an organism, its cells will be subjected to endogenous and exogenous chronic stressors, leading to aging of cells and consequently the organism. For these reasons we used fibroblasts at subconfluent levels and mimicked natural chronic stress by exposing fibroblasts to low concentrations of stressors up to one week.

In conclusion we report stress-induced responses of human cells *in vitro* reflect the propensity for human longevity of the subjects from whom these were derived.

References

(1) Harman D. Aging: a theory based on free radical and radiation chemistry. J Gerontol 1956;11(3):298-300.

(2) Yoon SO, Yun CH, Chung AS. Dose effect of oxidative stress on signal transduction in aging. Mech Ageing Dev 2002;123(12):1597-1604.

(3) Campisi J. Cancer and ageing: rival demons? Nat Rev Cancer 2003;3(5):339-349.

(4) van Heemst D, den Reijer PM, Westendorp RG. Ageing or cancer: a review on the role of caretakers and gatekeepers. Eur J Cancer 2007;43(15):2144-2152.

(5) Ben Porath I, Weinberg RA. When cells get stressed: an integrative view of cellular senescence. J Clin Invest 2004;113(1):8-13.

(6) Dierick JF, Eliaers F, Remacle J, Raes M, Fey SJ, Larsen PM *et al*. Stress-induced premature senescence and replicative senescence are different phenotypes, proteomic evidence. Biochem Pharmacol 2002;64(5-6):1011-1017.

(7) Warner HR, Hodes RJ, Pocinki K. What does cell death have to do with aging? J Am Geriatr Soc 1997;45(9):1140-1146.

(8) Harper JM, Salmon AB, Leiser SF, Galecki AT, Miller RA. Skin-derived fibroblasts from long-lived species are resistant to some, but not all, lethal stresses and to the mitochondrial inhibitor rotenone. Aging Cell 2007;6(1):1-13.

(9) Kapahi P, Boulton ME, Kirkwood TBL. Positive correlation between mammalian life span and cellular resistance to stress. Free Radical Biol Med 1999;26(5-6):495-500.

(10) Salmon AB, Murakami S, Bartke A, Kopchick J, Yasumura K, Miller RA. Fibroblast cell lines from young adult mice of long-lived mutant strains are resistant to multiple forms of stress. Am J Physiol Endocrinol Metab 2005;289(1):E23-E29.

(11) Donehower LA. p53: guardian AND suppressor of longevity? Exp Gerontol 2005;40(1-2):7-9.

(12) Bootsma-van der Wiel A, Gussekloo J, de Craen AJM, van Exel E, Bloem BR, Westendorp RGJ. Common chronic diseases and general impairments as determinants of walking disability in the oldest-old population. J Am Geriatr Soc 2002;50(8):1405-1410.

(13) Schoenmaker M, de Craen AJ, de Meijer PH, Beekman M, Blauw GJ, Slagboom PE *et al*. Evidence of genetic enrichment for exceptional survival using a family approach: the Leiden Longevity Study. Eur J Hum Genet 2006;14(1):79-84.

(14) Westendorp RG, van Heemst D, Rozing MP, Frolich M, Mooijaart SP, Blauw GJ *et al*. Nonagenarian siblings and their offspring display lower risk of mortality and morbidity than sporadic nonagenarians: The Leiden Longevity Study. J Am Geriatr Soc 2009;57(957):1634-1637.

(15) Maier AB, le Cessie S, Koning-Treurniet C, Blom J, Westendorp RG, van Heemst D. Persistence of high-replicative capacity in cultured fibroblasts from nonagenarians. Aging Cell 2007;6(1):27-33.

(16) Li N, Ragheb K, Lawler G, Sturgis J, Rajwa B, Melendez JA *et al*. Mitochondrial complex I inhibitor rotenone induces apoptosis through enhancing mitochondrial reactive oxygen species production. J Biol Chem 2003;278(10):8516-8525.

(17) Stockl P, Zankl C, Hutter E, Unterluggauer H, Laun P, Heeren G *et al*. Partial uncoupling of oxidative phosphorylation induces premature senescence in human fibroblasts and yeast mother cells. Free Radic Biol Med 2007;43(6):947-958.

(18) Chintapalli J, Yang S, Opawumi D, Goyal SR, Shamsuddin N, Malhotra A *et al*. Inhibition of wild-type p66ShcA in mesangial cells prevents glycooxidant-dependent FOXO3a regulation and promotes the survival phenotype. Am J Physiol Renal Physiol 2007;292(2):F523-F530.

(19) Blazer S, Khankin E, Segev Y, Ofir R, Yalon-Hacohen M, Kra-Oz Z *et al*. High glucose-induced replicative senescence: point of no return and effect of telomerase. Biochem Biophys Res Commun 2002;296(1):93-101.

(20) Noppe G, Dekker P, Koning-Treurniet C, Blom J, van Heemst D, Dirks RJ *et al*. Rapid flow cytometric method for measuring Senescence Associated â-galactosidase activity in human fibroblasts. Cytometry A 2009;75(11):910-916.

(21) Kurz DJ, Decary S, Hong Y, Erusalimsky JD. Senescence-associated beta-galactosidase reflects an increase in lysosomal mass during replicative ageing of human endothelial cells. J Cell Sci 2000;113(20):3613-3622.

(22) Dimri GP, Lee XH, Basile G, Acosta M, Scott C, Roskelley C *et al*. A Biomarker That Identifies Senescent Human-Cells in Culture and in Aging Skin In-Vivo. P Natl Acad Sci USA 1995;92(20):9363-9367.

(23) Herbig U, Ferreira M, Condel L, Carey D, Sedivy JM. Cellular senescence in aging primates. Science 2006;311(5765):1257.

(24) Jeyapalan JC, Ferreira M, Sedivy JA, Herbig U. Accumulation of senescent cells in mitotic tissue of aging primates. Mech Ageing Dev 2007;128(1):36-44.

(25) Ressler S, Bartkova J, Niederegger H, Bartek J, Scharffetter-Kochanek K, Jansen-Durr P *et al*. p16INK4A is a robust in vivo biomarker of cellular aging in human skin. Aging Cell 2006;5(5):379-389.

(26) Rubin H. The disparity between human cell senescence in vitro and lifelong replication in vivo. Nat Biotechnol 2002;20(7):675-681.

(27) Vicencio JM, Galluzzi L, Tajeddine N, Ortiz C, Criollo A, Tasdemir E *et al*. Senescence, apoptosis or autophagy? When a damaged cell must decide its path--a mini-review. Gerontology 2008;54(2):92-99.

(28) Itahana K, Zou Y, Itahana Y, Martinez JL, Beausejour C, Jacobs JJ *et al*. Control of the replicative life span of human fibroblasts by p16 and the polycomb protein Bmi-1. Mol Cell Biol 2003;23(1):389-401.

(29) Benanti JA, Galloway DA. Normal human fibroblasts are resistant to RAS-induced senescence. Mol Cell Biol 2004;24(7):2842-2852.

(30) Coates SS, Lehnert BE, Sharma S, Kindell SM, Gary RK. Beryllium induces premature senescence in human fibroblasts. J Pharmacol Exp Ther 2007;322(1):70-79.

(31) de Magalhaes JP, Chainiaux F, Remacle J, Toussaint O. Stress-induced premature senescence in BJ and hTERT-BJ1 human foreskin fibroblasts. FEBS Lett 2002;523(1-3):157-162.

(32) Killilea DW, Ames BN. Magnesium deficiency accelerates cellular senescence in cultured human fibroblasts. P Natl Acad Sci USA 2008;105(15):5768-5773.

(33) Kim KS, Seu YB, Baek SH, Kim MJ, Kim KJ, Kim JH *et al*. Induction of cellular senescence by insulin-like growth factor binding protein-5 through a p53-dependent mechanism. Mol Biol Cell 2007;18(11):4543-4552.

(34) Nyunoya T, Monick MM, Klingelhutz A, Yarovinsky TO, Cagley JR, Hunninghake GW. Cigarette smoke induces cellular senescence. Am J Respir Cell Mol Biol 2006;35(6):681-688.

(35) Xu D, Finkel T. A role for mitochondria as potential regulators of cellular life span. Biochem Biophys Res Commun 2002;294(2):245-248.

(36) Duan J, Zhang Z, Tong T. Senescence delay of human diploid fibroblast induced by anti-sense p16INK4a expression. J Biol Chem 2001;276(51):48325-48331.

(37) Cerami A. Hypothesis - Glucose As A Mediator of Aging. J Am Geriatr Soc 1985;33(9):626-634.

(38) Piper MD, Selman C, McElwee JJ, Partridge L. Separating cause from effect: how does insulin/IGF signalling control lifespan in worms, flies and mice? J Intern Med 2008;263(2):179-191.

(39) Roobrouck VD, Ulloa-Montoya F, Verfaillie CM. Self-renewal and differentiation capacity of young and aged stem cells. Exp Cell Res 2008;314(9):1937-1944.

(40) Francis MK, Appel S, Meyer C, Balin SJ, Balin AK, Cristofalo VJ. Loss of EPC-1/PEDF expression during skin aging in vivo. J Invest Dermatol 2004;122(5):1096-1105.

(41) Phillips DI, Barker DJ, Fall CH, Seckl JR, Whorwood CB, Wood PJ *et al*. Elevated plasma cortisol concentrations: a link between low birth weight and the insulin resistance syndrome? J Clin Endocrinol Metab 1998;1998(3):757-760.

(42) Coppe JP, Patil CK, Rodier F, Sun Y, Munoz DP, Goldstein J *et al*. Senescence-associated secretory phenotypes reveal cell-nonautonomous functions of oncogenic RAS and the p53 tumor suppressor. PLoS Biol 2008;6(12):2853-2868.

(43) Maier AB, Westendorp RG. Relation between replicative senescence of human fibroblasts and life history characteristics. Ageing Res Rev 2009;8(3):237-243.

Chapter 4

Relation between maximum replicative capacity and oxidative stress-induced responses in human skin fibroblasts *in vitro*

Pim Dekker, Mark de Lange, Roeland W. Dirks, Diana van Heemst, Hans J. Tanke, Rudi G.J. Westendorp, Andrea B. Maier

J Gerontol A Biol Sci Med Sci 2010; 66(1), 45-50

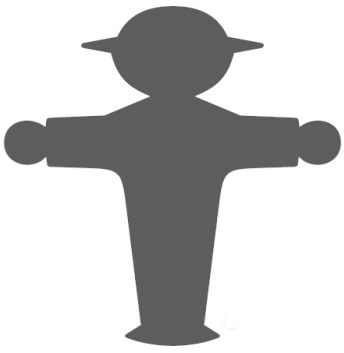

Summary

Cellular senescence, an important factor in aging phenotypes, can be induced by replicative exhaustion or by stress. We investigated the relation between maximum replicative capacity, telomere length, stress-induced cellular senescence and apoptosis/cell death in human primary fibroblast strains obtained from nonagenarians of the Leiden 85-plus Study. Fibroblast strains were cultured until replicative senescence and stressed with rotenone at low passage. Telomere length, Senescence Associated-β-galactosidase (SA-β-gal) activity, Sub-G1 content and Annexin-V/PI positivity were measured in non-stressed and stressed conditions. Fibroblast strains with a higher replicative capacity had longer telomeres ($p=0.054$). In non-stressed conditions replicative capacity was not associated with β-gal activity ($p=0.07$) and negatively with Sub-G1 ($p=0.008$). In rotenone-stressed conditions replicative capacity was negatively associated with β-gal activity ($p=0.034$) and positively with Sub-G1 ($p=0.07$). Summarizing, fibroblast strains with a higher maximum replicative capacity have longer telomeres, are less prone to go into stress-induced cellular senescence and more prone to die after stress.

Introduction

Cellular senescence and apoptosis are suggested to be important drivers of aging phenotypes and age related diseases such as diabetes mellitus and coronary heart disease (1). Cellular senescence is characterized by an irreversible state of replication arrest and can be induced by two factors. Firstly, after a finite number of cell population doublings (PDs) cells will cease to divide, a phenomenon also known as the Hayflick limit or Replicative Senescence (RS) (2). Current knowledge indicates that this form of senescence is mostly telomere driven, which means that with every cell division the telomere length shortens until it reaches a critical length after which the cell stops dividing (3). Secondly, cells can become senescent by exposure to stress which is called Stress-Induced-Premature-Senescence (SIPS) (4). Reactive oxygen species (ROS) seem to play a major role in this process because they cause damage to DNA and proteins, resulting in an accelerated accumulation of mutations which eventually causes early senescence (5).

Although cellular senescence can be induced by replicative exhaustion and by stress, the relation between RS and SIPS has remained largely unknown. It has been shown that fibroblasts aged *in vitro*, i.e. having undergone PDs *in vitro*, are more prone to go into stress-induced cellular senescence than fibroblasts that have undergone less PDs (6). If this is indeed the case, fibroblast strains from subjects of the same chronological age but with different maximum replicative capacities may have undergone different numbers of PDs during *in vivo* life history, affecting the response to stress-induced cellular senescence *in vitro*. Factors determining a long-term cell fate decision, undergoing senescence or apoptosis, are not yet fully understood, but there seems to be a clear dependence on cell type and the nature and extent of the damage (7). The transcriptional regulator p53 plays an important role in both senescence and apoptosis and in the interaction between these processes. DNA-damage is one of the important stimuli activating p53, which subsequently regulates the expression and activity of the cell cycle inhibitors p21 (8) and later p16 (9). If the DNA-damage is reversible, p53 activity will decrease after quick repair. However, when repair is slow and/or incomplete, p53 activity is sustained and p16 will also be induced in most cells, which will enter the senescence state. Indeed, earlier we showed that most

stress-induced Senescence Associated β-galactosidase (SA-β-gal) positive fibroblasts are also p16-positive, but not exclusively so (10). Furthermore, p53 plays a major role in replicative senescence induced by telomere erosion (11;12). When telomeres reach a critical length they will resemble broken DNA-strands which cells will recognize as DNA-damage and will respond accordingly, in a p16-independent fashion (8).

In order to investigate if there is a relation between RS and SIPS, we tested fibroblast strains with a range of maximum replicative capacities in non-stressed conditions and on their ability to react to oxidative stress. We are in the unique position to have access to a large number of fibroblasts strains which have been cultured to the end of their replicative potential, but which have also been stored frozen at low PDs. We hypothesize that fibroblast strains with a higher replicative capacity will have longer telomeres. Furthermore, if telomere shortening also plays an important role in SIPS, fibroblast strains with a higher replicative capacity will be more resistant to oxidative stress-induced cellular senescence and apoptosis/cell death at low PDs.

Materials and methods

Study design

The Leiden 85-Plus Study (13) is a prospective population-based study in which all inhabitants aged 85 year or older of the city of Leiden, the Netherlands, were invited to take part. Between September 1997 and September 1999, 599 out of 705 eligible subjects (85%) were enrolled. All participants were followed for mortality and 275 subjects survived to the age of 90 years. During the period December 2003 up to May 2004, a biobank was established from fibroblasts cultivated from skin biopsies from 68 of the 275 surviving 90-year-old participants.

Cell strains and maximum replicative capacity

Fibroblast strains were isolated from biopsies of the upper medial arm obtained from 68 participants of the Leiden 85-plus Study at the age of 90 years (14). All fibroblast strains were cultured under highly standardized conditions and serially passaged until the onset of replicative cellular senescence. Maximum replicative capacity was defined as maximum PDs and differed significantly between individual strains (14). Thirty strains with maximum replicative capacity, ranging from 51 to 108 PDs, were randomly selected. One strain with the highest maximum replicative capacity was found to yield results that were not in line with the results for the other strains. Since the highest maximum replicative capacity differed 3.5xSD of the mean of the other strains, this strain was considered to be an outlier and was not included in further analyses.

The relation between known maximum replicative capacity and markers of cellular senescence and apoptosis/cell death was determined at low passage, on average at PD 21±3 (±SD, range 17-30). Since the fibroblast strains entered phase IIb at PD 52 on average, ranging from PD 26 to 79, these strains were in phase IIa when the experiments were carried out.

Culture conditions

All fibroblasts cultures were grown in D-MEM:F-12 (1:1) medium supplemented with 10% fetal calf serum (FCS) (batch no. 40G4932F), 1 mM MEM sodium pyruvate, 10 mM HEPES, 2 mM glutamax I, antibiotics (100 Units/mL penicillin, 100 µg/mL streptomycin, and 0.25–2.5 µg/mL amphotericin B, all obtained from Gibco, Breda, the Netherlands) incubated at 37℃ with 5% CO_2 and 100% humidity. Trypsin (Sigma, St Louis, MO, USA) was used to split cells using a 1:4 ratio each time they reached 80-100% confluence.

Experimental set-up

To test the inducibility of SIPS, cells were thawed from frozen stocks on day zero. On day one, the medium was changed and on day four cells were passaged from 25-cm^2 flasks to 75-cm^2 flasks. Cells were passaged further on days six and eight. To have similar confluences for experiments, cells were counted on day 8 and subcultured in equal numbers.

On day 11, fibroblasts were seeded for the experiment, a remaining part was kept in culture for repeat experiments.

Fibroblasts were stressed using 600 µM rotenone (Sigma, St Louis, MO, USA) for three days. Rotenone is known to induce ROS at the mitochondrial level (15) and increased ROS induce cellular senescence (16). Rotenone-induced increased levels of ROS were confirmed for the experiments described here (data not shown). Because rotenone is light-sensitive, experiments were performed in darkness as much as possible. Samples were prepared three days after exposure to a stressor (day 14). Stock solutions of rotenone were prepared in DMSO at a concentration of 500 µM and stored at -40℃ (aliquots). Initial tests showed that DMSO (0.2%) did not affect the results. Experiments were repeated for each cell strain and each condition and were performed in batches of maximally four strains simultaneously.

Telomere length analysis

Telomere length was measured for 19 of 30 randomly chosen fibroblast strains in non-stressed conditions. To measure telomere length, a flow-FISH kit was used (DAKO, Heverlee, Belgium) and fibroblasts were treated according to the manufacturer protocol. In short, fibroblasts were trypsinized, mixed with the reference cell line (line 1301, Banca Biologica e Cell Factory, Genoa, Italy), hybridized without and with Cy3-labeled PNA-probe. After labeling with propidium iodide for DNA-content, samples were measured on a FACS Calibur II flow cytometer (Becton Dickinson, Franklin Lakes, USA). The probe-signal was measured in the FITC-channel and the PI signal in the PE-Texas Red channel. Results were calculated according to the manufacturer's protocol.

Flow cytometric measurement of SA-β-gal activity

Cells were seeded at 1000 cells/cm^2 in 25-cm^2 flasks. Cells were prepared as described recently (10). In short, to change the lysosomal pH to pH 6, cells were incubated with medium containing 100 nM bafilomycin A1 (VWR, Amsterdam, the Netherlands) for one hour. Cells were then incubated with 33 µM of the β-galactosidase substrate C_{12}FDG (Invitrogen, Breda, The Netherlands), in the presence of 100 nM bafilomycin. After trypsinisation, cells were washed once and resuspended in 200 µl ice cold PBS. Cells were measured in the

FITC-channel and analysis was performed on the median fluorescence intensity (MdFI) values.

Flow cytometric Annexin V/PI analysis

Cells were seeded at 1000 cells/cm^2 in 75-cm^2 flasks. Sample preparation was performed on ice. Aspirated medium and washes were collected so that any floating cells and cell debris indicating cell death would be included in the analysis. Cells were trypsinized and washed with phosphate buffered saline (PBS). The suspension was divided over two tubes, one for Annexin V/PI analysis and one for cell cycle analysis. For the Annexin V/propidium iodide (PI) analysis, the TACS Annexin V-FITC kit was used (R&D Systems, Abingdon, United Kingdom). Cells were processed according to the manufacturer's guidelines. Analysis was performed on a FACS Calibur II flow cytometer (Becton Dickinson). The Annexin V-FITC signal was measured in the FITC-channel and the PI signal in the PE-Texas Red channel. Cells were gated into quadrants and Annexin V positive/PI negative (Annexin V+/PI-) and Annexin V positive/PI positive (Annexin V+/PI+) fibroblasts were analyzed as percentages of the total cell population.

Flow cytometric cell cycle analysis

After trypsinisation, fibroblasts were centrifuged at 1000 rpm for five minutes, washed by resuspending in PBS, centrifuged again and resuspended in 200 µl 70% ethanol. Samples were kept at -40°C at least overnight. After adding 1 mL PBS, fibroblasts were centrifuged at 2000 rpm for 5 minutes and resuspended in 200 µl PBS containing 50 µg/mL PI and 20 µg/mL RNAse (Sigma, St Louis, MO, USA). Fibroblasts were stored overnight at 4°C and measured in the PE-Texas Red channel. In the resulting histograms, Sub-G1 events (dead cells and cell debris) were gated and analyzed as percentages of the total cell population.

Statistics

All analyses were performed with the software package SPSS 16.0.01 (SPSS Inc., Chicago, IL). Fibroblast strains were tested in batches of maximally four strains simultaneously. No intra-experiment replicates were used but experiments were repeated for each strain (in the same batches) one passage later. Values were acquired for non-stressed conditions and for

rotenone-treated conditions of each strain and parameter. The former was then subtracted from the latter to acquire rotenone-induced increases. For parameters of telomere length, cellular senescence and cell death/apoptosis, linear regression analysis was performed between values for the non-stressed condition and maximum replicative capacity and between rotenone-induced increases and maximum replicative capacity, using a linear mixed model taking into account the duplicate experiments as repeated measures and the batches of experiments as random effect. The different batches of strains were run in two rounds of multiple experiments. To be able to better compare the results of these two rounds, the data of the SA-β-gal assay were normalized by z-transforming the data within these rounds of experiments and use these values for the statistical analysis.

Results

Baseline characteristics of the subjects from whom the tested fibroblast strains were derived are summarized in Table 1. The mean maximum replicative capacity was 71±11 (mean±SD) PDs, ranging from 51 to 94. Table 2 shows the rotenone-induced increases in the measured parameters regardless of the maximum replicative capacity of the fibroblast strains. Telomere length was measured for fibroblast strains in non-stressed conditions. A positive relation was found between maximum replicative capacity and telomere length (p=0.054, Figure 1), which was borderline significant. For non-stressed fibroblasts no significant correlation was found between maximum replicative capacity and SA-β-gal activity (Table 3, Figure 2A), whereas rotenone-stressed fibroblasts showed a significant negative relation (Table 3, Figure 2B).

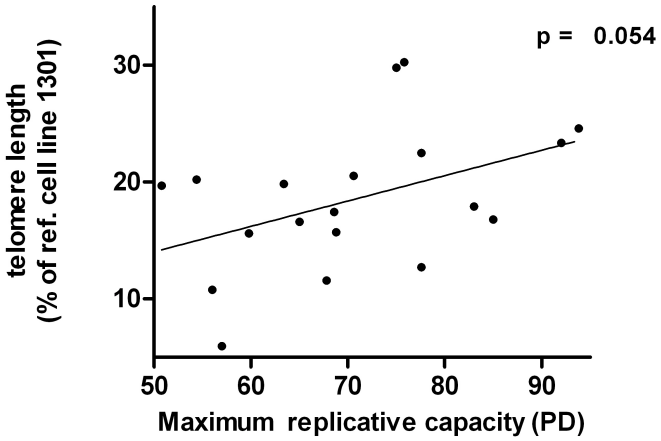

Figure 1. Correlation between maximum replicative capacity (PDs) of human fibroblasts and telomere length (% of telomere length of reference cell line 1301). P-value is result of linear mixed model.

Table 1. Clinical characteristics and fibroblast growth characteristics of subjects from the Leiden 85-plus Study (N=29).

	Leiden 85-plus Study
Demographic and anthropometric data	
N (female)	18
Age (years, mean ± SD)	90.0 (0.6)
Height (cm, mean ± SD)	162 (10)
Weight (kg, mean ± SD)	72.0 (11)
Current smokers – no./total known	2/29
Growth characteristics of fibroblast strains	
PD at which strains were tested (mean ± SD, range)	21 (3), 17-30
Onset phase IIb (PD, mean ± SD, range)*	52 (12), 26-79
Onset phase III, replicative capacity (PD, mean ± SD, range)†	71 (11), 51-94
Growth speed phase IIa (PD per day, mean ± SD, range)*	0.28 (0.04), 0.20-0.36
Growth speed phase IIb (PD per day, mean ± SD, range)*	0.09 (0.04), 0.03-0.19

* according to change-point model (14)

† number of observed PD during serial culturing

PD=population doubling

Table 2. Stress-induced increases in parameters measured in human fibroblasts (N=29 strains). Values are given as mean (SE).

Parameter	Non-treated	0.6 μM rotenone, 3 days	p
β-gal FACS, z-score of MdFI	-0.55 (0.83)	0.52 (0.79)	< 0.001
Sub-G1 (%)	5.4 (0.7)	22.7 (0.7)	< 0.001
Annexin V+/PI- cells, %	1.21 (0.38)	7.15 (0.38)	< 0.001
Annexin V+/PI+ cells, %	3.02 (0.46)	6.67 (0.46)	< 0.001

Data were analyzed with a linear mixed model, taking into account different batches of experiments and repeated measures (duplicate experiments). P-values are results of linear mixed models.

To determine the level of cell death, levels of Sub-G1 cell debris were measured. In non-stressed conditions there was a significant negative correlation between maximum replicative capacity and Sub-G1 content (Table 3, Figure 2C). In rotenone-stressed conditions a positive correlation was found, which was borderline significant (Table 3, Figure 2D). Apoptosis was assessed by the Annexin V/PI assay. Results were tested for correlations between maximum replicative capacity and percentage Annexin V+/PI- (early apoptotic) and Annexin V+/PI+ (late apoptotic or necrotic) fibroblasts. For both Annexin Annexin V+/PI-and Annexin V+/PI+ fibroblasts, no significant correlations were found under non-stressed conditions nor under rotenone-stressed conditions (Table 3).

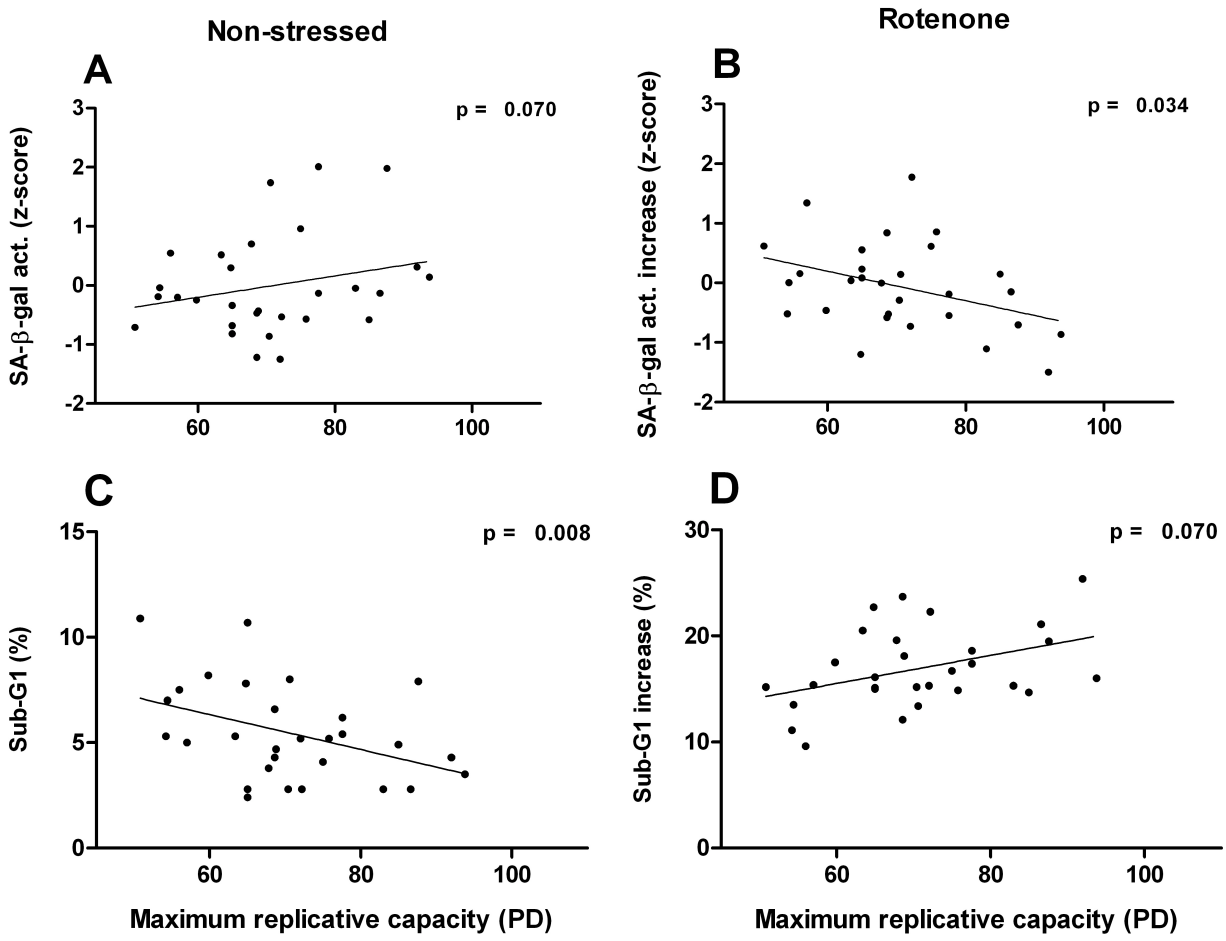

Figure 2. Correlation between maximum replicative capacity and markers of cellular senescence (SA- β-gal activity; A and B) and cell damage (sub-G1 cell debris; C and D) under non-stressed and rotenone-stressed conditions. Due to batch differences SA-β-gal values were z-tranformed.

Table 3. Relation between maximum replicative capacity, telomere length and markers of stress induced cellular senescence (SA-β-gal activity), cell damage (Sub-G1 cell debris) and apoptosis (AnnexinV/PI) under non-stressed and rotenone-stressed conditions in human fibroblasts (N=29 strains).

	Change/PD (SE)	p
Non-stressed		
Telomere length, % of ref. cell line 1301	0.193 (0.095)	0.054
SA-β-gal activity, z-score of MdFI	0.022 (0.011)	0.070
Sub-G1, %	-0.080 (0.029)	**0.008**
Annexin V+ / PI- cells, %	-0.003 (0.007)	0.69
Annexin V+ / PI+ cells, %	-0.005 (0.019)	0.81
600nM Rotenone, 3d		
SA-β-gal activity, z-score of MdFI	-0.024 (0.011)	**0.034**
Sub-G1, %	0.121 (0.066)	0.070
Annexin V+/PI- cells, %	0.044 (0.041)	0.29
Annexin V+/PI+ cells, %	-0.031 (0.031)	0.32

Data were analyzed with a linear mixed model, taking into account different batches of experiments and repeated measures (duplicate experiments). P-values are results of linear mixed models.

Discussion

The aim of this study was to investigate whether observed variations in maximum replicative capacities of fibroblast strains derived from the oldest old correlate with telomere length and inducibility of stress-induced parameters of cell death and cellular senescence *in vitro*. We found that fibroblast strains with a higher maximum replicative capacity have longer telomeres, are less prone to go into stress-induced cellular senescence and more prone to die after exposure to stress.

Telomere shortening and senescence

There is much variation in maximum replicative capacity of human fibroblast *in vitro* (14). This could be due to interindividual differences in number of PDs obtained during *in vivo* life history and/or differences in intrinsic replicative capacity and telomere length, which is supported by the observation that telomere length varies already considerable very early in life (17). Telomeres clearly play an important role in cellular senescence since *in vitro,* every cell lacking the enzyme telomerase can undergo a limited number of cell divisions before becoming senescent. Even so, murine cells *in vitro* senesce after a few PDs despite expressing telomerase (7). Hence it is questionable whether data that have been used for establishing the maximum replicative capacity of cells *in vitro* are a reliable reflection of the real maximum replicative capacity *in vivo*.

However, it has been described that telomere length is a good indicator for the maximum replicative capacity of fibroblasts (17). Indeed, we found that fibroblasts with a high maximum replicative capacity had long telomeres, although the correlation was borderline significant due to the small samples size tested. Thus, fibroblasts already having shorter telomeres (i.e. lower maximum replicative capacity) might enter the senescent state faster than fibroblasts with longer telomeres (i.e. higher maximum replicative capacity).

Oxidative stress accelerates the rate of telomere shortening, mainly because of insufficient repair mechanisms (18;19). We did not measure telomere length after induction of acute stress, but it is unlikely that after three days of stress telomeres would have shortened measurably within a cell, since shortening of telomeres is the result of cell division.

It has been shown that high passage fibroblasts *in vitro* (i.e. more PDs) show more stress-induced cellular senescence when compared with low passage fibroblasts of the same strain (6). It could be argued that a fibroblast strain with a higher maximum replicative capacitiy *in vitro*, underwent less PDs *in vivo* (and as such has longer telomeres), and would thus be less inclined to go into stress-induced cellular senescence at low passage *in vitro*. Our results seem to be consistent with the data of other workers (6) since we found a significant negative correlation between maximum replicative capacity and stress-induced cellular senescence as measured by SA-β-gal activity, suggesting that fibroblasts with a higher maximum replicative capacity would indeed be less prone to go into cellular senescence.

Since there is debate about the validity of SA-β-gal as a marker of cellular senescence, we earlier performed a proof-of-principle experiment to ascertain to what extent our SA-β-gal results are consistent with the more conventional marker of cellular senescence p16 (10). From this we concluded that the increase in SA-β-gal activity after rotenone treatment does indeed reflect senescence.

Apoptosis and senescence

Cell death, and more specifically apoptosis, is an important factor in tissue dysfunction during the aging process (7;20). Possibly, apoptosis contributes even more to this process than cellular senescence because dysfunctional cells are removed altogether. In healthy tissues these cells are replaced with new ones from a pool of proliferative cells to prevent tissue atrophy. It has already been described that, in contrast to cellular senescence, *in vitro* aged fibroblasts are increasingly resistant to oxidative stress-induced apoptosis (7;21). This would be consistent with the fact that we found a positive correlation between maximum replicative capacity and amounts of stress-induced sub-G1 cell debris. Furthermore, under non-stressed conditions there was a negative correlation between maximum replicative capacity and the amount of sub-G1 cell debris. This is especially striking since earlier we described that fibroblasts derived from chronologically young subjects, when compared with fibroblasts from chronologically old subjects, also show less sub-G1 cell debris under non-stressed conditions and more stress-induced sub-G1 cell debris (22). This would suggest that fibroblast strains with a high maximum replicative capacity but derived from old subjects are more comparable to fibroblasts strains from young subjects than from old subjects (with average maximum replicative capacity), i.e. are biologically younger. The sub-G1 results were not corroborated by the Annexin V/PI results, for which no significant relations were found. Possibly, we missed the early phase of the apoptotic response and were only able to measure the end result (sub-G1 cell debris).

Culture conditions

To determine stress resistance in fibroblasts, strains were selected on their maximum replicative capacity *in vitro* (14). Not much is known about the process of culturing itself but it is suggested to be an important stressor by which fibroblasts undergo cellular senescence

following the pathway of SIPS (23). An important factor in the process of culturing is the concentration of oxygen (pO_2) to which fibroblasts are exposed. The pO_2 in most tissues is much lower than the atmospheric pO_2 which is often used for cell culture. These hyperoxic conditions are a significant stress for cells. Murine fibroblasts go into senescence after only a few PDs at 20% oxygen but proliferate much longer at 5% oxygen (24). Although less dramatic, a similar effect can be observed for human fibroblasts, which grow considerably slower in 20% oxygen when compared with 5% oxygen (25). Additionally, the density at which fibroblasts are grown determines to what extent hyperoxic conditions affect growth speed (25). Furthermore, when fibroblasts are explanted from skin biopsies, they are removed from their normal environment in which they were exposed to lower pO_2, different levels and types of growth factors and many other factors (e.g. cytokines, metabolites).

Summarizing, fibroblast strains with a higher maximum replicative capacity seemed to have longer telomeres, are less prone to go into stress-induced cellular senescence and more sensitive to stress-induced stimuli, as measured by levels of sub-G1 cell debris. These results suggest that replicative cellular senescence and stress-induced premature cellular senescence share interacting cellular pathways, which should be determined within individual cell strains in further studies.

References

(1) Burton DGA. Cellular senescence, ageing and disease. Age 2009;31(1):1-9.

(2) Hayflick L, Moorhead PS. Serial Cultivation of Human Diploid Cell Strains. Exp Cell Res 1961;25(3):585-621.

(3) Rubin H. The disparity between human cell senescence in vitro and lifelong replication in vivo. Nat Biotechnol 2002;20(7):675-681.

(4) Toussaint O, Remacle J, Dierick JF, Pascal T, Frippiat C, Zdanov S *et al*. From the Hayflick mosaic to the mosaics of ageing. Role of stress-induced premature senescence in human ageing. Int J Biochem Cell Biol 2002;34(11):1415-1429.

(5) Kirkwood TB, Austad SN. Why do we age? Nature 2000;408(6809):233-238.

(6) Gurjala AN, Liu WR, Mogford JE, Procaccini PS, Mustoe TA. Age-dependent response of primary human dermal fibroblasts to oxidative stress: cell survival, pro-survival kinases, and entrance into cellular senescence. Wound Repair Regen 2005;13(6):565-575.

(7) Campisi J, d'Adda di Fagagna F. Cellular senescence: when bad things happen to good cells. Nat Rev Mol Cell Biol 2007;8(9):729-740.

(8) Herbig U, Jobling WA, Chen BP, Chen DJ, Sedivy JM. Telomere shortening triggers senescence of human cells through a pathway involving ATM, p53, and p21(CIP1), but not p16(INK4a). Mol Cell 2004;14(4):501-513.

(9) Stein GH, Drullinger LF, Soulard A, Dulic V. Differential roles for cyclin-dependent kinase inhibitors p21 and p16 in the mechanisms of senescence and differentiation in human fibroblasts. Mol Cell Biol 1999;19(3):2109-2117.

(10) Noppe G, Dekker P, Koning-Treurniet C, Blom J, van Heemst D, Dirks RJ *et al*. Rapid flow cytometric method for measuring Senescence Associated â-galactosidase activity in human fibroblasts. Cytometry A 2009;75(11):910-916.

(11) Chin L, Artandi SE, Shen Q, Tam A, Lee SL, Gottlieb GJ *et al*. p53 deficiency rescues the adverse effects of telomere loss and cooperates with telomere dysfunction to accelerate carcinogenesis. Cell 1999;97(4):527-538.

(12) Saretzki G, Walter T, Atkinson S, Passos JF, Bareth B, Keith WN *et al*. Downregulation of multiple stress defense mechanisms during differentiation of human embryonic stem cells. Stem Cells 2008;26(2):455-464.

(13) Bootsma-van der Wiel A, Gussekloo J, de Craen AJM, van Exel E, Bloem BR, Westendorp RGJ. Common chronic diseases and general impairments as determinants of walking disability in the oldest-old population. J Am Geriatr Soc 2002;50(8):1405-1410.

(14) Maier AB, le Cessie S, Koning-Treurniet C, Blom J, Westendorp RG, van Heemst D. Persistence of high-replicative capacity in cultured fibroblasts from nonagenarians. Aging Cell 2007;6(1):27-33.

(15) Li N, Ragheb K, Lawler G, Sturgis J, Rajwa B, Melendez JA *et al*. Mitochondrial complex I inhibitor rotenone induces apoptosis through enhancing mitochondrial reactive oxygen species production. J Biol Chem 2003;278(10):8516-8525.

(16) Stockl P, Zankl C, Hutter E, Unterluggauer H, Laun P, Heeren G *et al*. Partial uncoupling of oxidative phosphorylation induces premature senescence in human fibroblasts and yeast mother cells. Free Radic Biol Med 2007;43(6):947-958.

(17) Allsopp RC, Vaziri H, Patterson C, Goldstein S, Younglai EV, Futcher AB *et al*. Telomere length predicts replicative capacity of human fibroblasts. P Natl Acad Sci USA 1992;89(21):10114-10118.

(18) Passos JF, von Zglinicki T. Mitochondria, telomeres and cell senescence. Exp Gerontol 2005;40(6):466-472.

(19) von Zglinicki T. Oxidative stress shortens telomeres. Trends Biochem Sci 2002;27(7):339-344.

(20) Warner HR, Hodes RJ, Pocinki K. What does cell death have to do with aging? J Am Geriatr Soc 1997;45(9):1140-1146.

(21) Lee YH, Lee JC, Moon HJ, Jung JE, Sharma M, Park BH *et al*. Differential effect of oxidative stress on the apoptosis of early and late passage human diploid fibroblasts: implication of heat shock protein 60. Cell Biochem Funct 2008;26(4):502-508.

(22) Dekker P, Maier AB, van Heemst D, Koning-Treurniet C, Blom J, Dirks RW *et al*. Stress-induced responses of human skin fibroblasts *in vitro* reflect human longevity. Aging Cell 2009;8(5):595-603.

(23) Sherr CJ, DePinho RA. Cellular senescence: mitotic clock or culture shock? Cell 2000;102(4):407-410.

(24) Parrinello S, Samper E, Krtolica A, Goldstein J, Melov S, Campisi J. Oxygen sensitivity severely limits the replicative lifespan of murine fibroblasts. Nature Cell Biology 2003;5(8):741-747.

(25) Balin AK, Fisher AJ, Anzelone M, Leong I, Allen RG. Effects of establishing cell cultures and cell culture conditions on the proliferative life span of human fibroblasts isolated from different tissues and donors of different ages. Exp Cell Res 2002;274(2):275-287.

Chapter 5

Chronic inhibition of the respiratory chain in human fibroblast cultures: Differential responses related to subject chronological and biological age

Pim Dekker, Laurens M. van Baalen, Roeland W. Dirks, P. Slagboom , Diana van Heemst, Hans J. Tanke, Rudi G.J. Westendorp, Andrea B. Maier

J Gerontol A Biol Sci Med Sci 2011 Nov [Epub ahead of print]

Summary

Respiratory chain function becomes less efficient with age resulting in increased levels of damaging reactive oxygen species (ROS). We compared rotenone-exposed fibroblast strains from young and old subjects, and from offspring of nonagenarian siblings and the partners of the offspring. Rotenone increased ROS levels, inhibited growth rate and increased telomere shortening (all $p<0.05$). Non-stressed strains from young subjects showed lower ROS levels ($p=0.031$) and higher growth rates ($p=0.002$) than strains from old subjects. Stressed strains from young subjects showed smaller increases in ROS levels ($p=0.014$) and larger decreases in growth rate ($p<0.001$) than strains from old subjects. Telomere shortening rates were not different between groups. Stress-induced decreases in growth rate were larger in strains from offspring than from partners ($p=0.05$). Strains from young and old subjects are differentially affected by chronic inhibition of the respiratory chain. Changed growth rates in strains from offspring resemble those from strains from young subjects.

Introduction

Aging is determined by accumulation of molecular damage and a paucity of well functioning differentiated cells that lead to the loss of bodily functions and various age-related diseases (1). During the lifespan of an organism, damage to cellular components accumulates. Depending on the type of cell and adverse conditions, cells can repair the damage, arrest proliferation irreversibly (senescence), undergo programmed cell death (apoptosis) or die in an uncontrolled manner (necrosis). Senescent cells affect the integrity of tissues by altering their morphology and by excreting factors that promote tumour invasiveness (2). Furthermore, when cells are removed by apoptosis or necrosis, tissues are compromised if cells are not replaced by the proliferative pool of progenitor cells. A decreased proliferative capacity of progenitor cells is thought to be one of the hallmarks of *in vivo* aging (3).

There is much debate about the factors that determine if cells go into senescence. Telomere shortening has long been considered as a cellular clock (4). When telomeres are critically short, cells go into replicative senescence or, in case of loss of p53 function, die by necrosis after crisis (5). However, critically short telomeres are not a prerequisite for senescence since this state can also be induced by oxidative stress causing DNA-damage and changes in chromatin structure involving p53/Rb and p16/21 pathways. Furthermore, expression of certain oncogenes, mainly from the RAS pathways, can lead to senescence. Before cells undergo senescence, they show a decreased rate of proliferation. The fact that oxidative stress both accelerates telomere shortening (6) and can drive cells into senescence would imply that telomere length plays an important role in this stress-induced deceleration of proliferation. As early as 1956 Harman described that mitochondria become increasingly dysfunctional with age, leading to increased levels of reactive oxygen species (ROS) (7). It has been suggested that these increased ROS levels could accelerate telomere shortening (8). Conversely, it does not seem to be telomere length per se which determines the rate of proliferation, but rather the protective status of shortened telomeres (9) which inhibits proliferation.

Earlier we described that skin fibroblast strains derived from chronologically young subjects, when compared with fibroblast strains from very old subjects, are less prone to go into senescence and more prone to go into apoptosis, both under non-stressed and stressed conditions (10). These differences were mirrored by similar differences under stress-induced conditions between fibroblast strains derived from offspring of nonagenarian siblings within families enriched for longevity and their partners from the general population (11). Though of the same chronological age, these offspring were previously observed to be of a younger biological age than their partners as reflected by their beneficial glucose and lipid metabolism, preservation of insulin sensitivity and resistance to cellular stress (10;12;13). The fibroblast strains from these offspring resembled the responses of fibroblast strains from young subjects, i.e. were biologically younger. Here we study if chronic low-level inhibition of the respiratory chain induces increased rates of telomere shortening in human fibroblast strains and if this is related to growth rate, senescence and ROS levels. To allow telomere shortening, multiple population doublings are necessary and therefore we decided to culture fibroblasts for seven weeks rather than one week as described earlier (10). Our hypothesis is that chronic inhibition of the respiratory chain function by exposure to a low dose of rotenone, which decreases but does not arrest proliferation, leads to increased ROS levels, Senescence Associated-β-galactosidase (SA-β-gal) activity, decreased growth rates and concomitant acceleration of telomere shortening of fibroblasts depending on the chronological and biological age of the subject. For this study we compare the fibroblast strains from young versus old subjects and from offspring of nonagenarian siblings versus their partners.

Material and methods

Study designs

The Leiden 85-plus Study (14) is a prospective population-based study in which all inhabitants aged 85 years or older of the city of Leiden, the Netherlands, were invited to take part. Between September 1997 and September 1999, 599 out of 705 eligible subjects (85%) were enrolled. All participants were followed for mortality and 275 subjects survived to the

age of 90 years. During the period December 2003 up to May 2004, a biobank was established from fibroblasts cultivated from skin biopsies from 68 of the 275 surviving 90-year-old participants (15). During the period August to November 2006, we also established a biobank of fibroblast strains established from biopsies taken from 27 young subjects (23-29 years old).

The Leiden Longevity Study (LLS) (11) was set up to investigate the contribution of genetic factors to healthy longevity by establishing a cohort enriched for familial longevity. From July 2002 to May 2006, 421 families were recruited consisting of 944 long-lived Caucasian siblings together with their 1671 of their offspring and 744 of the partners thereof. There were no selection criteria on health or demographic characteristics. Compared with their partners, the offspring were shown to have a 30% lower mortality rate and a lower prevalence of cardio-metabolic diseases (11;12). During the period November 2006 and May 2008, a biobank was established from fibroblasts cultivated from skin biopsies from 150 offspring-partner couples.

Fibroblast Cultures

Three-mm (Leiden 85-plus Study) and 4-mm skin biopsies (LLS) were taken from the sun unexposed medial side of the upper arm. Fibroblasts were grown in D-MEM:F-12 (1:1) medium supplemented with 10% fetal calf serum (FCS), 1 mM MEM sodium pyruvate, 10 mM HEPES, 2 mM glutamax I, and antibiotics (100 Units/mL penicillin, 100 µg/mL streptomycin, and 0.25–2.5 µg/mL amphotericin B), all obtained from Gibco, Breda, the Netherlands. Different FCS batches were used for fibroblasts from the Leiden 85-plus Study (Gibco, batch no. 40G4932F) and for fibroblasts from the LLS (Bodinco, Alkmaar, the Netherlands, batch no. 162229). This medium will be referred to as standard medium. Fibroblasts were incubated at 37℃ with 5% CO2, under conditions of ambient oxygen and 100% humidity. All cultures that are used in the present study were grown under predefined, highly standardized conditions as published earlier (15). Trypsin (Sigma, St Louis, MO, USA) was used to split fibroblasts using a 1:4 ratio each time they reached 80-100% confluence to make sure that each strain had undergone the same number of population doublings.

Experimental set-up

Fibroblasts were thawed from frozen stocks on day zero. Passage 11 fibroblasts were used from young and old subjects and passage seven fibroblast strains from offspring and partners. On day four, seven and eleven fibroblasts were further passaged in order to multiply fibroblasts. On day 18 the experiments were started. Fibroblast strains were seeded at 2000 and 3300 cells/cm^2 in 25 cm^2 culture flasks for non-stressed and rotenone-stressed cultures respective-ly, in batches of eight strains per condition. To chronically stress fibroblast strains, medium was supplemented with rotenone (Sigma, St Louis, MO, USA), known to induce an increase in the intracellular production of ROS at the mitochondrial level (16). Since cell division was necessary for telomere shortening to occur, a low concentration of 20 nM was used in order to prevent complete arrest of proliferation. Because rotenone has a half-life of one to three days (17), medium was changed twice a week throughout a culture period of seven weeks. Fibroblast strains were counted every week and passaged at 2000 and 3300 cells/cm^2 again in new culture flasks. At day 49 fibroblast strains were seeded for assays measuring ROS levels, SA-β-gal activity and telomere length as described below.

Flow cytometric measurement of ROS

Levels of ROS were measured using the intracellular redox dye dihydrorhodamine 123 as described earlier (18). In short, fibroblasts were seeded at 2000 cells/cm^2 in 25-cm^2 flasks. After three days in culture fibroblasts were incubated in medium supplemented with 30 µM dihydrorhodamine 123 (Invitrogen, Breda, The Netherlands). One stock of dihydrorhodamine 123 was prepared and aliquotted before the experiments to prevent changes in fluorescence intensity due to probe oxidation, leading to results that are independent of ROS generation (19). To reduce quenching of the fluorescent probe, ambient light in the laboratory was reduced as much as possible. After incubation with dihydrorhodamine 123, fibroblasts were trypsinized, washed in ice-cold PBS, pelleted and resupended in 200 µl ice-cold PBS. Fibroblasts were kept on ice before measurement of median fluorescence intensity (MdFI) in the FITC-channel.

Flow cytometric measurement of SA-β-galactosidase activity

Fibroblasts were seeded at 2000 cells/cm^2 in 25-cm^2 flasks. Fibroblasts were prepared as described earlier (20). In short, to change the lysosomal pH to pH 6, fibroblasts were incubated with medium containing 100 nM bafilomycin A1 (VWR, Amsterdam, the Netherlands) for one hour. Fibroblasts were then incubated with 33 µM of the β-galactosidase substrate 5-dodecanoylaminofluorescein di-β-D-galactopyranoside (C12FDG, Invitrogen, Breda, The Netherlands), in the presence of 100 nM bafilomycin. After trypsinisation, fibroblasts were washed once and resuspended in 200 µl ice cold PBS. Fibroblasts were measured in the FITC-channel and analysis was performed on the MdFI values.

Telomere length analysis

To measure telomere length, a flow-FISH kit was used (DAKO, Heverlee, Belgium) and fibroblasts were treated according to the manufacturer protocol. In short, fibroblasts were trypsinised, mixed 1:1 with the reference cell line (line 1301, Banca Biologica e Cell Factory, Genoa, Italy), hybridised without and with Cy3-labeled PNA-probe. After labeling with propidium iodide (PI) for DNA-content, samples were measured on a LSRII flow cytometer (Becton Dickinson, Franklin Lakes, USA). The probe-signal was measured in the FITC-channel and the PI signal in the Cherry-Red channel. Results were calculated according to the manufacturer's protocol and telomere length was expressed as percentage of the reference cell line. To determine telomere shortening rates, telomere length was also measured at the beginning of the experiment at day 18. The shortening rate was calculated by dividing the difference in telomere length after seven weeks of culturing by the number of cumulative population doublings and was expressed as percentage per PD.

Statistics

All analyses were performed with the software package SPSS 16.0.01 (SPSS Inc., Chicago, IL). To study the effect of rotenone during seven weeks culturing, results were first analyzed regardless of young/old and offspring/partner comparisons. Since the FCS used for fibroblast strains from the 85-plus Study was a different batch than the batch used for the LLS, fibroblast strains from the former (young and old) were analyzed separately from the latter (offspring and partner). Differences in ROS levels, SA-β-gal activity, telomere length and

telomere shortening rate between groups (young/old, offspring/partner) in non-stressed conditions were analyzed using linear mixed models. In strains from the 85-plus Study, results were adjusted for gender only and in strains from the LLS for gender and age. The same analyses were applied to rotenone-stressed differences (non-stressed subtracted from rotenone-stressed) in these parameters.

Growth curves were produced by plotting cumulative population doublings against time. To analyze differences between groups, the slopes of the lines were compared by calculating the interaction terms time*young/old and time*offspring/partner in a linear mixed model, adjusting for gender in strains from the 85-plus Study and for gender and age in strains from the LLS.

Results

Baseline characteristics of subjects of different chronological and biological ages from whom fibroblast strains were established are shown in Table 1. Middle aged offspring from nonagenarian siblings and their partners were of similar age, height and weight.

Effect of chronic exposure to rotenone on ROS levels, SA-β-gal activity, growth rate and rate of telomere shortening

When compared with non-stressed fibroblast strains, levels of ROS and SA-β-gal activity were significantly increased in fibroblast strains stressed with rotenone for seven weeks (Table 2). Compared with non-stressed strains, growth rate was significantly decreased at all time points for rotenone-stressed fibroblast strains (Table 2, Figure 1A and B). For the strains from young and old subjects, telomere length decreased during seven weeks from 22.2±1.2% to 16.9±0.7% (±SEM) in non-stressed fibroblasts and from 22.2±1.2% to 17.1±0.6% in stressed fibroblasts. For the strains from offspring and partners telomere length decreased during seven weeks, from 23.7±1.3% to 18.8± 0.7% in non-stressed fibroblasts and from 23.7±1.3% to 19.2±0.6% in stressed fibroblasts. In all cases $p<0.001$ for the difference between 0 weeks and 7 weeks. Telomere length was not different between non-stressed fibroblast strains and rotenone-stressed fibroblasts after seven weeks of serial culturing.

However, since the rotenone-stressed fibroblast strains had undergone less population doublings (PDs), the rate of telomere shortening per PD was significantly higher in rotenone-stressed fibroblast strains (Table 2).

Table 1. Clinical characteristics of young and old subjects from the Leiden 85-plus Study representing a difference in chronological age and of offspring and partners from the Leiden Longevity Study who differ in biological age.

	Leiden 85-plus Study		Leiden Longevity Study	
	Young	Old	Offspring	Partners
	n=10	n=10	n=10	n=10
Demographic data				
Female	7	5	5	5
Age, years (mean±SD)	25.5 (1.8)	90.2 (0.3)	57.3 (7.6)	57.4 (8.7)
Anthropometric data				
Height, cm (mean±SD)	177 (10)	164 (7)	174 (12)	174 (7)
Weight, kg (mean±SD)	69.9 (11.1)	69.0 (9.3)	76.3 (19.2)	74.5 (13.5)
Current smoking - no./total known	1/8	1/10	2/10	1/10
Diseases				
Myocardial infarction, no.	0	1	0	0
Stroke, no.	0	1	0	1
Hypertension, no.	0	6	1	2
Diabetes mellitus, no.	0	1	0	3
Malignancies, no.	0	0	1	0
Chronic obstructive pulmonary disease, no.	0	1	0	1
Rheumatoid arthritis, no.	0	3	0	0

Table 2. Effect of chronic exposure to rotenone on levels of reactive oxygen species (ROS), Senescence Associated-β-galactosidase (SA-β-gal) activity, population doublings (PDs) and telomere length, measured after 7 weeks in human fibroblasts from the Leiden 85-plus Study and Leiden Longevity Study. Average rate of telomere shortening during 7 weeks was also calculated. Values are given as mean (SE).

	Leiden 85-plus Study			Leiden Longevity Study		
	Non-stressed n=20	Rotenone n=20	p	Non-stressed n=20	Rotenone n=20	p
ROS (MdFI)	1427 (109)	1571 (115)	<0.001	1380 (78)	1551 (88)	<0.001
SA-β-gal (MdFI)	4116 (398)	4743 (348)	<0.001	3964 (264)	4442 (284)	<0.001
PDs (no.)	16.13 (0.53)	10.85 (0.40)	<0.001	15.12 (0.48)	9.83 (0.39)	<0.001
Telomere length (% of ref. cell line)	16.9 (0.7)	17.1 (0.6)	0.82	18.8 (0.8)	19.2 (0.8)	0.67
Telomere shortening rate (%/PD)	-0.32 (0.07)	-0.49 (0.13)	0.002	-0.32 (0.08)	-0.43 (0.16)	0.042

MdFI: median fluorescence intensity. Data were analyzed with linear mixed models, adjusting for gender, batches of experiments, repeat measures and age (for offspring/partner comparison).

Differential effect of chronic exposure to rotenone on ROS levels, SA-β-gal activity, growth rate, telomere length and rate of telomere shortening dependent on chronological and biological age

Serial culturing under non-stressed conditions for seven weeks

ROS levels were significantly lower in fibroblast strains from young subjects compared with old subjects, but no differences were found in SA-β-gal activity. Fibroblast strains from young subjects showed a significantly higher growth rate when compared with fibroblast strains from oldest old subjects (Figure 1C). Telomere length was not different between strains from young and old subjects at 0 weeks (24.0±2.6% and 23.6±2.6% respectively, p=0.54) or at 7 weeks (17.0±0.9% and 17.3±0.9% respectively, p=0.86). Shortening rates were also not different between strains from young and old subjects (Table 3).

No statistically significant differences in ROS, SA-β-gal activity and growth rate were found between fibroblast strains from offspring and from their partners in non-stressed conditions, although ROS levels were consistently lower in fibroblast strains from offspring when compared with strains from partners (Table 3 and Figure 1D). Telomere length was not different between strains from offspring and partners at 0 weeks (25.2±2.5% and 25.1±2.5% respectively, p=0.93) or at seven weeks (19.2±0.8% and 18.7±0.8% respectively, p=0.61). Shortening rates were also not different between strains from offspring and partners (Table 3).

Chronic exposure to rotenone for seven weeks

Stress-induced ROS levels and SA-β-gal activity were lower in fibroblast strains from young subjects when compared with strains from old subjects. Stress-induced decreases (rotenone-stressed – non-stressed) in growth rate were larger for fibroblast strains from young subjects when compared with strains from old subjects (Figure 1E). No differences in telomere shortening rates were found between strains from young and old subjects after seven weeks culturing under stressed conditions (Table 3).

Differences in stress-induced ROS levels between fibroblast strains from offspring of nonagenarian siblings and partners were not statistically significant but were consistently lower in fibroblast strains from offspring. SA-β-gal activity was not different between fibroblast strains from offspring and strains from partners. When fibroblast strains from offspring and their partners were compared, stress-induced decreases in growth rate were larger for fibroblast strains from offspring when compared with strains from partners (Figure 1F). Telomere shortening rates showed no difference between fibroblast strains from offspring and strains from partners after seven weeks under stressed conditions.

Table 3. Effect of chronic exposure to rotenone on ROS levels (ROS), Senescence Associated-β-gal (SA-β-gal) activity and rate of telomere shortening measured in human fibroblasts from young and old subjects from the Leiden 85-plus Study, representing a difference in chronological age, and of offspring and partners from the Leiden Longevity Study who differ in biological age.

	Leiden 85-plus Study			Leiden Longevity Study		
	Young	Old		Offspring	Partner	
	n=10	n=10	p	n=10	n=10	p
ROS (MdFI)						
Non-stressed	1282 (108)	1573 (183)	**0.031**	1329 (87)	1431 (132)	0.39
Rotenone – Non-stressed	+81 (59)	+234 (35)	**0.014**	+146 (68)	+207 (65)	0.43
Bgal (MdFI)						
Non-stressed	3756 (319)	3814 (360)	0.47	4120 (423)	3790 (315)	0.67
Rotenone – Non-stressed	+472 (238)	+960 (238)	0.076	+598 (166)	+660 (120)	0.90
Telomere shortening rate (%/PD)						
Non-stressed	-0.43 (0.13)	-0.41 (0.13)	0.85	-0.39 (0.16)	-0.42 (0.16)	0.79
Rotenone	-0.68 (0.25)	-0.64 (0.25)	0.72	-0.60 (0.30)	-0.59 (0.30)	0.93

MdFI: median fluorescence intensity. Data were analyzed with linear mixed models, adjusting for gender, batches of experiments, repeat measures and age (for the offspring/partner comparison). Values in bold are statistically significant at $p<0.05$

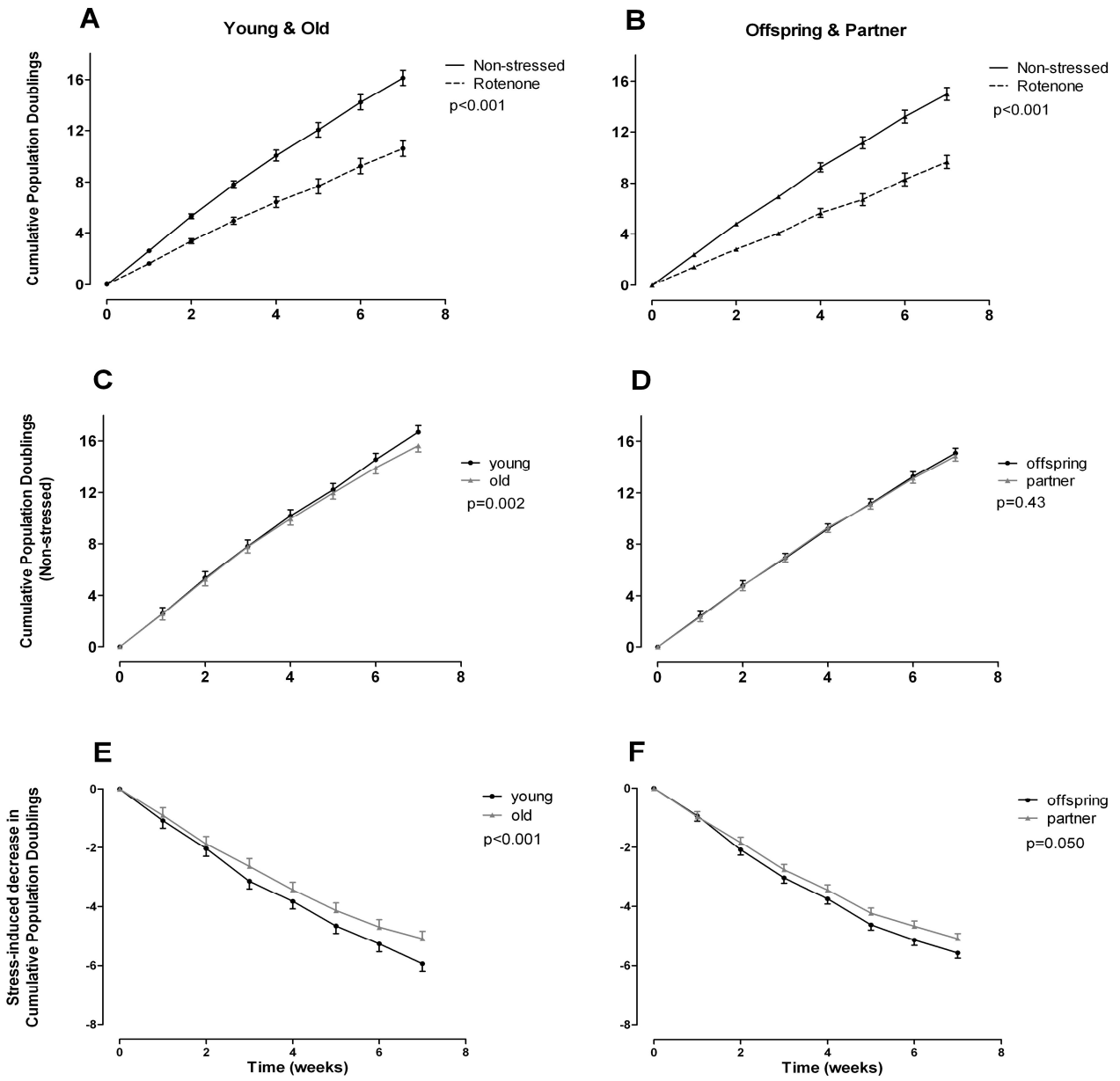

Figure 1. Cumulative population doublings under non-stressed conditions and chronic exposure to rotenone for 7 weeks comparing young/old subjects and off-spring/partner subjects (stress-induced decreases: rotenone stressed and non-stressed). A, rotenone effect on young and old subjects. B, rotenone effect on offspring and partners. C, young and old subjects compared under non-stressed conditions. D, offspring and partners compared under non-stressed conditions. E, rotenone-induced decrease compared between young and old subjects. F, rotenone-induced decrease compared between offspring and partners. Data were analyzed using linear mixed models adjusting for gender and batches of experiments. Values are given as mean (SE). p Values indicate differences between the slopes of the curves.

Discussion

The main findings of our study are that chronic inhibition of the respiratory chain with rotenone differentially affects ROS levels, SA-β-gal activity and growth rate, but not telomere shortening rate, when fibroblast strains from young subjects are compared with strains from old subjects. Even more importantly, the stress-induced changes in growth rate of fibroblast strains from offspring of nonagenarian siblings resemble the changes in growth rate of strains from young subjects.

According to the free radical theory of aging the respiratory chain function decreases with age, resulting in increased levels of ROS which will damage proteins and DNA (7). Indeed, the efficiency of oxidative phosphorylation in human skin fibroblasts becomes less efficient with chronological age (21). We aimed to simulate this process *in vitro* by inhibiting mitochondrial activity with the mitochondrial complex I inhibitor rotenone, which is known to decrease cellular respiration, paralleled by increased ROS levels (16). A low concentration of rotenone was used in order not to completely arrest proliferation. Also, it is known that long-term inhibition of mitochondrial complex I with concentrations of rotenone inducing 100% inhibition, leads to secondary toxicity (22) resulting in massive cell death (16).

As expected, fibroblast strains exposed to rotenone showed increased levels of ROS and increased SA-β-gal activity, indicating senescence (23), albeit not much is known about long-term culturing conditions of fibroblasts under chronic oxidative stress. Koopman *et al*. showed that human fibroblast exposed to low concentrations of rotenone (100nM) for up to three days show depolarisation of the $\Delta\psi$ paralleled by increased levels of ROS (16). They also reported that despite unchanging numbers of mitochondria, rotenone-treatment did induce changes in the shape of mitochondria and the extent and speed of movement of mitochondria.

Decreased growth rate due to oxidative stress was also found by von Zglinicki *et al*. who showed that hyperoxic condition markedly slowed proliferation (24). With the flow-FISH method we were able to measure that the telomere length shortened significantly after seven weeks of culturing. There were no differences in telomere length between non-stressed and

rotenone-stressed fibroblast strains after seven weeks of culturing, but taking into account the lower number of population doublings of the rotenone-stressed fibroblast strains, rotenone did induce a significantly faster telomere shortening rate per PD. This is consistent with the current consensus that increased oxidative stress accelerates telomere shortening (6;24).

In line with our hypothesis, strains from young subjects showed lower ROS levels when compared with fibroblast strains from old subjects, both under non-stressed and stressed conditions. For non-stressed conditions these results are supported by recent findings from Koziel *et al*. who showed higher levels of ROS, coinciding with lower mitochondrial membrane potential (Δψ), in fibroblast strains from old subjects (25). We used the fluorescent probe dihydrorhodamine 123 for the quantification of ROS. This assay is sensitive to such factors as plasma membrane efflux pumps (ABC transporters) (26), so it should be realized that any differences in these pumps between fibroblast strains from young and from old subjects may attribute to changes in the fluorescent signal. *In vivo*, ROS levels have been reported to increase with age in various tissues from animal models (27). We also found consistently lower ROS levels in strains from offspring when compared with strains from partners, albeit not significantly so. This is most probably due to the relatively low number of strains tested. Despite the lack of significance for the offspring-partner comparison, the results are support our earlier findings (10). Future studies with higher numbers of strains will have to confirm if fibroblast strains from offspring indeed show lower levels of rotenone-induced ROS when chronically exposed. Additionally, to study differences in mitochondrial functionality, it would be insightful to compare Δψ and the number, shape and (speed of) movement of mitochondria and the effect of rotenone on ROS generation by mitochondria respiring on different substrates. In model organisms it has indeed been shown that isolated mitochondria respiring on different substrates will differentially represent *in vivo* the longevity of the organisms they were derived from (28). Furthermore, with aging the binding affinities of mitochondrial proteins in the electron transport chain decrease, causing increased ROS leakage (29).

We did not find differences in SA-β-gal activity under non-stressed conditions between fibroblast strains from young subjects and from old subjects, whereas earlier we showed

lower numbers of senescent fibroblasts for strains from young subjects (10). It should be noted that in the experiments described here, fibroblasts were cultured for seven weeks whereas in the experiments described earlier fibroblasts were cultured for one week. Since it is well known that the number of senescence fibroblasts increases with increased duration of culturing (30), higher background levels of senescence after seven weeks of culturing might mask the difference in SA-β-gal activity between strains from young and old subjects. Also we did not find differences in SA-β-gal activity between strains from offspring and strains from partners under non-stressed conditions. When chronically stressed with rotenone, increases in SA-β-gal activity in strains from young subjects were lower when compared with fibroblast strains from old subjects, but no differences in stress-induced increases in SA-β-gal activity were found between fibroblast strains from offspring and partners, probably due to the relatively low number of strains tested.

Under non-stressed conditions the growth rate of fibroblast strains from young subjects was higher when compared with strains from old subjects. Similar *in vitro* results were described already in 1976 by Schneider *et al*. (31) and comparable differences were thought to exist *in vivo* (32). No differences in non-stressed growth rate were found between fibroblast strains from offspring of nonagenarian siblings when compared with strains from partners. It should be realized that we cultured the fibroblast strains under ambient oxygen conditions. The oxygen concentration in most tissues is much lower than the atmospheric oxygen concentration which is often used for cell culture. Human fibroblasts grow considerably slower in 20% oxygen when compared with 5% oxygen (33). Relatively large decreases in growth rate caused by the ambient oxygen conditions might mask the much smaller differences between fibroblast strains from offspring and partners.

Stress-induced decreases in growth rate were larger for fibroblast strains from young subjects and offspring when compared with strains from old subjects and partners, respectively, so in this respect fibroblast strains from offspring resemble the responses of strains from young subjects, both being more responsive to oxidative stress when compared with strains from old subjects and partners, respectively. Again these results confirm our earlier findings that fibroblast strains from offspring seem to be biologically younger than strains from their partners (10).

Contrary to our hypothesis, telomere shortening rates were not different between fibroblast strains from young subjects and fibroblast strains from old subjects. These results suggest that higher ROS levels in fibroblast strains from old subjects do not lead to measurably higher telomere shortening rates compared with young subjects. It is important to differentiate between *in vivo* age (chronological age of donors of fibroblast strains) and *in vitro* age (number of cumulative population doublings *in vitro* of those strains). After seven weeks of culturing we found stress-induced acceleration of telomere shortening which coincided with increased ROS levels, suggesting that with increasing *in vitro* age, ROS levels are related to accelerated telomere shortening. Indeed, it has already been described that ROS levels increase in human fibroblasts in later proliferation stages *in vitro* (34). However, there seems to be an uncoupling of ROS and telomere shortening when fibroblasts strains are compared based on *in vivo* age of the subjects. The results described here suggest that increased ROS levels affect growth rate independently of telomere shortening rate. The differences in growth rate dependent on chronological age and biological age under stressed conditions were not accompanied by differences in telomere length, suggesting that changes in growth rate with increasing *in vivo* age of subjects do not depend on changes in telomere length. This finding is in line with the results of Karlseder *et al*. who suggested that it is not telomere length per se which induces senescence but rather the protected status of shortened telomeres (9). More recently these results were supported by Sahin *et al*. (35) who reported results supporting a link between telomere and mitochondrial biology. The flow-FISH method for measuring telomere length has been developed for blood cells. When applied to other cell types, for instance to epithelial cells with a large cytoplasm, the method is known to be less accurate (36). Although the flow-FISH method was found sensitive enough in this study to measure telomere shortening in human fibroblasts during seven weeks of culturing, it is important to realize that this method might not be sensitive enough to measure subtle differences between fibroblast strains from young and old subjects and from offspring and partners.

Differences between cellular phenotypes of fibroblast are dependent on differences in gene expression. Fibroblast strains from old subjects were shown to express lower levels of mRNA for genes related to oxidative stress, growth and differentiation, cell cycle or metabolic

enzymes whereas higher expression was seen for genes related to protein processing and docking, extracellular matrix, immune response, EGF-signaling and transcription (37;38). Similar findings were reported *in vivo* (39). Stress-induced differences in mRNA expression of these genes are also dependent on the age of the subject, showing blunted responses in fibroblast strains from old subjects (40). Age-dependent differences in transcription are reflected in differences in translation, as suggested by considerable age-dependent differences in cytoplasmic levels of proteins involved in metabolism and stress response (e.g. heat shock and anti-oxidant proteins) (41). Taken together, these findings support the theory that aging is the result of accumulation of random damage (42) to the (mitochondrial) genome and to synthetic and degradative pathways, modulating the whole cell machinery.

An important strength of this study is the long-term character of the experiments, mimicking age-related decreases in mitochondrial function by inhibiting mitochondrial respiratory chain function. Furthermore, the tested strains were obtained from subjects of various chronological and biological ages, collected and stored in a highly standardized manner. We chose to study stress-induced senescence rather than replicative senescence, since it has been shown that the maximum number of population doublings does not reflect human life history trajectories (43). This suggests that stress-induced senescence might better differentiate between cellular phenotypes of individual subjects. A weakness of the study is the relatively low number of strains tested.

In conclusion we report that chronic inhibition of the respiratory chain differentially affects ROS levels, SA-β-gal activity and growth rate, but not telomere shortening when fibroblast strains from young subjects are compared with strains from old subjects. Even more importantly, the stress-induced changes in growth rate of fibroblast strains from offspring of nonagenarian siblings resemble the changes in growth rate of strains from young subjects, indicating that these offspring are biologically younger when compared with the general population. When fibroblast strains from offspring are compared with strains from partners, the effects of the biological age difference are likely to be smaller than those resulting from the 70 years difference between strains from young and old subjects. This might partly explain the lack of differences in ROS-levels and SA-β-gal acitivity between fibroblast strains

from offspring and partners. On the other hand the differences between the chronological and biological age contrasts could involve different biological phenomena. Future work will have to elucidate which signaling pathways are responsible for these differences.

References

(1) Krtolica A. Stem cell: balancing aging and cancer. Int J Biochem Cell Biol 2005;37:935-941.

(2) Coppe JP, Patil CK, Rodier F, Sun Y, Munoz DP, Goldstein J, Nelson PS, Desprez PY, Campisi J. Senescence-associated secretory phenotypes reveal cell-nonautonomous functions of oncogenic RAS and the p53 tumor suppressor. PLoS Biol 2008;6:2853-2868.

(3) Stolzing A, Jones E, McGonagle D, Scutt A. Age-related changes in human bone marrow-derived mesenchymal stem cells: consequences for cell therapies. Mech Ageing Dev 2008;129:163-173.

(4) Oeseburg H, de Boer RA, van Gilst WH, van der HP. Telomere biology in healthy aging and disease. Pflugers Arch 2010;459:259-268.

(5) Campisi J, d'Adda di Fagagna F. Cellular senescence: when bad things happen to good cells. Nat Rev Mol Cell Biol 2007;8:729-740.

(6) Richter T, von Zglinicki T. A continuous correlation between oxidative stress and telomere shortening in fibroblasts. Exp Gerontol 2007;42:1039-1042.

(7) Harman D. Aging: a theory based on free radical and radiation chemistry. J Gerontol 1956;11:298-300.

(8) von Zglinicki T. Oxidative stress shortens telomeres. Trends Biochem Sci 2002;27:339-344.

(9) Karlseder J, Smogorzewska A, de LT. Senescence induced by altered telomere state, not telomere loss. Science 2002;295:2446-2449.

(10) Dekker P, Maier AB, van HD, de Koning-Treurniet C, Blom J, Dirks RW, Tanke HJ, Westendorp RG. Stress-induced responses of human skin fibroblasts in vitro reflect human longevity. Aging Cell 2009;8:595-603.

(11) Schoenmaker M, de Craen AJM, de Meijer PHEM, Beekman M, Blauw GJ, Slagboom PE, Westendorp RGJ. Evidence of genetic enrichment for exceptional survival using a family approach: the Leiden Longevity Study. Eur J Hum Genet 2006;14:79-84.

(12) Westendorp RG, van Heemst D, Rozing MP, Frolich M, Mooijaart SP, Blauw GJ, Beekman M, Heijmans BT, de Craen AJ, Slagboom PE. Nonagenarian siblings and their offspring display lower risk of mortality and morbidity than sporadic nonagenarians: The Leiden Longevity Study. J Am Ger Soc 2009;57:1634-1637.

(13) Wijsman CA, Rozing MP, Streefland TC, Le CS, Mooijaart SP, Slagboom PE, Westendorp RG, Pijl H, van HD. Familial longevity is marked by enhanced insulin sensitivity. Aging Cell 2010;10-9726.

(14) Bootsma-van der Wiel A, Gussekloo J, de Craen AJM, van Exel E, Bloem BR, Westendorp RGJ. Common chronic diseases and general impairments as determinants of walking disability in the oldest-old population. J Am Ger Soc 2002;50:1405-1410.

(15) Maier AB, le Cessie S, Koning-Treurniet C, Blom J, Westendorp RG, van Heemst D. Persistence of high-replicative capacity in cultured fibroblasts from nonagenarians. Aging Cell 2007;6:27-33.

(16) Koopman WJ, Nijtmans LG, Dieteren CE, Roestenberg P, Valsecchi F, Smeitink JA, Willems PH. Mammalian mitochondrial complex I: biogenesis, regulation, and reactive oxygen species generation. Antioxid Redox Signal 2010;12:1431-1470.

(17) Cabras P, Caboni P, Cabras M, Angioni A, Russo M. Rotenone residues on olives and in olive oil. J Agric Food Chem 2002;50:2576-2580.

(18) Wondrak GT, Roberts MJ, Cervantes-Laurean D, Jacobson MK, Jacobson EL. Proteins of the extracellular matrix are sensitizers of photo-oxidative stress in human skin cells. J Invest Dermatol 2003;121:578-586.

(19) Boulton S, Anderson A, Swalwell H, Henderson JR, Manning P, Birch-Machin MA. Implications of using the fluorescent probes, dihydrorhodamine 123 and 2',7'-dichlorodihydrofluorescein diacetate, for the detection of UVA-induced reactive oxygen species. Free Radic Res 2011;45:139-146.

(20) Noppe G, Dekker P, Koning-Treurniet C, Blom J, van Heemst D, Dirks RJ, Tanke HJ, Westendorp RG, Maier AB. Rapid flow cytometric method for measuring Senescence Associated â-galactosidase activity in human fibroblasts. Cytometry A 2009;75:910-916.

(21) Greco M, Villani G, Mazzucchelli F, Bresolin N, Papa S, Attardi G. Marked aging-related decline in efficiency of oxidative phosphorylation in human skin fibroblasts. FASEB J 2003;17:1706-1708.

(22) Barrientos A, Moraes CT. Titrating the effects of mitochondrial complex I impairment in the cell physiology. J Biol Chem 1999;274:16188-16197.

(23) Toussaint O, Medrano EE, von Zglinicki T. Cellular and molecular mechanisms of stress-induced premature senescence (SIPS) of human diploid fibroblasts and melanocytes. Exp Gerontol 2000;35:927-945.

(24) von Zglinicki T, Saretzki G, Docke W, Lotze C. Mild hyperoxia shortens telomeres and inhibits proliferation of fibroblasts: a model for senescence? Exp Cell Res 1995;220:186-193.

(25) Koziel R, Greussing R, Maier AB, Declercq L, Jansen-Durr P. Functional interplay between mitochondrial and proteasome activity in skin aging. J Invest Dermatol 2011;131:594-603.

(26) Prochazkova J, Kubala L, Kotasova H, Gudernova I, Sramkova Z, Pekarova M, Sarkadi B, Pachernik J. ABC transporters affect the detection of intracellular oxidants by fluorescent probes. Free Radic Res 2011;45:779-787.

(27) Sohal RS, Ku HH, Agarwal S, Forster MJ, Lal H. Oxidative damage, mitochondrial oxidant generation and antioxidant defenses during aging and in response to food restriction in the mouse. Mech Ageing Dev 1994;74:121-133.

(28) Melvin RG, Ballard JW. Intraspecific variation in survival and mitochondrial oxidative phosphorylation in wild-caught Drosophila simulans. Aging Cell 2006;5:225-233.

(29) Ames BN. Optimal micronutrients delay mitochondrial decay and age-associated diseases. Mech Ageing Dev 2010;131:473-479.

(30) Dimri GP, Lee XH, Basile G, Acosta M, Scott C, Roskelley C, Medrano EE, Linskens M, Rubelj I, Pereirasmith O, Peacocke M, Campisi J. A Biomarker That Identifies Senescent Human-Cells in Culture and in Aging Skin In-Vivo. P Natl Acad Sci USA 1995;92:9363-9367.

(31) Schneider EL, Mitsui Y. The relationship between in vitro cellular aging and in vivo human age. P Natl Acad Sci USA 1976;73:3584-3588.

(32) Rubin H. Cell aging in vivo and in vitro. Mech Ageing Dev 1997;98:1-35.

(33) Balin AK, Fisher AJ, Anzelone M, Leong I, Allen RG. Effects of establishing cell cultures and cell culture conditions on the proliferative life span of human fibroblasts isolated from different tissues and donors of different ages. Exp Cell Res 2002;274:275-287.

(34) Lee HC, Yin PH, Chi CW, Wei YH. Increase in mitochondrial mass in human fibroblasts under oxidative stress and during replicative cell senescence. J Biomed Sci 2002;9:517-526.

(35) Sahin E, Colla S, Liesa M, Moslehi J, Muller FL, Guo M, Cooper M, Kotton D, Fabian AJ, Walkey C, Maser RS, Tonon G, Foerster F, Xiong R, Wang YA, Shukla SA, Jaskelioff M, Martin ES, Heffernan TP, Protopopov A, Ivanova E, Mahoney JE, Kost-Alimova M, Perry SR, Bronson R, Liao R, Mulligan R, Shirihai OS, Chin L, DePinho RA. Telomere dysfunction induces metabolic and mitochondrial compromise. Nature 2011;470:359-365.

(36) Wieser M, Stadler G, Bohm E, Borth N, Katinger H, Grillari J, Voglauer R. Nuclear flow FISH: isolation of cell nuclei improves the determination of telomere lengths. Exp Gerontol 2006;41:230-235.

(37) Braam B, Langelaar-Makkinje M, Verkleij A, Bluyssen H, Verrips T, Koomans HA, Joles JA, Post JA. Anti-oxidant sensitivity of donor age-related gene expression in cultured fibroblasts. Eur J Pharmacol 2006;542:154-161.

(38) Ly DH, Lockhart DJ, Lerner RA, Schultz PG. Mitotic misregulation and human aging. Science 2000;287:2486-2492.

(39) Lener T, Moll PR, Rinnerthaler M, Bauer J, Aberger F, Richter K. Expression profiling of aging in the human skin. Exp Gerontol 2006;41:387-397.

(40) Kyng KJ, May A, Kolvraa S, Bohr VA. Gene expression profiling in Werner syndrome closely resembles that of normal aging. P Natl Acad Sci USA 2003;100:12259-12264.

(41) Boraldi F, Bini L, Liberatori S, Armini A, Pallini V, Tiozzo R, Pasquali-Ronchetti I, Quaglino D. Proteome analysis of dermal fibroblasts cultured in vitro from human healthy subjects of different ages. Proteomics 2003;3:917-929.

(42) Kirkwood TB. Molecular gerontology. J Inherit Metab Dis 2002;25:189-196.

(43) Maier AB, Westendorp RG. Relation between replicative senescence of human fibroblasts and life history characteristics. Ageing Res Rev 2009;8:237-243.

Chapter 6

Microarray-based identification of age-dependent differences in gene expression of human dermal fibroblasts

Pim Dekker, David Gunn, Tony McBryan, Roeland W. Dirks, Diana van Heemst, Fei-Ling Lim, Aart G. Jochemsen, Matty Verlaan-de Vries, Julia Nagel, Peter D. Adams, Hans J. Tanke, Rudi G.J. Westendorp, Andrea B. Maier

Submitted for publication

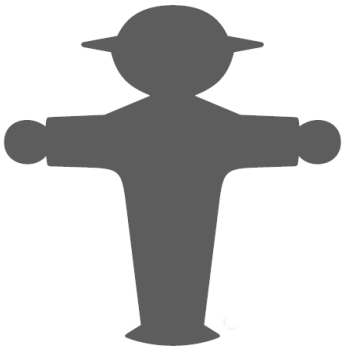

Summary

Senescence is thought to play an important role in the progressive age-related decline in tissue integrity and concomitant diseases, but not much is known about the complex interplay between upstream regulators and downstream effectors. We profiled whole genome gene expression of non-stressed and rotenone-stressed human fibroblast strains from young and oldest old subjects, and measured Senescence Associated-β-gal (SA-β-gal) activity. Microarray results identified gene sets involved in carbohydrate metabolism, Wnt/β-catenin signaling, the cell cycle, glutamate signaling, RNA-processing and mitochondrial function as being differentially regulated with chronological age. The most significantly differentially regulated mRNA corresponded to the p16 gene. p16 was then investigated using qPCR, Western blotting and immunocytochemistry (ICC). In conclusion, we have identified cellular pathways that are differentially expressed between fibroblast strains from young and old subjects.

Introduction

In addition to apoptosis, senescence is thought to contribute to the progressive age-related decline in tissue integrity and the concomitant diseases (1). It was found that various types of stressors (e.g. cytokines, oxidative agents) could induce premature senescence, implying a significant role for environmental factors in accelerating the aging process. In the past, studying senescence *in vivo* was thwarted by the lack of markers that indubitably identify senescent cells. Meanwhile studies into the signal transduction pathways of senescence have led to identification of many proteins that have overlapping roles in senescence, apoptosis and DNA-damage sensing (2).

Despite the fact that senescence, apoptosis and DNA-damage repair have been shown to play pivotal roles in the aging process, not much is known about the complex interplay between upstream and downstream pathways that operate intracellularly and between tissues on the systemic level. Gene expression array technologies may help to find a specific profile of differential gene expression as a marker of senescence. Comparisons of gene expression profiles have been made between various tissues of chronologically young and old mammalian model organisms (3-13) and humans (14-24). These studies show that different tissues in various species show similar changes in expression of genes involved in DNA-damage repair, cell cycle progression, senescence, apoptosis, stress response, immune response and metabolism. However, there are also many species-dependent and tissue-dependent differences that these studies did not address, and it is also not clear which changes are the results of the aging process and which drive the aging process. We have already reported that human skin fibroblast strains derived from chronologically young subjects, when compared with fibroblast strains from oldest old subjects (90 years of age), are less prone to go into senescence and more prone to go into apoptosis, both under non-stressed and stressed conditions (25). Also, fibroblast strains from middle aged offspring of nonagenarian siblings exhibited less senescence and more apoptosis when compared with fibroblasts from the partners of the offspring, representing the general population. Thus, fibroblasts from the offspring demonstrated younger cellular characteristics than fibroblasts from age-matched controls.

Here, we aimed to identify the cellular pathways that drive the differences with chronological age in cell senescence and apoptosis. We performed whole genome gene expression profiling of non-stressed and rotenone-stressed human fibroblast strains from young and old subjects. We expected the rotenone treatment to exacerbate differences in gene mRNA levels with age and, in particular, affect genes involved in senescence, apoptosis, DNA-damage repair, cell cycle progression, stress responses and metabolism. We validated the most significant mRNA change by qPCR and then performed a replication experiment in independent strains to investigate whether mRNA changes were reflected by protein level changes.

Material and methods

Study design

The Leiden 85-plus Study (26) is a prospective population-based study in which all inhabitants aged 85 years or older of the city of Leiden, the Netherlands, were invited to take part. Between September 1997 and September 1999, 599 out of 705 eligible subjects (85%) were enrolled. All participants were followed for mortality and 275 subjects survived to the age of 90 years. During the period December 2003 up to May 2004, a biobank was established from fibroblasts cultivated from skin biopsies from 68 of the 275 surviving 90-year-old participants (27). These participants were in good physical and mental condition and were able to come to the research institute, where the same qualified physician carried out the procedures. During the period August to November 2006, we also established a biobank of fibroblast strains established from biopsies taken from 27 young subjects (23-29 years old).

Fibroblast cultures and experimental setup

Three-mm biopsies were taken from the sun unexposed medial side of the upper arm. Fibroblasts were grown in D-MEM:F-12 (1:1) medium supplemented with 10% fetal calf serum (FCS, Gibco, batch no. 40G4932F), 1 mM MEM sodium pyruvate, 10 mM HEPES, 2

mM glutamax I, and antibiotics (100 Units/mL penicillin, 100 µg/mL streptomycin, and 0.25–2.5 µg/mL amphotericin B), all obtained from Gibco, Breda, the Netherlands. This medium will be referred to as standard medium. Fibroblasts were incubated at 37^{o}C with 5% CO_2 and 100% humidity. All cultures that are used in the present study were grown under predefined, highly standardized conditions as published earlier (27) and frozen at low passage. Trypsin (Sigma, St Louis, MO, USA) was used to split fibroblasts using a 1:4 ratio each time they reached 80-100% confluence.

Passage 11 fibroblasts were thawed from frozen stocks on day zero. On day four, seven and 11 fibroblasts were further passaged in order to multiply fibroblasts. On day 18 the experiments were started. For the microarray experiments, fibroblast strains were seeded at 5200 and 7500 cells/cm^2 for non-stressed and rotenone-stressed cultures respectively. For the replication experiments, fibroblast strains were seeded at 2300 and 3900 cells/cm^2 for non-stressed and rotenone-stressed cultures respectively. Strains were seeded in batches of eight strains per condition.

To chronically stress fibroblast strains, medium was supplemented with 0.6 µM rotenone (Sigma, St Louis, MO, USA), known to induce an increase in the intracellular production of reactive oxygen species (ROS) at the mitochondrial level (28). After three days fibroblast strains were assessed for SA-β-gal, ROS, microarray experiments, p16 on the mRNA level and the protein level as described below. In order to check early response genes samples were also taken at three hours for the microarray experiments.

Flow cytometric measurement of SA-β-galactosidase activity

Fibroblasts were prepared as described earlier (29). In short, to change the lysosomal pH to pH 6, fibroblasts were incubated with medium containing 100 nM bafilomycin A1 (VWR, Amsterdam, the Netherlands) for 1 hour. Fibroblasts were then incubated with 33 µM of the β-galactosidase substrate C_{12}FDG (Invitrogen, Breda, The Netherlands), in the presence of 100 nM bafilomycin. After trypsinisation, fibroblasts were washed once and resuspended in 200 µl ice cold PBS. Fibroblasts were measured in the FITC-channel and analysis was performed on the Median Fluorescence Intensity (MdFI) values.

Flow cytometric measurement of ROS

Fibroblasts were incubated in medium supplemented with 30 µM dihydrorhodamine 123 (Invitrogen, Breda, The Netherlands). They were then trypsinized, washed in ice-cold PBS, pelleted and resupended in 200 µl ice-cold PBS. Fibroblasts were kept on ice before measurement of MDI in the FITC-channel.

Microarray Analysis

All products were purchased from Agilent Technologies UK Ltd (Wokingham, Berkshire, UK) and used according to manufacturer's protocol unless stated otherwise. All samples (n=12) were isolated and run on microarrays separately. Total mRNA was isolated using the RNeasy Mini Kit (Qiagen Ltd, Crawley, UK) and 300ng was mixed with an appropriate amount of One-Color RNA Spike-In RNA and converted into labelled cRNA (One-Color Low RNA Input Linear Amplification Kit PLUS). Labelled cRNA was purified using an RNeasy Mini Kit (Qiagen Ltd, Crawley, UK) and 2µg was hybridised to Agilent human whole genome Oligo Arrays (G4112F; 41094 probes) using reagents supplied in the Agilent Hybridisation Kit (One-Color Microarray-Based Gene Expression Analysis Protocol). Microarray slides were hybridised for 17 h at 65 ºC and subsequently washed in acetonitrile for 1 min followed by 30s in Agilent Stabilisation and Drying Solution. Scanning of the slides was performed with the Agilent G2565BA Microarray Scanner System. The Agilent G2567AA Feature Extraction Software (v.9.1) was used to extract data and check the quality. To comply with MIAME requirements the data discussed in this publication have been deposited in NCBI's Gene Expression Omnibus (GEO) (30;31) and are accessible through GEO Series accession number GSE28300 (http://www.ncbi.nlm.nih.gov/geo/query/acc.cgi?acc=GSE28300).

Validation/replication of p16 by qPCR

cDNA syntheses of total RNA extracted from non-stressed fibroblast strains or rotenone-stressed fibroblast strains was carried out using 0.5µg total RNA per reaction. Synthesis of cDNA was via AMV first strand synthesis kit (Roche Applied Science, Hertfordshire, UK) according to the manufacturer's instructions. All PCR mixes were prepared in triplicate, comprising 0.1µl of freshly prepared cDNA, 1 x SYBR Green PCR master mix (Bio-Rad Laboratories Ltd, Hemel Hempstead, UK) and 1 x QuantiTect PCR primers (Qiagen Ltd,

Crawley, UK) specific for the genes CDKN2A/p16 (QT00089964) or to PPIA/cyclophilin A (QT00062311). Semi-quantitative PCR was performed on a Bio-Rad iCycler. Transcript levels were normalized to PPIA and data analysis was performed using the comparative cycle threshold method (ΔΔCT).

p16 immunoblotting

Fibroblasts were lysed in RIPA buffer (20mM Triethanolamine-HCL, ph 7.8, 140 mM NaCl, 0.1% Natrium deoxycholaat, 0.1% Natrium dodecylsulfaat (SDS) and 0.1% Triton X-100) with protease inhibitors (SIGMA*FAST* ™ Protease Inhibitor Cocktail Tablets, EDTA-free) used according to the manufacturer's protocol. Proteinlysates of the fibroblasts were stored at -80℃. Protein content was determined by Pierce BCA Protein Assay Kit (Thermo Scientific, Breda, the Netherlands). Proteins were fractionated by 10% and 15% SDS-polyacrylamide gel electrophoresis. For every strain the loaded amounts of protein were the same for the unstressed and for the rotenone-stressed condition. Samples of three subjects were not used for immunoblots because of very low protein content. Proteins were blotted onto a PVDF membrane (Immobilon-P, Millipore, Billerica, USA). Membranes were blocked in Tris-Buffered Saline Tween-20 (TBST) containing 10% non-fat dry milk. Primary antibodies were prepared in TBST solution with 10% dry milk. Membranes were incubated overnight at 4℃ with the following primary antibodies: α-p16 JC8 (Santa Cruz Biotechnology, 1:500) and α-Hausp Pab (Bethyl laboratories, Montgomery 1:1000). After incubation, membranes were washed three times with TBST and incubated with goat anti-mouse or goat anti-rabbit antibody coupled to horse-radish-peroxidase for one h at room temperature. Antibody binding was visualized using Super Signal West Dura (Thermo Scientific, Breda, the Netherlands) and exposure to X-ray film. The software package Odyssey (LI-COR Biosciences, Lincoln, USA) was used to quantify the values from the Immunoblot signals, the values of which were expressed in arbitrary units (AU). All values were normalized for loading control before they were used further for statistical analyses.

Immunocytochemical staining for p16

Fibroblasts were fixed with 4% paraformaldehyde in PBS for four minutes. After permeabilization for 20 minutes in 0.2% Triton (Sigma, St Louis, MO, USA) in PBS, samples were

blocked with blocking buffer (3% BSA in PBS) for one hour at room temperature and incubated for two hours with anti-p16 (JC8) antibody (Santa Cruz Biotechnology Inc., Santa Cruz, USA), diluted 1/100 in blocking buffer. After five washes with PBS, cells were treated with 0.3% H_2O_2 in methanol to reduce background peroxidase activity. Fibroblasts were then stained using an anti-mouse IgG Vectastain Elite ABC kit (Vector laboraties, Burlingame, CA, USA) and a DAB Peroxidase Substrate Kit (Vector laboraties, Burlingame, CA, USA), according to the manufacturer's protocols. Fibroblasts were counterstained with Hematoxylin (Vector laboraties, Burlingame, CA, USA) for five minutes and incubated with NH4OH in 70% ethanol for one minute. After washing in water, slides were mounted with Faramount Mounting Medium (DAKO, Heverlee, Belgium) and photographed with a Leica microscope (Leica Microsystems, Rijswijk, the Netherlands). Per sample 500 randomly chosen cells were assessed for p16 positivity.

Statistics

Raw data produced from microarrays were imported into R version 2.11.0 (2010-04-22) (32), an open source statistical analysis program, using custom code. Background correction was performed using the normexp+offset method and data were log-transformed (33). Differential expression of genes was determined by fitting a linear model using the lmFit function from the limma package and moderated t-statistics were computed using the ebayes function (34). The linear model included parameters for treatment, age, gender and batch effects. Bonferroni-Holm multiple testing correction was also applied (FDR(p) < 0.05).

For the probes showing significant differences in expression of mRNA between fibroblast strains from young and old strains, variation in expression between strains from different subjects was presented as a heatmap.

The Bonferroni-Holm data set was uploaded into the Ingenuity application [www.ingenuity.com]. Each probe identifier was mapped to its corresponding object/gene in Ingenuity's Knowledge Base. These molecules, called Network Eligible molecules, were overlaid onto a global molecular network developed from information contained in Ingenuity's Knowledge Base. Networks of Network Eligible Molecules were then algorithmically generated based on their connectivity. The Functional Analysis identified the biological functions and/or diseases that were most significant to the data set. Right-tailed Fisher's

exact test was used to calculate a p-value determining the probability that each biological function and/or disease assigned to that data set is due to chance alone. Canonical pathways analysis identified the pathways from the Ingenuity Pathways Analysis library of canonical pathways that were most significant to the data set. The significance of the association between the data set and the canonical pathway was measured in 2 ways: 1) A ratio of the number of molecules from the data set that map to the pathway divided by the total number of molecules that map to the canonical pathway is displayed. 2) Fisher's exact test was used to calculate a p-value determining the probability that the association between the genes in the dataset and the canonical pathway is explained by chance alone.

Gene Set Enrichment Analysis (GSEA; www.broad.mit.edu\gsea) (35;36) was applied for functional pathway analysis between comparative conditions. Probes from the microarray were collapsed into 17517 gene features and ordered by signal to noise ratio into a rank ordered list (L). For each gene set (S) an enrichment score (ES) is calculated which reflects the degree to which it is overrepresented at the extremes (top or bottom) of the entire ranked list L based on the Kolmogorov-Smirnov statistic. Briefly, the score is calculated by traversing the list L and increasing a running-sum statistic when a gene is encountered which is in S and decreasing it when genes are encountered which are not in S. The magnitude of the increment corresponds to the degree that the gene correlates to the phenotype. Statistical significance (nominal P-value) of the ES is determined by empirical phenotype-based permutation; specifically the phenotype labels are permuted and the ES of the gene set is recalculated to generate a null distribution for the ES. Nominal p-value is computed relative to this null distribution. Significance levels are then adjusted to account for multiple hypotheses testing first by normalizing the ES for each gene set to account for the size of the set (NES) and then by controlling the proportion of false positives by calculating the FDR corresponding to each NES. Gene sets were obtained from the Broad Institute Molecular Signatures Database.

All other analyses were performed with the software package SPSS 16.0.01 (SPSS Inc., Chicago, IL). Since the AU values from the Western blotting results were not normally distributed, they were normalised by log-transformation. Rotenone-induced effects were

analysed using linear mixed models (LMMs), adjusting for batches of experiments, repeat experiments and gender (and also age in case of offspring/partner comparison). Differences between groups (young/old, offspring/partner) in non-stressed and rotenone-stressed conditions were analysed using similar linear mixed models.

Results

Microarray analysis dependent on chronological age

SA-β-gal activity was measured in fibroblasts from young and old subjects under non-stressed and stressed conditions to assure that rotenone treatment for three days would increase levels of senescence, as previously observed (29). Six young subjects and six old subjects were randomly chosen (age: 23.1±1.6 [mean±SD] and 90.3±0.5 years, respectively, three males and three females for both young and old). All subjects were in good physical and mental condition and were able to come to the research institute. There was a significant increase in SA-β-gal activity in all fibroblast strains after three days of exposure to 0.6 μM rotenone (non-stressed: 2365±236 [MdFI in arbitrary units; mean±SE], rotenone: 4366±489, $p<0.001$). Furthermore, strains from old subjects showed a higher SA-β-gal activity under non-stressed conditions and a higher stress-induced increase in SA-β-gal activity (Supplemental table 2).

Gene expression profiles were generated using fibroblast strains from young and old subjects under non-stressed conditions and stressed for three hours and three days with rotenone. After quantile normalisation of the data, a linear regression model was used in conjunction with a Bonferroni-Holm multiple testing correction ($p<0.05$) to detect mRNAs that were differentially expressed between fibroblast strains from young and old subjects. A total of 215 out of 41094 probes were identified whose expression was significantly different between the fibroblast strains from young and old subjects (Supplemental table 1). Variation in expression between strains from different subjects was presented as a heatmap (Supplemental figure 1). These differences between young and old were present in the untreated samples as well as in the samples obtained after treatment with rotenone for three hours and after treatment with

rotenone for three days. The 215 differentially expressed probes could be mapped to 106 genes (Table 1).

Pathway analysis

To identify cellular pathways that could be responsible for the age-dependent changes in gene expression, Ingenuity Pathway Analysis was performed using all data and applying a Bonferroni-Holm cutoff to generate a target list for further study. The 215 probes could be mapped to 106 genes eligible for Ingenuity network analysis and 100 genes allowing function and canonical pathway analysis. Twelve over-represented gene networks were identified, with the most significant Ingenuity network containing p16 (CDKN2A) at its centre (Figure 1) and corresponding to the biological functions Tumour Morphology, Cell Cycle progression and Cellular Development. The biological function most significantly enriched in the 100 genes was Carbohydrate Metabolism. For the canonical pathway analysis Wnt/β-Catenin signaling was the most significantly enriched. The top 10 functions and canonical pathways derived from these analyses are shown in Figure 2.

To complement the Ingenuity analysis, a GSEA-based analysis was performed as this approach uses significance data across all the probes rather than a division of the list via a significant cutoff. When the data from old subjects were compared with that from young subjects, 446 of 967 gene sets were more highly expressed in the strains from the old subjects. Using a false discovery rate (FDR) cutoff of 0.25, the Glutamate Signaling Pathway appeared to be significantly enriched (nominal p-value: 0.006, FDR: 0.22, ES: 0.68, NES: -17.7) due to the differential regulation of the genes HOMER2, GRIA3, GRIN2B and GRIK2. In fibroblast strains from young subjects, 521 of 967 gene sets were more highly expressed when compared with strains from old subjects and 29 gene sets were significantly enriched at a FDR cutoff of 0.25 (Table 2). These gene sets were mainly involved in mitochondrial processes, the cytoskeleton (especially the machinery needed for mitosis) and RNA-processing.

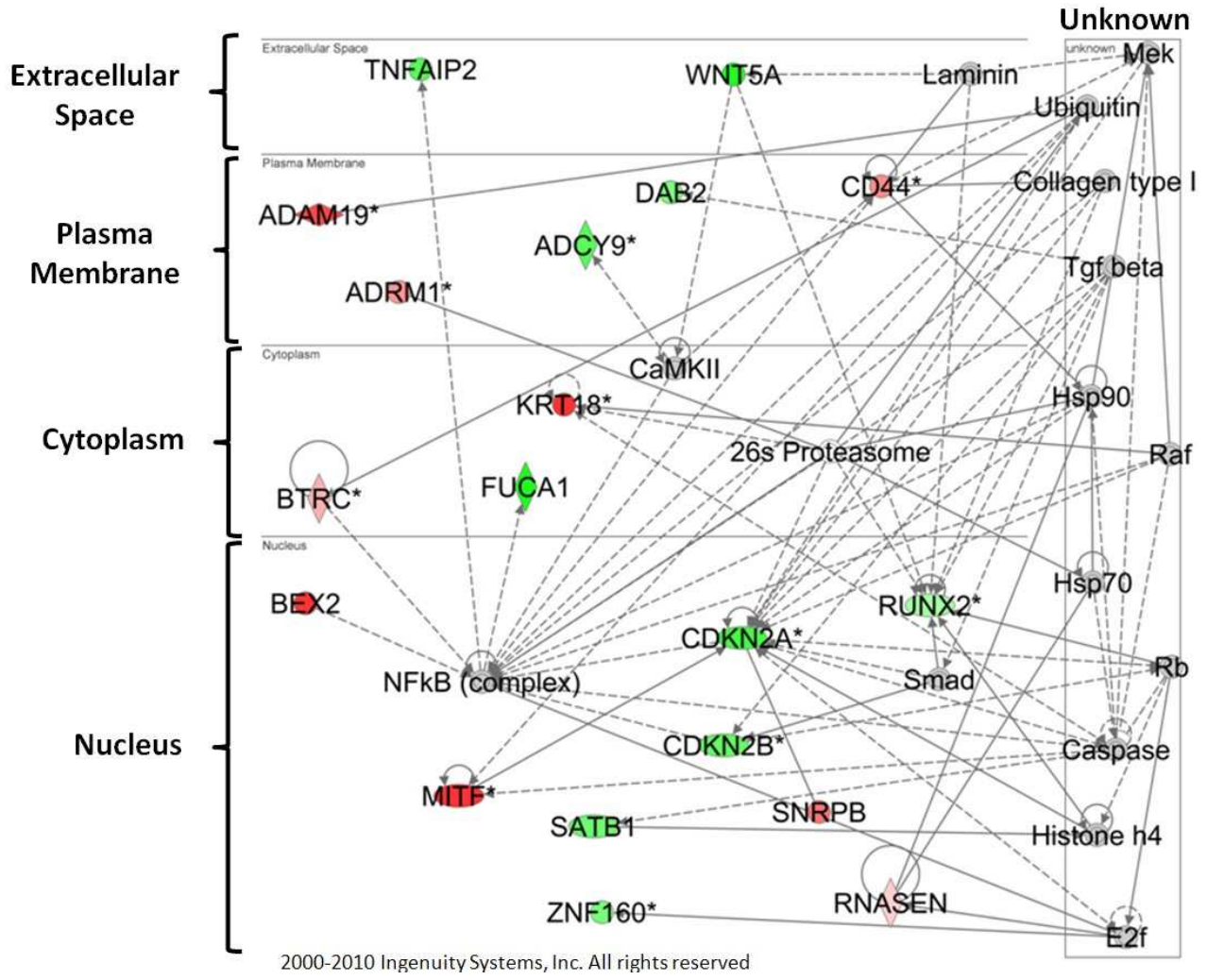

Figure 1. Top network generated by the use of Ingenuity Pathway Analysis (IPA), carried out on comparing young with old subjects with the Bonferroni-Holm cutoff applied ($p<0.05$). Molecules are represented as nodes, and the biological relationship between two nodes is represented as a line. The intensity of the node color indicates the degree of up- (red) or down- (green) regulation in fibroblast strains from young subjects. Nodes are displayed using various shapes that represent the functional class of the gene product (diamond: enzyme, horizontal oval: transcription factor, circle: other).

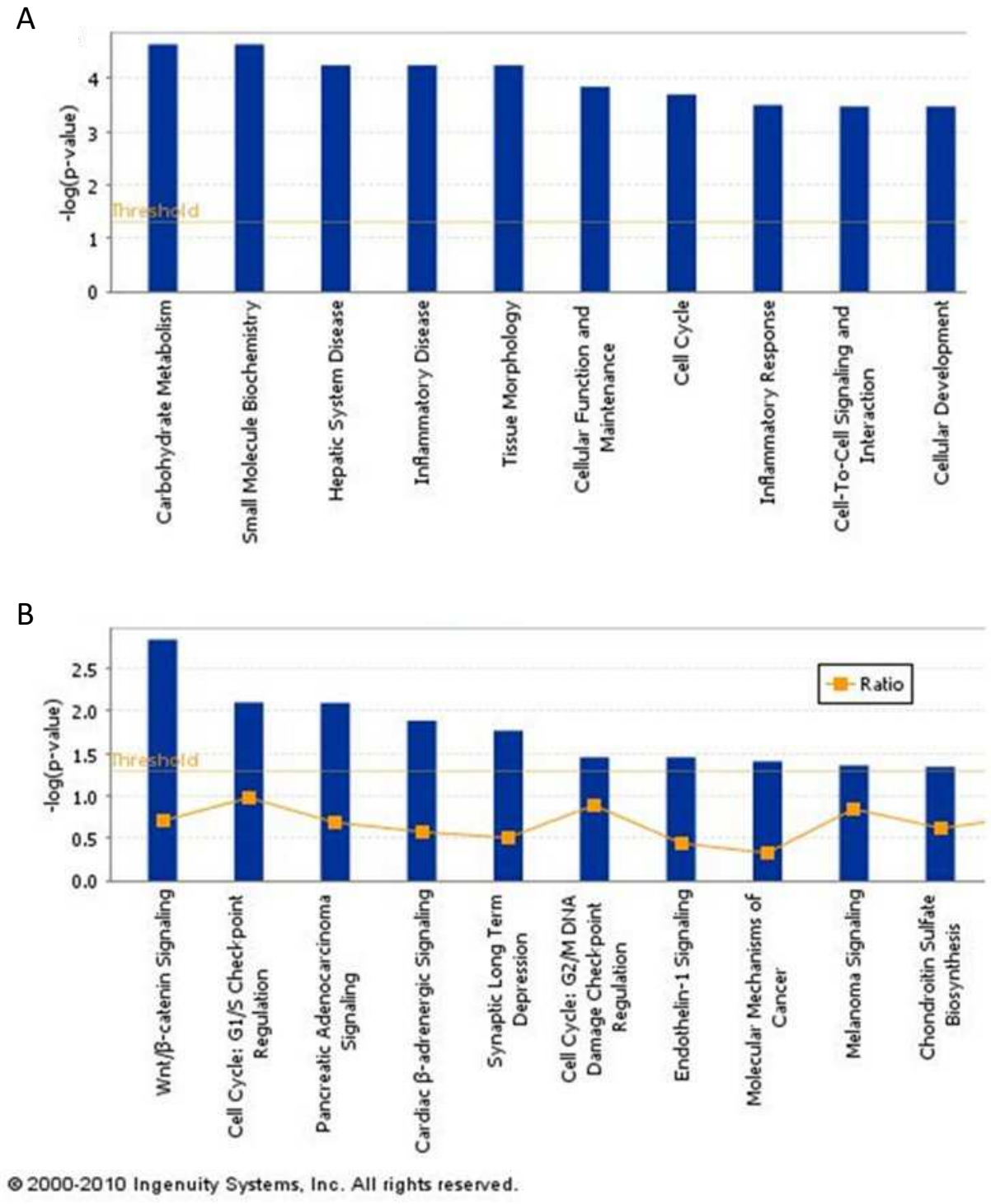

Figure 2. Ingenuity analysis. A, top 10 biological functions; B, top ten canonical pathways. Analysis was carried out on comparing young with old subjects with the Bonferroni-Holm cutoff applied ($p<0.05$). Ratio: expression in young/expression in old.

Table 1. List of genes to which the 215 differentially expressed probes could be mapped.

ID	Symbol	Entrez Gene Name	Location	Type(s)
A_23_P14515	ACOT4	acyl-CoA thioesterase 4	Cytoplasm	enzyme
A_23_P374082	ADAM19	ADAM metallopeptidase domain 19	Plasma Membrane	peptidase
A_24_P935103	ADCY9	adenylate cyclase 9	Plasma Membrane	enzyme
A_23_P68665	ADRM1	adhesion regulating molecule 1	Plasma Membrane	other
A_23_P317105	AKAP10	A kinase (PRKA) anchor protein 10	Cytoplasm	other
A_23_P158231	APBA2	amyloid beta (A4) precursor protein-binding, family A, member 2	Cytoplasm	transporter
A_23_P41166	B3GALNT1	beta-1,3-N-acetylgalactosaminyltransferase 1 (globoside blood group)	Cytoplasm	enzyme
A_23_P159952	BEX1	brain expressed, X-linked 1	Cytoplasm	other
A_23_P22735	BEX2	brain expressed X-linked 2	Nucleus	other
A_23_P35427	BTRC	beta-transducin repeat containing	Cytoplasm	enzyme
A_24_P201404	C11orf54	chromosome 11 open reading frame 54	Nucleus	other
A_32_P162183	C2	complement component 2	Extracellular Space	peptidase
A_23_P40315	C20orf12	chromosome 20 open reading frame 12	unknown	other
A_32_P142700	C22orf15	chromosome 22 open reading frame 15	unknown	other
A_32_P160972	C6orf115	chromosome 6 open reading frame 115	unknown	other
A_23_P73012	C9orf3	chromosome 9 open reading frame 3	Cytoplasm	peptidase
A_23_P155106	CCDC134	coiled-coil domain containing 134	unknown	other
A_23_P24870	CD44	CD44 molecule (Indian blood group)	Plasma Membrane	other
A_24_P42633	CDC42	cell division cycle 42 (GTP binding protein, 25kDa)	Cytoplasm	enzyme
A_23_P43484	CDKN2A	cyclin-dependent kinase inhibitor 2A (melanoma, p16, inhibits CDK4)	Nucleus	transcription regulator
A_24_P360674	CDKN2B	cyclin-dependent kinase inhibitor 2B (p15, inhibits CDK4)	Nucleus	transcription regulator
A_32_P99171	CHST11	carbohydrate (chondroitin 4) sulfotransferase 11	Cytoplasm	enzyme
A_24_P351435	CRBN	cereblon	Cytoplasm	enzyme
A_24_P76666	CSNK2A1	casein kinase 2, alpha 1 polypeptide	Cytoplasm	kinase
A_23_P202448	CXCL12	chemokine (C-X-C motif) ligand 12	Extracellular Space	cytokine
A_23_P257871	DAB2	disabled homolog 2, mitogen-responsive phosphoprotein (Drosophila)	Plasma Membrane	other
A_32_P230547	DOCK7	dedicator of cytokinesis 7	Plasma Membrane	other
A_23_P217079	DPM2	dolichyl-phosphate mannosyltransferase polypeptide 2, regulatory subunit	Cytoplasm	enzyme
A_23_P103232	DUSP23	dual specificity phosphatase 23	Cytoplasm	phosphatase
A_24_P375609	EIF5A	eukaryotic translation initiation factor 5A	Cytoplasm	translation regulator
A_23_P154806	EPB41L1	erythrocyte membrane protein band 4.1-like 1	Plasma Membrane	other
A_24_P166613	EPDR1	ependymin related protein 1 (zebrafish)	Nucleus	other
A_23_P71981	ERAL1	Era G-protein-like 1 (E. coli)	Cytoplasm	other
A_24_P314451	F8	coagulation factor VIII, procoagulant component	Extracellular Space	other
A_32_P39093	FAM108C1	family with sequence similarity 108, member C1	unknown	enzyme
A_23_P167599	FAM134B	family with sequence similarity 134, member B	Cytoplasm	other
A_24_P38316	FOXP2	forkhead box P2	Nucleus	transcription

				regulator
A_23_P11543	FUCA1	fucosidase, alpha-L- 1, tissue	Cytoplasm	enzyme
A_23_P25964	GALC	galactosylceramidase	Cytoplasm	enzyme
A_24_P217489	GLRB	glycine receptor, beta	Plasma Membrane	ion channel
A_23_P416581	GNAZ	guanine nucleotide binding protein (G protein), alpha z polypeptide	Plasma Membrane	enzyme
A_32_P132317	GPR155	G protein-coupled receptor 155	Plasma Membrane	G-protein coupled receptor
A_23_P139864	GSG1	germ cell associated 1	Cytoplasm	other
A_23_P98431	HMBS	hydroxymethylbilane synthase	Cytoplasm	enzyme
A_32_P50924	HNRNPA1L2	heterogeneous nuclear ribonucleoprotein A1-like 2	Nucleus	other
A_23_P170687	HSPBP1	HSPA (heat shock 70kDa) binding protein, cytoplasmic cochaperone 1	unknown	other
A_23_P48513	IFI27	interferon, alpha-inducible protein 27	Cytoplasm	other
A_23_P343954	IGF2BP1	insulin-like growth factor 2 mRNA binding protein 1	Cytoplasm	translation regulator
A_23_P19987	IGF2BP3	insulin-like growth factor 2 mRNA binding protein 3	Cytoplasm	translation regulator
A_23_P257956	ILF2	interleukin enhancer binding factor 2, 45kDa	Nucleus	transcription regulator
A_32_P87872	IMMP2L	IMP2 inner mitochondrial membrane peptidase-like (S. cerevisiae)	Cytoplasm	peptidase
A_23_P19852	IQCE	IQ motif containing E	Cytoplasm	other
A_23_P324523	IQCK	IQ motif containing K	unknown	other
A_23_P112201	KDM4C	lysine (K)-specific demethylase 4C	Nucleus	other
A_32_P151544	KRT18	keratin 18	Cytoplasm	other
A_23_P93750	LSM5	LSM5 homolog, U6 small nuclear RNA associated (S. cerevisiae)	Cytoplasm	other
A_24_P314640	MDGA1	MAM domain containing glycosylphosphatidylinositol anchor 1	Plasma Membrane	other
A_23_P61945	MITF	microphthalmia-associated transcription factor	Nucleus	transcription regulator
A_23_P135474	MRPL37	mitochondrial ribosomal protein L37	Cytoplasm	enzyme
A_32_P117170	NAPEPLD	N-acyl phosphatidylethanolamine phospholipase D	Cytoplasm	enzyme
A_24_P367752	NDST1	N-deacetylase/N-sulfotransferase (heparan glucosaminyl) 1	Cytoplasm	enzyme
A_23_P300600	NEFH	neurofilament, heavy polypeptide	Cytoplasm	other
A_23_P91328	NOP56	NOP56 ribonucleoprotein homolog (yeast)	Nucleus	other
A_23_P59547	NT5C3	5'-nucleotidase, cytosolic III	Cytoplasm	phosphatase
A_24_P360206	PCDHA11	protocadherin alpha 11	Plasma Membrane	other
A_32_P116857	PDE11A	phosphodiesterase 11A	Cytoplasm	enzyme
A_23_P411723	PLAG1	pleiomorphic adenoma gene 1	Nucleus	transcription regulator
A_23_P17914	PNPLA3	patatin-like phospholipase domain containing 3	Cytoplasm	enzyme
A_24_P570049	PPARA	peroxisome proliferator-activated receptor alpha	Nucleus	ligand-dependent nuclear receptor
A_23_P60458	PPP2R4	protein phosphatase 2A activator, regulatory subunit 4	Cytoplasm	phosphatase
A_23_P146554	PTGDS	prostaglandin D2 synthase 21kDa (brain)	Cytoplasm	enzyme
A_23_P203729	RAB6A	RAB6A, member RAS oncogene family	Cytoplasm	enzyme
A_23_P166087	RASSF2	Ras association (RalGDS/AF-6) domain family member 2	Nucleus	other
A_23_P9056	RB1CC1	RB1-inducible coiled-coil 1	Nucleus	other

A_23_P133596	DROSHA	drosha, ribonuclease type III	Nucleus	enzyme
A_24_P199500	RNF2	ring finger protein 2	Nucleus	transcription regulator
A_23_P6802	RRP9	ribosomal RNA processing 9, small subunit (SSU) processome component, homolog (yeast)	Nucleus	other
A_32_P161762	RUNX2	runt-related transcription factor 2	Nucleus	transcription regulator
A_23_P259741	SATB1	SATB homeobox 1	Nucleus	transcription regulator
A_23_P152548	SCPEP1	serine carboxypeptidase 1	Cytoplasm	peptidase
A_23_P150092	SEPHS1	selenophosphate synthetase 1	unknown	enzyme
A_23_P106299	SERF2	small EDRK-rich factor 2	unknown	other
A_32_P4595	SGCD	sarcoglycan, delta (35kDa dystrophin-associated glycoprotein)	Cytoplasm	other
A_23_P139260	SLC22A18	solute carrier family 22, member 18	Plasma Membrane	transporter
A_23_P436179	SLC25A5	solute carrier family 25 (mitochondrial carrier; adenine nucleotide translocator), member 5	Cytoplasm	transporter
A_23_P24345	SLC39A13	solute carrier family 39 (zinc transporter), member 13	unknown	transporter
A_23_P50167	SLC39A6	solute carrier family 39 (zinc transporter), member 6	Plasma Membrane	transporter
A_23_P154675	SNRPB	small nuclear ribonucleoprotein polypeptides B and B1	Nucleus	other
A_32_P43711	SOCS7	suppressor of cytokine signaling 7	Cytoplasm	other
A_32_P89755	SSR1	signal sequence receptor, alpha	Cytoplasm	other
A_23_P36076	SSRP1	structure specific recognition protein 1	Nucleus	other
A_23_P43164	SULF1	sulfatase 1	Cytoplasm	enzyme
A_23_P96965	SYNC	syncoilin, intermediate filament protein	Cytoplasm	other
A_32_P66881	TLR4	toll-like receptor 4	Plasma Membrane	transmembrane receptor
A_23_P103282	TMEM59	transmembrane protein 59	Plasma Membrane	other
A_23_P216522	TMEM8B	transmembrane protein 8B	Plasma Membrane	other
A_23_P421423	TNFAIP2	tumor necrosis factor, alpha-induced protein 2	Extracellular Space	other
A_23_P363344	TPM1 (includes EG:22003)	tropomyosin 1 (alpha)	Cytoplasm	other
A_23_P16683	TRMT1	TRM1 tRNA methyltransferase 1 homolog (S. cerevisiae)	unknown	enzyme
A_23_P79510	VPS24	vacuolar protein sorting 24 homolog (S. cerevisiae)	Cytoplasm	other
A_23_P141394	WIPI1	WD repeat domain, phosphoinositide interacting 1	Cytoplasm	other
A_23_P211926	WNT5A	wingless-type MMTV integration site family, member 5A	Extracellular Space	cytokine
A_32_P34516	XKR6	XK, Kell blood group complex subunit-related family, member 6	unknown	other
A_23_P134527	YKT6	YKT6 v-SNARE homolog (S. cerevisiae)	Cytoplasm	enzyme

Table 2. Gene sets more higly expressed in fibroblast strains from young subjects when compared with strains from old subjects, and significantly enriched at FDR<0.25, identified by GSEA.

Gene set	p	FDR	ES	NES
MITOCHONDRIAL_INNER_MEMBRANE	0.010	0.163	-0.58	-17.72
SPINDLE	0.000	0.217	-0.85	-16.00
NUCLEAR_EXPORT	0.024	0.218	-0.54	-15.76
PORE_COMPLEX	0.027	0.220	-0.63	-16.04
MICROTUBULE_ORGANIZING_CENTER	0.010	0.225	-0.58	-15.81
SPINDLE_POLE	0.004	0.226	-0.84	-15.77
SPLICEOSOME	0.048	0.228	-0.55	-15.92
MITOCHONDRIAL_PART	0.054	0.229	-0.44	-16.05
RNA_DEPENDENT_ATPASE_ACTIVITY	0.008	0.230	-0.71	-16.15
MITOCHONDRIAL_RIBOSOME	0.052	0.231	-0.62	-1.62
MICROTUBULE_ORGANIZING_CENTER_PART	0.024	0.231	-0.65	-15.82
RNA_BINDING	0.017	0.233	-0.36	-15.86
MITOCHONDRIAL_MEMBRANE	0.008	0.235	-0.52	-17.75
MICROTUBULE_CYTOSKELETON	0.020	0.235	-0.57	-1.55
NUCLEOLUS	0.008	0.235	-0.48	-16.61
SMALL_NUCLEAR_RIBONUCLEOPROTEIN_COMPLEX	0.012	0.239	-0.66	-17.21
MITOCHONDRIAL_MEMBRANE_PART	0.076	0.239	-0.52	-15.51
CYTOSKELETAL_PART	0.018	0.239	-0.52	-15.48
MITOCHONDRIAL_ENVELOPE	0.039	0.240	-0.46	-1.63
NUCLEAR_LUMEN	0.010	0.240	-0.41	-15.31
VIRAL_REPRODUCTIVE_PROCESS	0.006	0.242	-0.64	-16.05
ORGANELLE_INNER_MEMBRANE	0.020	0.244	-0.53	-17.03
FEMALE_GAMETE_GENERATION	0.029	0.244	-0.72	-15.32
RNA_HELICASE_ACTIVITY	0.013	0.246	-0.68	-16.42
VIRAL_REPRODUCTION	0.011	0.246	-0.59	-15.40
RIBOSOMAL_SUBUNIT	0.063	0.247	-0.63	-15.51
ORGANELLAR_RIBOSOME	0.052	0.247	-0.62	-1.62
ATP_DEPENDENT_HELICASE_ACTIVITY	0.004	0.247	-0.69	-16.67
TRANSLATION_FACTOR_ACTIVITY__NUCLEIC_ACID_BINDING	0.044	0.248	-0.53	-15.36

FDR: false discovery rate, ES: enrichment score, NES: normalised enrichment score

p16

An expression probe corresponding to p16 was the most significantly differentially expressed probe between fibroblast strains from young and old subjects, being higher in strains from old subjects. Rotenone-treatment resulted in decreases in p16 mRNA expression after three hours and even more so after three days which were similar for fibroblast strains from young and old subjects, i.e. there was no significant rotenone-age interaction. This was validated by qPCR (non-stressed=1, fold change 3 hours rotenone [mean±SE]: 0.74±0.04, fold change 3 days rotenone: 0.67±0.04, $p<0.001$). For each condition, p16 mRNA levels were found to be higher in fibroblast strains from old subjects (Supplemental table 2). To verify these results, we performed a replication experiment on fibroblast strains from a new set of ten young and ten old subjects (age: 25.5±1.8 [mean±SD] and 90.2±0.3 years). To assess the rotenone-induced stress response, levels of reactive oxygen species (ROS [MdFI in arbitrary units] non-stressed: 1580±70 [mean±SE], rotenone: 2181±124, $p<0.001$) and SA-β-gal activity ([MdFI in arbitrary units] non-stressed: 2793±278, rotenone: 4278±330, $p<0.001$) were measured. There was no difference in SA-β-gal activity between strains from young and old subjects, but strains from old subjects did show a greater rotenone-induced increase in SA-β-gal activity (Supplemental table 2). Under non-stressed conditions ROS levels were higher in strains from old subjects (MdFI in arbitrary units, young: 1500±150, old: 1656±148, $p=0.027$), but there were no differences in rotenone-induced increases. p16 was measured by qPCR, Western blotting and immunocytochemistry (ICC). Consistent with the microarray experiments, p16 mRNA expression decreased (non-stressed=1, rotenone: 0.74±0.04, $p<0.001$). Under non-stressed conditions, fibroblast strains from old subjects showed significantly lower levels of p16 mRNA when compared with strains of young subjects (Supplemental table 2), contrary to the microarray results of the microarray experiment. Under stressed conditions there was no difference in p16 mRNA expression or protein levels. Western blotting demonstrated neither rotenone-induced changes in p16 protein levels, nor any differences between strains from young and old subjects. ICC showed rotenone-induced increases in p16 positive fibroblasts (Non-stressed: 2.40±0.31%, rotenone: 7.02±0.72%, $p<0.001$). Under non-stressed conditions percentages of p16-positive fibroblasts were higher for strains from old subjects when compared with strains from young subjects (young:

+1.39±0.31%, old: +3.05±0.31%, p<0.001), as were rotenone-induced increases in p16 positive percentages (young: +3.43±0.65%, old: +5.08±0.65%, p=0.060).

Discussion

In this study we addressed which pathways could be responsible for the reported differences in senescence and apoptosis between fibroblast strains from young and old subjects (25;37) using microarray methodology. Age-dependent differences were found in pathways involved in carbohydrate metabolism, Wnt/β-catenin signalling, the cytoskeleton, cell cycle, RNA-processing and mitochondrial function. No significant rotenone-age interactions were detected in this analysis indicating that the differences with age in mRNA levels were generally similar in stressed and non-stressed conditions.

Ingenuity analysis

Ingenuity analysis identified carbohydrate metabolism as the biological function that was most differentially expressed between strains from young and old subjects. The most significant pathway within this function was modification of glycosaminoglycans (GAGs), which are important components of the extracellular matrix (ECM). In support of this finding, it has been reported that physiological aging is associated with ECM remodeling, reflected by plasma GAGs concentrations (38). Genes involved in carbohydrate metabolism identified by Ingenuity were, amongst others, CD44, CXCL12 and TLR4. CD44 is a cell-surface glycoprotein important for cell-cell interactions, cell adhesion and migration (39;40). In aged fibroblasts, TGF-1-induced association between CD44 and EGF-R is lost with resultant suppression of ERK1/2 activation (41) and this might explain the lower CD44-expression in fibroblast strains from old subjects that we observed. In addition, CD44 is a receptor for hyaluran (HA), which is an important component of the ECM. HA acts through TLR4 and CD44 to stimulate an immune response against the septic response (42). Lower TLR4 activity has also been linked to reduced inflammatory response and successful aging (43), consistent with the higher TLR4-expression in fibroblast strains from old subjects observed in

the study reported here. CXCL12/SDF-1 is a chemotactic cytokine involved in cell motility (44) and showed lower expression in fibroblast strains from old subjects, correlating well with the decreased expression with age reported in animal models (45). Taken together, these results suggest that differences in cell to cell signaling might explain the differential regulation of carbohydrate metabolism between fibroblast strains from young and old subjects.

The most significant canonical pathway identified by the Ingenuity analysis was the Wnt/β-catenin pathway, which is frequently deregulated in cancer (46;47) and consists of, amongst others, the genes B-TRCP, CK2, CDKN2A (or p14/p16: see below) and WNT5A. WNT5A-expression was higher in fibroblast strains from old subjects, consistent with reduced cell proliferation in fibroblast strains from old subjects (25) and age-dependent increased WNT5A-expression reported for animal models (48). In support of this, the top Ingenuity network indicated reduced cell proliferation in fibroblast strains from old subjects via the increases found in p15, p16 and RUNX2 mRNA. However, the expression levels of some genes were opposite to that expected. For example, B-TRCP is involved in ubiquitination and degradation of β-catenin which, as a consequence, leads to cell cycle arrest (49) and CK2 is activated by Wnt/β-catenin signalling (50). We found lower B-TRCP and CK2 expression in fibroblast strains from old subjects, suggesting increased cell proliferation. Thus, although the Ingenuity analysis indicated reduced cellular proliferation in fibroblast strains from old subjects, some contradictory findings warrant further pathway analysis to validate the findings.

GSEA analysis

GSEA pathway analysis resulted in gene sets such as spindle, spindle pole and microtubule organizing centre showing lower expression in fibroblast strains from old subjects, supporting the view that there was inhibition of the cell cycle in fibroblast strains from the old subjects. In addition, there was an increased activity of pathways linked to RNA processing in the young strains, consistent with the idea that with cellular aging (senescence) the expression of many genes required for the cell cycle decrease (51). Indeed, fewer senescent fibroblasts are observed in strains from young subjects (25). Combined with the Ingenuity analysis, these

results suggest a reduced cellular proliferation rate in fibroblast strains from old subjects, as we indeed showed recently (37).

Mitochondrial function was also detected by the GSEA analysis. This was striking because rotenone binds to the electron transport chain in mitochondria, disrupting the production of ATP (52). Our previous results demonstrated that rotenone treatment exacerbated differences in the number of fibroblasts entering cellular senescence and apoptosis between strains from young and old subjects (25). Thus, as mitochondrial membrane potential is impaired in fibroblasts from old subjects (53), rotenone insult could lead to greater ROS production in the fibroblasts from the old subjects and consequently more cellular senescence.

GSEA analysis also identified the Glutamate Signaling Pathway gene set as the most differentially upregulated pathway in the fibroblast strains from the old subjects. Although fibroblasts are known to utilize glutamate signaling (54), very little is known about the role glutamate signaling plays in fibroblast function. These results are the first to indicate that glutamate signaling is upregulated with age in skin fibroblasts and the consequences of these changes on fibroblast function now requires further examination.

Boraldi et al. (55) also compared fibroblast strains from young and old subjects (ex vivo aging model) at early and late CPDs (in vitro aging model). While showing the majority of differences, like stress response, endoplasmic reticulum and cell membrane compartments and post-translational protein modifications, for in vitro aging, they did not observe many differences dependent on the age of subjects. It must be noted, though, that they used only three strains per age group. Although the effect was more pronounced in in vitro aging, they did find that deterioration of the redox balance depended on the subjects' age, consistent with the difference in expression of genes involved in mitochondrial function that reported here. Furthermore, elastin and fibulin-5 expression, both important ECM components, were differently expressed in cultures between fibroblast strains from young and old donors, consistent with the different expression of genes involved in ECM remodeling, cell-cell interactions and cell adhesion reported here.

p16

The gene most differentially expressed between fibroblast strains from young and old subjects was p16 and this microarray finding was confirmed by qPCR. p16 is regarded as a robust marker for cellular aging and senescence (2;56) and increasing numbers of p16-positive cells can indeed be found in mitotic aging of aging primates (57;58). We hypothesized that increased numbers of senescent cells (SA-β-gal activity) would be paralleled by p16 mRNA after rotenone-treatment. However, a decrease was observed in both the microarray experiment and the replication experiment. Furthermore, Western blot analyses could not show rotenone-induced differences in p16 protein levels whereas ICC did show rotenone-induced increased numbers of p16-positive fibroblasts. Thus, p16 mRNA levels were not reflected by p16 protein levels as measured by Western blot analysis and ICC.

Regulation of p16 activity can occur at different levels: transcription, mRNA stability, translation and protein stability. p16 mRNA stability is controlled by genes regulating the degradation of p16 mRNA which are down-regulated in late passage fibroblasts (59;60). In addition, p16 protein levels can increase in the absence of changes to p16 mRNA levels via changes to p16 protein stability (61;62). Thus, in senescent cells p16 mRNA and protein levels are likely to be stable whereas p16 protein stabilization rather than increased p16 mRNA levels could be responsible for non-senescent cells entering cell arrest. Another explanation could be that the microarray and qPCR probes both corresponded to the 3' end of the gene which is common to at least two gene transcripts (p14 and p16) whereas the proteins transcribed from the locus are unique in sequence (63). Thus, differential regulation of the different transcripts between the two experiments might well dissociate any concordance that actually exists between p16 mRNA and protein levels. The discrepancies between ICC and Western blotting could be explained by the fact that the ICC method scores each fibroblast dichotomously, while Western blotting measures the average level of all fibroblasts, underestimating the p16 positivity of some fibroblasts and overestimating the negativity of other fibroblasts, resulting in no average change.

In the microarray experiments the fibroblast strains from the old subjects showed higher levels of p16 mRNA expression for all three conditions (non-stressed, 3 hours and 3 days rotenone) consistent with increasing numbers of p16-positive fibroblasts in aging primates (57;64). No differences in the rotenone-induced fold changes in p16 mRNA expression were detected. In contrast to the microarray experiments the replication experiments showed lower expression of p16 mRNA in strains from old subjects (non-stressed) and rotenone induced a smaller decrease in p16 mRNA expression in these strains. The consistency of the p16 mRNA results across strains within each experiment, and the concordance of the ICC results across experiments indicated that the cause of this difference was technical in nature and specific to the mRNA. For example, a higher seeding density (to maximize mRNA yield) used for the microarray experiment compared with the replication experiments could have lead to differential regulation of p16 expression (65). Alternatively, changes to the expression of the housekeeping gene used in the qPCR experiments could have resulted in different qPCR results. Further detailed work investigating differences in p16 mRNA between fibroblast strains from young and old subjects, along with epistatic control of p16 mRNA levels is now required. However, as the most accurate reflection of p16 function, the ICC results reflected the gene array pathway analyses, the SA-β-gal activity and previous reported work (29) that cell cycle arrest is higher in fibroblasts strains from old subjects compared with young subjects. These results suggest that mRNA is not necessarily the best marker of p16 and ICC might be a better candidate.

In conclusion, from the microarray analyses emerged pathways involved in carbohydrate metabolism, cell cycle, mitochondrial function, glutamate signaling and RNA processing. The cell cycle inhibitor p16, involved in senescence, was the most significantly differentially expressed mRNA between fibroblast strains from young and old subjects. The discrepancies between the microarray experiments and the replication experiments could be explained by non-representative strain selection and/or technical issues regarding seeding density. Future work with higher numbers of fibroblast strains will need to identify common pathways between the contrast in chronological age and biological age (e.g. familial longevity). These pathways might then be manipulated, resulting in biologically old cells becoming biologically younger, i.e. resemble chronologically cells.

References

(1) Campisi J. Cellular senescence and apoptosis: how cellular responses might influence aging phenotypes. Exp Gerontol 2003;38:5-11.

(2) Ben-Porath I, Weinberg RA. The signals and pathways activating cellular senescence. Int J Biochem Cell Biol 2005;37:961-976.

(3) Han E, Hilsenbeck SG, Richardson A, Nelson JF. cDNA expression arrays reveal incomplete reversal of age-related changes in gene expression by calorie restriction. Mech Ageing Dev 2000;20;115:157-174.

(4) Prolla TA. DNA microarray analysis of the aging brain. Chem Senses 2002;27:299-306.

(5) Crott JW, Choi SW, Ordovas JM, Ditelberg JS, Mason JB. Effects of dietary folate and aging on gene expression in the colonic mucosa of rats: implications for carcinogenesis. Carcinogenesis 2004;25:69-76.

(6) Ida H, Boylan SA, Weigel AL, Hjelmeland LM. Age-related changes in the transcriptional profile of mouse RPE/choroid. Physiol Genomics 2003;15:258-262.

(7) Lluel P, Palea S, Ribiere P, Barras M, Teillet L, Corman B. Increased adrenergic contractility and decreased mRNA expression of NOS III in aging rat urinary bladders. Fundam Clin Pharmacol 2003;17:633-641.

(8) Vazquez-Padron RI, Lasko D, Li S, Louis L, Pestana IA, Pang M, Liotta C, Fornoni A, Aitouche A, Pham SM. Aging exacerbates neointimal formation, and increases proliferation and reduces susceptibility to apoptosis of vascular smooth muscle cells in mice. J Vasc Surg 2004;40:1199-1207.

(9) Edwards MG, Anderson RM, Yuan M, Kendziorski CM, Weindruch R, Prolla TA. Gene expression profiling of aging reveals activation of a p53-mediated transcriptional program. BMC Genomics 2007;8:80.:80.

(10) Meyer RA, Jr., Desai BR, Heiner DE, Fiechtl J, Porter S, Meyer MH. Young, adult, and old rats have similar changes in mRNA expression of many skeletal genes after fracture despite delayed healing with age. J Orthop Res 2006;24:1933-1944.

(11) Edwards MG, Sarkar D, Klopp R, Morrow JD, Weindruch R, Prolla TA. Impairment of the transcriptional responses to oxidative stress in the heart of aged C57BL/6 mice. Ann N Y Acad Sci 2004;1019:85-95.:85-95.

(12) Tollet-Egnell P, Parini P, Stahlberg N, Lonnstedt I, Lee NH, Rudling M, Flores-Morales A, Norstedt G. Growth hormone-mediated alteration of fuel metabolism in the aged rat as determined from transcript profiles. Physiol Genomics 2004;16:261-267.

(13) Park SK, Prolla TA. Gene expression profiling studies of aging in cardiac and skeletal muscles. Cardiovasc Res 2005;66:205-212.

(14) Kyng KJ, May A, Kolvraa S, Bohr VA. Gene expression profiling in Werner syndrome closely resembles that of normal aging. P Natl Acad Sci USA 2003;100:12259-12264.

(15) Geigl JB, Langer S, Barwisch S, Pfleghaar K, Lederer G, Speicher MR. Analysis of gene expression patterns and chromosomal changes associated with aging. Cancer Res 2004;64:8550-8557.

(16) Melk A, Mansfield ES, Hsieh SC, Hernandez-Boussard T, Grimm P, Rayner DC, Halloran PF, Sarwal MM. Transcriptional analysis of the molecular basis of human kidney aging using cDNA microarray profiling. Kidney Int 2005;68:2667-2679.

(17) Lazuardi L, Herndler-Brandstetter D, Brunner S, Laschober GT, Lepperdinger G, Grubeck-Loebenstein B. Microarray analysis reveals similarity between CD8+CD28- T cells from young and elderly persons, but not of CD8+CD28+ T cells. Biogerontology 2009;10:191-202.

(18) Welle S, Brooks A, Thornton CA. Senescence-related changes in gene expression in muscle: similarities and differences between mice and men. Physiol Genomics 2001;5:67-73.

(19) Hazane-Puch F, Bonnet M, Valenti K, Schnebert S, Kurfurst R, Favier A, Sauvaigo S. Study of fibroblast gene expression in response to oxidative stress induced by hydrogen peroxide or UVA with skin aging. Eur J Dermatol 2010;20:308-320.

(20) Lener T, Moll PR, Rinnerthaler M, Bauer J, Aberger F, Richter K. Expression profiling of aging in the human skin. Exp Gerontol 2006;41:387-397.

(21) Ma H, Li R, Zhang Z, Tong T. mRNA level of alpha-2-macroglobulin as an aging biomarker of human fibroblasts in culture. Exp Gerontol 2004;39:415-421.

(22) Welle S, Brooks AI, Delehanty JM, Needler N, Bhatt K, Shah B, Thornton CA. Skeletal muscle gene expression profiles in 20-29 year old and 65-71 year old women. Exp Gerontol 2004;39:369-377.

(23) Welle S, Brooks AI, Delehanty JM, Needler N, Thornton CA. Gene expression profile of aging in human muscle. Physiol Genomics 2003;14:149-159.

(24) Thomas RP, Guigneaux M, Wood T, Evers BM. Age-associated changes in gene expression patterns in the liver. J Gastrointest Surg 2002;6:445-453.

(25) Dekker P, Maier AB, van HD, de Koning-Treurniet C, Blom J, Dirks RW, Tanke HJ, Westendorp RG. Stress-induced responses of human skin fibroblasts in vitro reflect human longevity. Aging Cell 2009;8:595-603.

(26) Bootsma-van der Wiel A, Gussekloo J, de Craen AJM, van Exel E, Bloem BR, Westendorp RGJ. Common chronic diseases and general impairments as determinants of walking disability in the oldest-old population. J Am Geriatr Soc 2002;50:1405-1410.

(27) Maier AB, le Cessie S, Koning-Treurniet C, Blom J, Westendorp RG, van Heemst D. Persistence of high-replicative capacity in cultured fibroblasts from nonagenarians. Aging Cell 2007;6:27-33.

(28) Li N, Ragheb K, Lawler G, Sturgis J, Rajwa B, Melendez JA, Robinson JP. Mitochondrial complex I inhibitor rotenone induces apoptosis through enhancing mitochondrial reactive oxygen species production. J Biol Chem 2003;278:8516-8525.

(29) Noppe G, Dekker P, Koning-Treurniet C, Blom J, van Heemst D, Dirks RJ, Tanke HJ, Westendorp RG, Maier AB. Rapid flow cytometric method for measuring Senescence Associated â-galactosidase activity in human fibroblasts. Cytometry A 2009;75:910-916.

(30) Edgar R, Domrachev M, Lash AE. Gene Expression Omnibus: NCBI gene expression and hybridization array data repository. Nucleic Acids Res 2002;30:207-210.

(31) Barrett T, Troup DB, Wilhite SE, Ledoux P, Evangelista C, Kim IF, Tomashevsky M, Marshall KA, Phillippy KH, Sherman PM, Muertter RN, Holko M, Ayanbule O, Yefanov A, Soboleva A. NCBI GEO: archive for functional genomics data sets--10 years on. Nucleic Acids Res 2011;39:D1005-D1010.

(32) Ihaka R, Gentleman R. R: a language for data analysis and graphics. J Comput Graph Stat 1996;5:299-314.

(33) Ritchie ME, Silver J, Oshlack A, Holmes M, Diyagama D, Holloway A, Smyth GK. A comparison of background correction methods for two-colour microarrays. Bioinformatics 2007;23:2700-2707.

(34) Smyth GK. Linear models and empirical bayes methods for assessing differential expression in microarray experiments. Stat Appl Genet Mol Biol 2004;3:Article3.

(35) Subramanian A, Tamayo P, Mootha VK, Mukherjee S, Ebert BL, Gillette MA, Paulovich A, Pomeroy SL, Golub TR, Lander ES, Mesirov JP. Gene set enrichment analysis: a knowledge-based approach for interpreting genome-wide expression profiles. P Natl Acad Sci USA 2005;102:15545-15550.

(36) Mootha VK, Lindgren CM, Eriksson KF, Subramanian A, Sihag S, Lehar J, Puigserver P, Carlsson E, Ridderstrale M, Laurila E, Houstis N, Daly MJ, Patterson N, Mesirov JP, Golub TR, Tamayo P, Spiegelman B, Lander ES, Hirschhorn JN, Altshuler D, Groop LC. PGC-1alpha-responsive genes involved in oxidative phosphorylation are coordinately downregulated in human diabetes. Nat Genet 2003;34:267-273.

(37) Dekker P, van Baalen LM, Dirks RW, Slagboom PE, van Heemst D, Tanke HJ, Westendorp RGJ, Maier AB. Chronic inhibition of the respiratory chain differentially affects fibroblast strains from young and old subjects. J Gerontol A Biol Sci Med Sci 2011 Nov 10 [Epub ahead of print].

(38) Komosinska-Vassev K, Olczyk P, Winsz-Szczotka K, Klimek K, Olczyk K. Age- and gender-dependent changes in circulating concentrations of tumor necrosis factor-alpha, soluble tumor necrosis factor receptor-1 and sulfated glycosaminoglycan in healthy people. Clin Chem Lab Med 2011;49:121-127.

(39) Naor D, Nedvetzki S. CD44 in rheumatoid arthritis. Arthritis Res Ther 2003;5:105-115.

(40) Robert L, Robert AM, Renard G. Biological effects of hyaluronan in connective tissues, eye, skin, venous wall. Role in aging. Pathol Biol (Paris) 2010;58:187-198.

(41) Simpson RM, Wells A, Thomas D, Stephens P, Steadman R, Phillips A. Aging fibroblasts resist phenotypic maturation because of impaired hyaluronan-dependent CD44/epidermal growth factor receptor signaling. Am J Pathol 2010;176:1215-1228.

(42) Muto J, Yamasaki K, Taylor KR, Gallo RL. Engagement of CD44 by hyaluronan suppresses TLR4 signaling and the septic response to LPS. Mol Immunol 2009;47:449-456.

(43) Balistreri CR, Candore G, Listi F, Fazio T, Gangi S, Incalcaterra E, Caruso M, Vecchi ML, Lio D, Caruso C. Role of TLR4 polymorphisms in inflammatory responses: implications for unsuccessful aging. Ann N Y Acad Sci 2007;1119:203-7.:203-207.

(44) Bleul CC, Fuhlbrigge RC, Casasnovas JM, Aiuti A, Springer TA. A highly efficacious lymphocyte chemoattractant, stromal cell-derived factor 1 (SDF-1). J Exp Med 1996;184:1101-1109.

(45) Loh SA, Chang EI, Galvez MG, Thangarajah H, El-ftesi S, Vial IN, Lin DA, Gurtner GC. SDF-1 alpha expression during wound healing in the aged is HIF dependent. Plast Reconstr Surg 2009;123:65S-75S.

(46) Fodde R, Brabletz T. Wnt/beta-catenin signaling in cancer stemness and malignant behavior. Curr Opin Cell Biol 2007;19:150-158.

(47) Dominguez I, Sonenshein GE, Seldin DC. Protein kinase CK2 in health and disease: CK2 and its role in Wnt and NF-kappaB signaling: linking development and cancer. Cell Mol Life Sci 2009;66:1850-1857.

(48) Rauner M, Sipos W, Pietschmann P. Age-dependent Wnt gene expression in bone and during the course of osteoblast differentiation. Age (Dordr) 2008;30:273-282.

(49) Sahasrabuddhe AA, Dimri M, Bommi PV, Dimri GP. Beta TrCP regulates BMI1 protein turnover via ubiquitination and degradation. Cell Cycle 2011;10.

(50) Gao Y, Wang HY. Casein kinase 2 Is activated and essential for Wnt/beta-catenin signaling. J Biol Chem 2006;281:18394-18400.

(51) Chen KY. Transcription factors and the down-regulation of G1/S boundary genes in human diploid fibroblasts during senescence. Front Biosci 1997;2:d417-26.:d417-d426.

(52) Koopman WJ, Nijtmans LG, Dieteren CE, Roestenberg P, Valsecchi F, Smeitink JA, Willems PH. Mammalian mitochondrial complex I: biogenesis, regulation, and reactive oxygen species generation. Antioxid Redox Signal 2010;12:1431-1470.

(53) Koziel R, Greussing R, Maier AB, Declercq L, Jansen-Durr P. Functional interplay between mitochondrial and proteasome activity in skin aging. J Invest Dermatol 2011;131:594-603.

(54) Zeng Y, Lv X, Zeng S, Shi J. Activity-dependent neuronal control of gap-junctional communication in fibroblasts. Brain Res 2009;1280:13-22.

(55) Boraldi F, Annovi G, Tiozzo R, Sommer P, Quaglino D. Comparison of ex vivo and in vitro human fibroblast ageing models. Mech Ageing Dev 2010;131:625-635..

(56) Campisi J, d'Adda di Fagagna F. Cellular senescence: when bad things happen to good cells. Nat Rev Mol Cell Biol 2007;8:729-740.

(57) Jeyapalan JC, Ferreira M, Sedivy JA, Herbig U. Accumulation of senescent cells in mitotic tissue of aging primates. Mechanisms of Ageing and Development 2007;128:36-44.

(58) Ressler S, Bartkova J, Niederegger H, Bartek J, Scharffetter-Kochanek K, Jansen-Durr P, Wlaschek M. p16INK4A is a robust in vivo biomarker of cellular aging in human skin. Aging Cell 2006;5:379-389.

(59) Chang N, Yi J, Guo G, Liu X, Shang Y, Tong T, Cui Q, Zhan M, Gorospe M, Wang W. HuR uses AUF1 as a cofactor to promote p16INK4 mRNA decay. Mol Cell Biol 2010;30:3875-3886.

(60) Wang W, Martindale JL, Yang X, Chrest FJ, Gorospe M. Increased stability of the p16 mRNA with replicative senescence. EMBO Rep 2005;6:158-164.

(61) Welcker M, Lukas J, Strauss M, Bartek J. Enhanced protein stability: a novel mechanism of D-type cyclin over-abundance identified in human sarcoma cells. Oncogene 1996;13:419-425.

(62) Al-Khalaf HH, Hendrayani SF, Aboussekhra A. The Atr Protein Kinase Controls UV-Dependent Upregulation of p16INK4A Through Inhibition of Skp2-Related Polyubiquitination/Degradation. Mol Cancer Res 2011;9:311-319.

(63) Collins CJ, Sedivy JM. Involvement of the INK4a/Arf gene locus in senescence. Aging Cell 2003;2:145-150.

(64) Herbig U, Ferreira M, Condel L, Carey D, Sedivy JM. Cellular senescence in aging primates. Science 2006;311:1257.

(65) Yanagisawa K, Kosaka A, Iwahana H, Nakanishi M, Tominaga S. Opposite regulation of the expression of cyclin-dependent kinase inhibitors during contact inhibition. J Biochem 1999;125:36-40.

Supplemental Table 1. List of 215 probes which were differentially expressed between fibroblast strains from young and old subjects

ID_REF	Log fold change	Fold change	Average Expression	t	*P* value	Adjusted *P* value	Beta	Systematic Name	Gene Symbol	GeneName
34090	-0.38	-1.46	7.48	-13.71	1.44E-14	6.49E-10	22.33	NM_058197	CDKN2A	cyclin-dependent kinase inhibitor 2A (melanoma, p16, inhibits CDK4)
1631	-0.21	-1.24	5.79	-11.82	6.64E-13	2.99E-08	18.93	NM_000132	F8	coagulation factor VIII, procoagulant component (hemophilia A)
9872	-1.08	-2.94	7.21	-11.53	1.23E-12	5.52E-08	18.38	NM_000063	C2	complement component 2
14382	0.20	1.22	5.84	11.39	1.67E-12	7.50E-08	18.10	NM_053042	KIAA1729	KIAA1729 protein
27247	-0.38	-1.46	7.58	-11.09	3.24E-12	1.46E-07	17.50	NM_058197	CDKN2A	cyclin-dependent kinase inhibitor 2A (melanoma, p16, inhibits CDK4)
16994	-0.30	-1.35	8.27	-10.87	5.29E-12	2.38E-07	17.05	NM_025163	PIGZ	phosphatidylinositol glycan anchor biosynthesis, class Z
44819	-0.36	-1.44	7.33	-10.71	7.49E-12	3.37E-07	16.73	NM_058197	CDKN2A	cyclin-dependent kinase inhibitor 2A (melanoma, p16, inhibits CDK4)
16344	-0.37	-1.45	7.58	-10.62	9.23E-12	4.16E-07	16.54	NM_058197	CDKN2A	cyclin-dependent kinase inhibitor 2A (melanoma, p16, inhibits CDK4)
13213	-0.38	-1.46	7.55	-10.56	1.05E-11	4.73E-07	16.42	NM_058197	CDKN2A	cyclin-dependent kinase inhibitor 2A (melanoma, p16, inhibits CDK4)
23491	-0.61	-1.84	6.30	-10.18	2.57E-11	1.16E-06	15.60	NM_001034850	FLJ20152	hypothetical protein FLJ20152
33922	-0.42	-1.52	5.95	-9.76	6.82E-11	3.07E-06	14.70	NM_000063	C2	complement component 2
38638	-0.34	-1.40	8.59	-9.58	1.06E-10	4.77E-06	14.29	NM_001116	ADCY9	adenylate cyclase 9
7444	0.21	1.23	8.03	9.31	2.04E-10	9.16E-06	13.68	NM_004704	RRP9	RRP9, small subunit (SSU) processome component, homolog (yeast)
32445	-0.32	-1.38	7.61	-9.15	3.04E-10	1.37E-05	13.31	NM_058197	CDKN2A	cyclin-dependent kinase inhibitor 2A (melanoma, p16, inhibits CDK4)
8451	0.41	1.50	5.90	9.10	3.46E-10	1.56E-05	13.18	NM_006546	IGF2BP1	insulin-like growth factor 2 mRNA binding protein 1
20244	-0.41	-1.51	6.11	-9.05	3.88E-10	1.75E-05	13.08	NM_138554	TLR4	toll-like receptor 4
41115	-0.21	-1.23	5.77	-8.99	4.51E-10	2.03E-05	12.94	NM_153487	MDGA1	MAM domain containing glycosylphosphatidylinositol anchor 1
13770	0.36	1.43	5.56	8.76	7.94E-10	3.57E-05	12.41	NM_005503	APBA2	amyloid beta (A4) precursor protein-binding, family A, member 2 (X11-like)
21416	0.48	1.62	5.81	8.61	1.18E-09	5.32E-05	12.03	NM_198159	MITF	microphthalmia-associated transcription factor
36293	-0.51	-1.66	8.85	-8.54	1.38E-09	6.22E-05	11.89	NM_032823	C9orf3	chromosome 9 open reading frame 3
32467	-0.73	-2.07	6.33	-8.43	1.86E-09	8.38E-05	11.61	NM_053276	VIT	vitrin
36113	-0.74	-2.09	8.71	-8.42	1.91E-09	8.58E-05	11.58	AF010236		
23396	-0.33	-1.40	7.66	-8.41	1.93E-09	8.67E-05	11.57	NM_058197	CDKN2A	cyclin-dependent kinase inhibitor 2A (melanoma, p16, inhibits CDK4)
11285	-0.25	-1.29	5.58	-8.39	2.06E-09	9.29E-05	11.51	NM_001034850	FLJ20152	hypothetical protein FLJ20152
8703	0.14	1.15	6.31	8.33	2.42E-09	1.09E-04	11.36	NM_177559	CSNK2A1	casein kinase 2, alpha 1 polypeptide
17352	-0.88	-2.41	5.83	-8.31	2.49E-09	1.12E-04	11.33	BC041856	LOC400879	hypothetical gene supported by AK096951
8334	-0.34	-1.40	5.86	-8.29	2.62E-09	1.18E-04	11.28	NM_138554	TLR4	toll-like receptor 4
42807	-0.24	-1.28	6.28	-8.24	3.02E-09	1.36E-04	11.15	NM_052937	PCMTD1	protein-L-isoaspartate (D-aspartate) O-methyltransferase domain containing 1
29312	-0.48	-1.62	7.14	-8.23	3.09E-09	1.39E-04	11.13	A_32_P225328		
29118	-0.32	-1.37	7.54	-8.23	3.09E-09	1.39E-04	11.13	NM_058197	CDKN2A	cyclin-dependent kinase inhibitor 2A (melanoma, p16, inhibits CDK4)
2500	-0.30	-1.35	5.78	-8.22	3.16E-09	1.42E-04	11.11	NM_138554	TLR4	toll-like receptor 4
12396	0.63	1.87	6.37	8.21	3.29E-09	1.48E-04	11.07	BC018626		
36691	-0.33	-1.39	5.78	-8.06	4.84E-09	2.18E-04	10.70	NM_138554	TLR4	toll-like receptor 4
41441	-0.52	-1.68	6.04	-8.00	5.58E-09	2.51E-04	10.57	NM_017549	EPDR1	ependymin related protein 1 (zebrafish)
31781	-0.34	-1.40	5.88	-7.97	6.16E-09	2.77E-04	10.48	NM_138554	TLR4	toll-like receptor 4
22430	0.19	1.20	5.56	7.96	6.27E-09	2.82E-04	10.46	THC2657663		
41609	-0.31	-1.36	5.73	-7.95	6.36E-09	2.86E-04	10.45	NM_138554	TLR4	toll-like receptor 4
12121	0.30	1.35	5.87	7.90	7.28E-09	3.27E-04	10.32	NM_022897	RANBP17	RAN binding protein 17
38751	-0.17	-1.18	5.95	-7.76	1.05E-08	4.72E-04	9.97	NM_001099407	C20orf12	chromosome 20 open reading frame 12
15998	-0.35	-1.41	7.49	-7.76	1.06E-08	4.76E-04	9.97	BC012888	NDST1	N-deacetylase/N-sulfotransferase (heparan glucosaminyl) 1
44393	-0.23	-1.26	10.21	-7.76	1.07E-08	4.81E-04	9.96	NM_017983	WIPI1	WD repeat domain, phosphoinositide interacting 1
14866	-0.50	-1.66	7.35	-7.75	1.07E-08	4.83E-04	9.95	NM_000147	FUCA1	fucosidase, alpha-L- 1, tissue
9503	-0.32	-1.37	5.84	-7.67	1.34E-08	6.03E-04	9.74	NM_138554	TLR4	toll-like receptor 4
44741	-0.15	-1.16	6.55	-7.63	1.49E-08	6.70E-04	9.64	NM_198181	FLJ40113	golgi autoantigen, golgin subfamily a-like pseudogene
39212	1.05	2.86	7.39	7.62	1.55E-08	6.97E-04	9.60	NM_006547	IGF2BP3	insulin-like growth factor 2 mRNA binding protein 3
32971	0.84	2.31	6.65	7.57	1.76E-08	7.90E-04	9.48	NM_021076	NEFH	neurofilament, heavy polypeptide 200kDa
10808	0.15	1.16	9.91	7.54	1.89E-08	8.51E-04	9.41	NM_006559	KHDRBS1	KH domain containing, RNA binding, signal transduction associated 1
31481	-0.29	-1.34	5.82	-7.54	1.92E-08	8.63E-04	9.40	NM_138554	TLR4	toll-like receptor 4
21362	-0.62	-1.86	7.54	-7.52	1.98E-08	8.91E-04	9.37	NM_025225	PNPLA3	patatin-like phospholipase domain containing 3
9389	1.43	4.19	8.44	7.52	2.01E-08	9.06E-04	9.35	XR_018843	LOC649233	similar to Keratin, type I cytoskeletal 18 (Cytokeratin-18) (CK-18) (Keratin-18) (K18)
38867	1.28	3.59	7.16	7.46	2.37E-08	1.06E-03	9.20	XR_019231	LOC442249	hypothetical LOC442249
40424	0.57	1.77	5.95	7.44	2.47E-08	1.11E-03	9.16	NM_198159	MITF	microphthalmia-associated transcription factor
22402	-0.34	-1.41	5.91	-7.42	2.64E-08	1.19E-03	9.10	NM_138554	TLR4	toll-like receptor 4
10241	0.22	1.24	11.21	7.39	2.84E-08	1.28E-03	9.03	NM_000610	CD44	CD44 molecule (Indian blood group)
36253	0.18	1.20	7.84	7.38	2.90E-08	1.31E-03	9.01	NM_044472	CDC42	cell division cycle 42 (GTP binding protein, 25kDa)
11681	0.14	1.15	6.33	7.36	3.06E-08	1.38E-03	8.96	NM_177559	CSNK2A1	casein kinase 2, alpha 1 polypeptide
11737	-0.52	-1.69	6.93	-7.35	3.17E-08	1.42E-03	8.92	NM_002073	GNAZ	guanine nucleotide binding protein (G protein), alpha z polypeptide
1686	0.30	1.35	6.00	7.34	3.27E-08	1.47E-03	8.90	NM_182520	C22orf15	chromosome 22 open reading frame 15
28832	-0.38	-1.46	6.19	-7.31	3.47E-08	1.56E-03	8.84	NM_020777	SORCS2	sortilin-related VPS10 domain containing receptor 2
2909	-0.31	-1.36	5.59	-7.29	3.69E-08	1.66E-03	8.78	NM_000063	C2	complement component 2
44689	1.20	3.32	6.96	7.27	3.94E-08	1.77E-03	8.72	A_24_P383660	LOC643471	similar to Keratin, type I cytoskeletal 18 (Cytokeratin-18) (CK-18) (Keratin-18) (K18)
42458	-0.40	-1.50	8.91	-7.26	3.99E-08	1.79E-03	8.71	NM_012156	EPB41L1	erythrocyte membrane protein band 4,1-like 1
36702	-0.27	-1.31	7.95	-7.26	4.01E-08	1.80E-03	8.70	NM_001002009	NT5C3	5'-nucleotidase, cytosolic III
34895	1.19	3.29	7.03	7.21	4.64E-08	2.09E-03	8.56	A_24_P418687	LOC731794	similar to Keratin, type I cytoskeletal 18 (Cytokeratin-18) (CK-18) (Keratin-18) (K18)
12527	1.43	4.17	8.55	7.20	4.69E-08	2.11E-03	8.55	NM_000224	KRT18	keratin 18
33355	1.31	3.72	7.68	7.20	4.69E-08	2.11E-03	8.55	A_24_P161733		
6848	1.34	3.81	7.42	7.20	4.75E-08	2.13E-03	8.54	NM_000224	KRT18	keratin 18
9893	0.26	1.29	10.20	7.20	4.77E-08	2.14E-03	8.54	NM_001152	SLC25A5	solute carrier family 25 (mitochondrial carrier; adenine nucleotide translocator), member 5
10253	-0.76	-2.14	5.74	-7.19	4.87E-08	2.19E-03	8.52	BG118529		
16140	-0.17	-1.19	6.42	-7.18	4.96E-08	2.23E-03	8.50	NM_052937	PCMTD1	protein-L-isoaspartate (D-aspartate) O-methyltransferase domain containing 1
38804	1.79	6.00	7.06	7.15	5.43E-08	2.44E-03	8.41	NM_018476	BEX1	brain expressed, X-linked 1
17731	-0.60	-1.83	7.43	-7.12	5.87E-08	2.64E-03	8.34	NM_138554	TLR4	toll-like receptor 4

6264	0.26	1.30	8.83	7.12	5.88E-08	2.64E-03	8.34	NM_198216	SNRPB	small nuclear ribonucleoprotein polypeptides B and B1
12633	-0.08	-1.08	5.41	-7.12	5.96E-08	2.68E-03	8.32	NM_000132	F8	coagulation factor VIII, procoagulant component (hemophilia A)
23023	0.23	1.25	8.08	7.09	6.44E-08	2.89E-03	8.25	NM_178001	PPP2R4	protein phosphatase 2A, regulatory subunit B' (PR 53)
19790	-0.39	-1.48	8.51	-7.08	6.59E-08	2.96E-03	8.23	NM_032823	C9orf3	chromosome 9 open reading frame 3
1258	0.13	1.14	5.71	7.08	6.65E-08	2.99E-03	8.22	NM_014598	SOCS7	suppressor of cytokine signaling 7
14815	-0.19	-1.21	10.06	-7.07	6.78E-08	3.05E-03	8.20	NM_198868	TBC1D9B	TBC1 domain family, member 9B (with GRAM domain)
14598	0.15	1.16	9.18	7.06	6.87E-08	3.09E-03	8.19	NM_012247	SEPHS1	selenophosphate synthetase 1
25318	0.26	1.29	12.20	7.05	7.10E-08	3.19E-03	8.16	NM_001037808	EIF3S8	eukaryotic translation initiation factor 3, subunit 8, 110kDa
37363	-0.32	-1.37	6.37	-7.04	7.24E-08	3.25E-03	8.14	NM_031289	GSG1	germ cell associated 1
20510	0.48	1.62	8.14	7.04	7.29E-08	3.28E-03	8.13	NM_001970	EIF5A	eukaryotic translation initiation factor 5A
37652	-0.21	-1.23	11.25	-7.03	7.46E-08	3.35E-03	8.11	NM_152264	SLC39A13	solute carrier family 39 (zinc transporter), member 13
44533	-0.14	-1.15	5.34	-7.03	7.58E-08	3.40E-03	8.10	AK056135		
21753	-0.27	-1.31	6.26	-7.02	7.82E-08	3.51E-03	8.07	ENST00000270457	ZNF160	zinc finger protein 160
29622	-0.30	-1.35	6.29	-7.01	7.85E-08	3.53E-03	8.06	NM_000824	GLRB	glycine receptor, beta
4527	-0.32	-1.38	7.33	-6.96	9.01E-08	4.05E-03	7.93	NM_153208	IQCK	IQ motif containing K
7859	0.45	1.57	11.13	6.96	9.17E-08	4.12E-03	7.91	NM_199168	CXCL12	chemokine (C-X-C motif) ligand 12 (stromal cell-derived factor 1)
33380	-0.40	-1.49	8.41	-6.95	9.45E-08	4.25E-03	7.88	NM_000153	GALC	galactosylceramidase
38585	0.18	1.20	9.28	6.94	9.54E-08	4.29E-03	7.88	NM_016491	MRPL37	mitochondrial ribosomal protein L37
20182	1.83	6.24	7.58	6.94	9.57E-08	4.30E-03	7.87	NM_032621	BEX2	brain expressed X-linked 2
39594	-0.23	-1.26	9.69	-6.92	1.01E-07	4.55E-03	7.82	NM_016079	VPS24	vacuolar protein sorting 24 homolog (S, cerevisiae)
2154	-0.23	-1.26	7.04	-6.91	1.04E-07	4.68E-03	7.79	NM_005036	PPARA	peroxisome proliferator-activated receptor alpha
2770	1.04	2.84	6.48	6.89	1.11E-07	5.01E-03	7.73	XR_016695	LOC345430	similar to Keratin, type I cytoskeletal 18 (Cytokeratin-18) (CK-18) (Keratin-18) (K18)
32638	-0.35	-1.42	9.39	-6.88	1.13E-07	5.09E-03	7.71	NM_006291	TNFAIP2	tumor necrosis factor, alpha-induced protein 2
17317	-1.16	-3.19	8.59	-6.87	1.18E-07	5.28E-03	7.68	NM_017549	EPDR1	ependymin related protein 1 (zebrafish)
304	-0.11	-1.12	5.62	-6.86	1.20E-07	5.37E-03	7.66	AK091348		
4565	0.20	1.22	8.25	6.82	1.33E-07	5.97E-03	7.56	NM_007002	ADRM1	adhesion regulating molecule 1
7041	-0.15	-1.16	6.16	-6.82	1.33E-07	5.97E-03	7.56	NM_152331	ACOT4	acyl-CoA thioesterase 4
31016	-0.31	-1.37	5.90	-6.81	1.36E-07	6.10E-03	7.54	NM_138554	TLR4	toll-like receptor 4
6486	0.17	1.18	10.75	6.80	1.43E-07	6.43E-03	7.49	NM_001011724	RP11-78J21,1	heterogeneous nuclear ribonucleoprotein A1-like
19297	-0.35	-1.42	9.20	-6.78	1.47E-07	6.62E-03	7.46	NM_030786	SYNC1	syncoilin, intermediate filament 1
14513	0.15	1.16	9.61	6.78	1.49E-07	6.69E-03	7.45	NM_021243	C6orf115	chromosome 6 open reading frame 115
42541	-0.13	-1.14	6.32	-6.77	1.55E-07	6.94E-03	7.42	NM_002869	RAB6A	RAB6A, member RAS oncogene family
12338	1.23	3.42	7.21	6.76	1.58E-07	7.08E-03	7.40	XR_019330	LOC647162	similar to Keratin, type I cytoskeletal 18 (Cytokeratin-18) (CK-18) (Keratin-18) (K18)
27679	1.14	3.13	6.93	6.76	1.59E-07	7.14E-03	7.39	XR_019568	LOC343326	similar to Keratin, type I cytoskeletal 18 (Cytokeratin-18) (CK-18) (Keratin-18) (K18)
5415	0.15	1.16	6.22	6.75	1.64E-07	7.37E-03	7.36	NM_033637	BTRC	beta-transducin repeat containing
26043	-0.30	-1.35	6.06	-6.74	1.68E-07	7.57E-03	7.33	AA428090		
18066	-0.37	-1.44	8.09	-6.73	1.73E-07	7.75E-03	7.31	AK057167		
14884	1.16	3.18	6.81	6.72	1.75E-07	7.84E-03	7.30	XR_016590	LOC647913	similar to keratin complex 1, acidic, gene 18
22348	1.28	3.58	7.69	6.72	1.77E-07	7.97E-03	7.28	XR_018193	LOC391819	similar to Keratin, type I cytoskeletal 18 (Cytokeratin-18) (CK-18) (Keratin-18) (K18)
41523	-0.24	-1.27	7.30	-6.71	1.79E-07	8.05E-03	7.28	NM_003144	SSR1	signal sequence receptor, alpha (translocon-associated protein alpha)
3098	0.25	1.28	6.94	6.71	1.79E-07	8.06E-03	7.27	XM_001718519		
6769	0.25	1.28	9.03	6.71	1.84E-07	8.25E-03	7.25	NM_012322	LSM5	LSM5 homolog, U6 small nuclear RNA associated (S, cerevisiae)
13046	-0.24	-1.28	7.67	-6.70	1.89E-07	8.48E-03	7.23	AK095603	KIAA1822	KIAA1822
5070	0.23	1.26	10.54	6.69	1.91E-07	8.58E-03	7.21	NM_003146	SSRP1	structure specific recognition protein 1
19228	-0.44	-1.55	6.86	-6.68	1.95E-07	8.76E-03	7.19	AF131762		
29456	-0.28	-1.33	7.38	-6.68	1.96E-07	8.81E-03	7.19	AV721971		
18366	-0.07	-1.08	5.38	-6.67	2.01E-07	9.02E-03	7.17	NM_018902	PCDHA11	protocadherin alpha 11
2943	0.16	1.18	6.25	6.67	2.04E-07	9.17E-03	7.15	NM_177559	CSNK2A1	casein kinase 2, alpha 1 polypeptide
6232	0.15	1.16	8.03	6.67	2.05E-07	9.19E-03	7.15	NM_003863	DPM2	dolichyl-phosphate mannosyltransferase polypeptide 2, regulatory subunit
20957	0.35	1.42	8.90	6.66	2.09E-07	9.36E-03	7.13	NM_033274	ADAM19	ADAM metallopeptidase domain 19 (meltrin beta)
12807	1.24	3.44	7.41	6.65	2.13E-07	9.57E-03	7.11	XR_018311	LOC139060	similar to Keratin, type I cytoskeletal 18 (Cytokeratin-18) (CK-18) (Keratin-18) (K18)
38821	-0.33	-1.39	9.04	-6.65	2.14E-07	9.59E-03	7.11	NM_024692	RSNL2	restin-like 2
21311	0.42	1.52	8.67	6.65	2.14E-07	9.62E-03	7.11	NM_001970	EIF5A	eukaryotic translation initiation factor 5A
649	1.08	2.94	6.61	6.65	2.15E-07	9.64E-03	7.10	XR_018938	LOC132391	similar to Keratin, type I cytoskeletal 18 (Cytokeratin-18) (CK-18) (Keratin-18) (K18)
34773	-0.31	-1.37	6.35	-6.63	2.25E-07	1.01E-02	7.06	NM_078487	CDKN2B	cyclin-dependent kinase inhibitor 2B (p15, inhibits CDK4)
19295	0.47	1.60	5.92	6.61	2.37E-07	1.06E-02	7.01	THC2535223		
35951	-0.93	-2.55	8.21	-6.61	2.39E-07	1.07E-02	7.00	NM_005532	IFI27	interferon, alpha-inducible protein 27
10887	1.19	3.27	6.95	6.61	2.42E-07	1.08E-02	6.99	XR_017211	LOC651696	similar to Keratin, type I cytoskeletal 18 (Cytokeratin-18) (CK-18) (Keratin-18) (K18)
33899	-0.30	-1.34	7.12	-6.60	2.45E-07	1.10E-02	6.98	NM_002971	SATB1	special AT-rich sequence binding protein 1 (binds to nuclear matrix/scaffold-associating DNA's)
4209	0.14	1.15	5.52	6.59	2.51E-07	1.13E-02	6.95	XR_018641	LOC649545	similar to Keratin, type II cytoskeletal 8 (Cytokeratin-8) (CK-8) (Keraton-8) (K8)
38629	1.06	2.88	6.62	6.59	2.52E-07	1.13E-02	6.95	XR_019037	LOC391271	hypothetical LOC391271
40982	0.89	2.43	6.21	6.58	2.61E-07	1.17E-02	6.92	A_24_P6850		
36957	-0.19	-1.21	8.06	-6.58	2.61E-07	1.17E-02	6.92	NM_014781	RB1CC1	RB1-inducible coiled-coil 1
14987	-0.20	-1.23	8.01	-6.57	2.66E-07	1.20E-02	6.90	NM_012319	SLC39A6	solute carrier family 39 (zinc transporter), member 6
40074	-0.15	-1.16	7.16	-6.56	2.71E-07	1.22E-02	6.88	NM_016302	CRBN	cereblon
30487	1.06	2.88	6.70	6.56	2.71E-07	1.22E-02	6.88	XR_018749	LOC442405	similar to Keratin, type I cytoskeletal 18 (Cytokeratin-18) (CK-18) (Keratin-18) (K18)
40222	0.31	1.36	6.92	6.56	2.73E-07	1.22E-02	6.88	NM_021214	LOC58489	hypothetical protein from EUROIMAGE 588495
18800	-0.24	-1.28	8.44	-6.56	2.74E-07	1.23E-02	6.87	NM_021626	SCPEP1	serine carboxypeptidase 1
34991	-0.73	-2.08	6.89	-6.55	2.84E-07	1.27E-02	6.84	NM_014737	RASSF2	Ras association (RalGDS/AF-6) domain family 2
31712	-0.12	-1.12	5.49	-6.54	2.90E-07	1.30E-02	6.82	NM_080676	C20orf133	chromosome 20 open reading frame 133
41927	-0.38	-1.46	11.98	-6.52	3.07E-07	1.38E-02	6.76	NM_212482	FN1	fibronectin 1
39571	-0.22	-1.25	5.96	-6.51	3.11E-07	1.40E-02	6.75	ENST00000328711		
10395	0.41	1.50	11.20	6.51	3.19E-07	1.43E-02	6.73	NM_199168	CXCL12	chemokine (C-X-C motif) ligand 12 (stromal cell-derived factor 1)
34939	-0.13	-1.13	6.57	-6.49	3.35E-07	1.50E-02	6.68	THC2505349		
3557	-0.32	-1.37	7.03	-6.48	3.42E-07	1.53E-02	6.66	NM_032549	IMMP2L	IMP2 inner mitochondrial membrane peptidase-like (S, cerevisiae)
16302	-0.16	-1.17	7.04	-6.48	3.44E-07	1.54E-02	6.65	XR_019214	LOC649551	similar to nuclear receptor binding factor 2
4882	0.23	1.26	10.04	6.48	3.45E-07	1.55E-02	6.65	THC2509446		
11654	0.17	1.18	11.39	6.46	3.61E-07	1.62E-02	6.61	NM_000610	CD44	CD44 molecule (Indian blood group)
9170	-0.89	-2.45	8.34	-6.46	3.66E-07	1.64E-02	6.60	NM_005532	IFI27	interferon, alpha-inducible protein 27
37711	-0.26	-1.30	7.24	-6.44	3.88E-07	1.74E-02	6.54	NM_001038628	B3GALNT1	beta-1,3-N-acetylgalactosaminyltransferase 1 (globoside blood group)
32308	1.25	3.47	7.36	6.43	3.89E-07	1.74E-02	6.54	NM_173624	FLJ40504	hypothetical protein FLJ40504

4695	-0.35	-1.42	12.09	-6.41	4.22E-07	1.89E-02	6.46	NM_212482	FN1	fibronectin 1
12773	0.09	1.09	9.82	6.39	4.36E-07	1.95E-02	6.43	NM_013235	RNASEN	ribonuclease III, nuclear
1999	1.15	3.15	6.80	6.39	4.38E-07	1.96E-02	6.42	XR_019198	LOC391589	similar to Keratin, type I cytoskeletal 18 (Cytokeratin-18) (CK-18) (Keratin-18) (K18)
3756	-0.93	-2.53	8.18	-6.38	4.51E-07	2.02E-02	6.39	NM_005532	IFI27	interferon, alpha-inducible protein 27
23972	-0.34	-1.41	11.58	-6.38	4.57E-07	2.05E-02	6.38	NM_015170	SULF1	sulfatase 1
40185	-0.19	-1.21	10.94	-6.37	4.70E-07	2.11E-02	6.35	NM_001018108	SERF2	small EDRK-rich factor 2
39793	0.16	1.18	8.03	6.36	4.73E-07	2.12E-02	6.35	NM_012267	HSPBP1	hsp70-interacting protein
11020	1.23	3.42	7.43	6.36	4.79E-07	2.15E-02	6.34	THC2524582		
24675	-0.29	-1.34	12.21	-6.36	4.79E-07	2.15E-02	6.34	NM_212482	FN1	fibronectin 1
13271	-0.12	-1.13	10.59	-6.35	4.97E-07	2.23E-02	6.30	NM_004872	TMEM59	transmembrane protein 59
9064	-0.24	-1.28	7.10	-6.34	5.02E-07	2.25E-02	6.29	NM_014039	C11orf54	chromosome 11 open reading frame 54
35349	-0.12	-1.13	5.85	-6.34	5.03E-07	2.26E-02	6.29	AK024516		
11062	0.20	1.23	8.46	6.33	5.23E-07	2.34E-02	6.25	NM_006555	YKT6	YKT6 v-SNARE homolog (S, cerevisiae)
44582	-0.18	-1.19	8.03	-6.33	5.24E-07	2.35E-02	6.25	NM_033407	DOCK7	dedicator of cytokinesis 7
28684	-0.15	-1.16	8.01	-6.32	5.31E-07	2.38E-02	6.24	NM_016446	C9orf127	chromosome 9 open reading frame 127
41988	0.16	1.18	7.73	6.30	5.73E-07	2.57E-02	6.17	NM_044472	CDC42	cell division cycle 42 (GTP binding protein, 25kDa)
14270	-0.33	-1.39	10.75	-6.28	6.00E-07	2.69E-02	6.12	NM_000366	TPM1	tropomyosin 1 (alpha)
8943	-0.26	-1.30	7.56	-6.28	6.03E-07	2.70E-02	6.12	NM_058197	CDKN2A	cyclin-dependent kinase inhibitor 2A (melanoma, p16, inhibits CDK4)
13215	1.03	2.80	6.49	6.28	6.06E-07	2.72E-02	6.11	XR_018953	LOC391179	similar to Keratin, type I cytoskeletal 18 (Cytokeratin-18) (CK-18) (Keratin-18) (K18)
27651	0.38	1.47	6.96	6.27	6.15E-07	2.76E-02	6.10	NM_002655	PLAG1	pleiomorphic adenoma gene 1
5168	-0.19	-1.21	8.13	-6.27	6.15E-07	2.76E-02	6.10	NM_178564	NRBP2	nuclear receptor binding protein 2
27609	0.11	1.12	6.38	6.27	6.23E-07	2.79E-02	6.09	NM_177559	CSNK2A1	casein kinase 2, alpha 1 polypeptide
43036	1.04	2.82	6.73	6.25	6.55E-07	2.94E-02	6.04	XR_018420	LOC391827	similar to Keratin, type I cytoskeletal 18 (Cytokeratin-18) (CK-18) (Keratin-18) (K18)
40951	0.24	1.27	6.77	6.24	6.63E-07	2.97E-02	6.03	NM_007212	RNF2	ring finger protein 2
959	1.13	3.09	6.90	6.24	6.65E-07	2.98E-02	6.02	A_24_P281443	LOC649375	similar to Keratin, type I cytoskeletal 18 (Cytokeratin-18) (CK-18) (Keratin-18) (K18)
1296	1.31	3.72	7.65	6.24	6.71E-07	3.01E-02	6.02	XR_019191	LOC121054	similar to Keratin, type I cytoskeletal 18 (Cytokeratin-18) (CK-18) (Keratin-18) (K18)
9569	0.98	2.67	6.41	6.24	6.76E-07	3.03E-02	6.01	XR_019060	LOC644030	similar to Keratin, type I cytoskeletal 18 (Cytokeratin-18) (CK-18) (Keratin-18) (K18)
6183	-0.34	-1.40	12.08	-6.23	6.87E-07	3.08E-02	5.99	NM_212482	FN1	fibronectin 1
7752	-0.54	-1.72	9.02	-6.23	6.87E-07	3.08E-02	5.99	NM_003392	WNT5A	wingless-type MMTV integration site family, member 5A
16674	-0.32	-1.37	12.16	-6.22	7.02E-07	3.15E-02	5.97	NM_212482	FN1	fibronectin 1
752	0.18	1.20	8.48	6.22	7.16E-07	3.21E-02	5.95	NM_017722	TRMT1	TRM1 tRNA methyltransferase 1 homolog (S, cerevisiae)
36709	-0.34	-1.41	8.55	-6.22	7.17E-07	3.21E-02	5.95	NM_183233	SLC22A18	solute carrier family 22 (organic cation transporter), member 18
25357	-1.18	-3.27	7.94	-6.22	7.17E-07	3.21E-02	5.95	NM_000954	PTGDS	prostaglandin D2 synthase 21kDa (brain)
15294	-0.24	-1.27	9.98	-6.20	7.52E-07	3.37E-02	5.91	NM_017823	DUSP23	dual specificity phosphatase 23
34641	0.16	1.17	7.90	6.19	7.66E-07	3.43E-02	5.89	NM_044472	CDC42	cell division cycle 42 (GTP binding protein, 25kDa)
19368	0.12	1.13	6.94	6.18	7.87E-07	3.53E-02	5.86	NM_005702	ERAL1	Era G-protein-like 1 (E, coli)
2342	-0.13	-1.14	5.43	-6.18	7.96E-07	3.57E-02	5.85	NM_002302	LECT2	leukocyte cell-derived chemotaxin 2
27606	0.14	1.15	9.48	6.17	8.07E-07	3.62E-02	5.84	NM_006392	NOL5A	nucleolar protein 5A (56kDa with KKE/D repeat)
3553	0.22	1.24	8.66	6.17	8.14E-07	3.65E-02	5.83	NM_018188	ATAD3A	ATPase family, AAA domain containing 3A
2158	0.05	1.05	5.32	6.16	8.44E-07	3.78E-02	5.80	XR_018787	LOC339396	similar to neurofilament, heavy polypeptide
7946	0.18	1.19	8.61	6.16	8.46E-07	3.79E-02	5.79	NM_007002	ADRM1	adhesion regulating molecule 1
2841	0.16	1.17	10.61	6.16	8.50E-07	3.81E-02	5.79	A_32_P179205	LOC402562	similar to Heterogeneous nuclear ribonucleoprotein A1 (Helix-destabilizing protein) (Single-strand binding protein) (hnRNP core protein A1) (HDP-1) (Topoisomerase-inhibitor suppressed)
41866	-0.15	-1.17	6.46	-6.15	8.60E-07	3.85E-02	5.78	NM_007202	AKAP10	A kinase (PRKA) anchor protein 10
30168	0.08	1.09	5.36	6.15	8.71E-07	3.91E-02	5.77	AK056119		
6538	-0.26	-1.30	9.98	-6.14	8.89E-07	3.99E-02	5.75	NM_001343	DAB2	disabled homolog 2, mitogen-responsive phosphoprotein (Drosophila)
41042	0.21	1.24	10.01	6.13	9.02E-07	4.04E-02	5.73	NM_004515	ILF2	interleukin enhancer binding factor 2, 45kDa
7984	0.36	1.43	9.18	6.12	9.30E-07	4.17E-02	5.70	NM_021214	LOC58489	hypothetical protein from EUROIMAGE 588495
44649	0.99	2.68	6.56	6.12	9.32E-07	4.18E-02	5.70	XR_018462	LOC391803	similar to Keratin, type I cytoskeletal 18 (Cytokeratin-18) (CK-18) (Keratin-18) (K18)
13274	-0.32	-1.37	6.72	-6.12	9.40E-07	4.21E-02	5.69	ENST00000393500		
31708	0.20	1.22	6.56	6.12	9.51E-07	4.26E-02	5.68	NM_024821	CCDC134	coiled-coil domain containing 134
33989	-0.18	-1.20	6.92	-6.11	9.68E-07	4.34E-02	5.67	NM_004348	RUNX2	runt-related transcription factor 2
33242	-0.19	-1.21	6.88	-6.10	9.84E-07	4.41E-02	5.65	NM_001122838	NAPE-PLD	N-acyl-phosphatidylethanolamine-hydrolyzing phospholipase D
5588	0.22	1.25	9.37	6.10	9.93E-07	4.45E-02	5.64	NM_000190	HMBS	hydroxymethylbilane synthase
38712	-0.24	-1.27	9.88	-6.09	1.01E-06	4.52E-02	5.63	NM_005780	LHFP	lipoma HMGIC fusion partner
11818	-0.27	-1.31	5.45	-6.09	1.03E-06	4.60E-02	5.61	NM_016953	PDE11A	phosphodiesterase 11A
25250	-0.84	-2.33	8.25	-6.08	1.04E-06	4.64E-02	5.60	NM_005532	IFI27	interferon, alpha-inducible protein 27
39603	-0.24	-1.27	6.09	-6.08	1.05E-06	4.72E-02	5.59	NM_001033045	GPR155	G protein-coupled receptor 155
39313	-0.16	-1.18	5.46	-6.08	1.06E-06	4.73E-02	5.58	NM_181643	C1orf88	chromosome 1 open reading frame 88
7675	0.17	1.19	5.67	6.07	1.07E-06	4.79E-02	5.57	NM_000679	ADRA1B	adrenergic, alpha-1B-, receptor
41277	-0.20	-1.22	7.08	-6.07	1.08E-06	4.86E-02	5.56	NM_015061	JMJD2C	jumonji domain containing 2C
36866	-0.27	-1.32	8.69	-6.06	1.10E-06	4.91E-02	5.55	NM_152558	IQCE	IQ motif containing E
26233	1.03	2.80	6.64	6.06	1.11E-06	4.98E-02	5.53	A_24_P358406		

Supplemental table 2. ROS levels, Senescence Associated-β-gal activity and p16 expression measured at the mRNA level in non-stressed and rotenone stressed human fibroblasts from young and old subjects from the Leiden 85-plus Study. Values are given as mean (SE).

	Young	Old	p
Micro-array experiments	n=6	n=6	
SA-β-gal (MdFI)			
Non-stressed	2078 (357)	2634 (360)	0.045
Rotenone-induced increase	+11433 (463)	2395 (472)	0.056
p16 (fold change)			
array	1	1.46	**<0.0001**
qPCR Non-stressed	1	1.43 (0.08)	**0.005**
qPCR Rotenone, 3h	1	1.37 (0.14)	**0.060**
qPCR Rotenone, 3d	1	1.42 (0.11)	**0.031**
Replication experiments	n=10	n=10	
SA-β-gal (MdFI)			
Non-stressed	3146 (368)	22740 (363)	0.23
Rotenone-induced increase	+1132 (260)	+1638 (255)	**0.052**
p16 (fold change)			
qPCR Non-stressed, 3d	1	0.74 (0.05)	**<0.001**
qPCR Rotenone, 3d	1	0.99 (0.07)	0.52

Supplemental Figure 1. Variation in expression between strains from different subjects presented as a heatmap

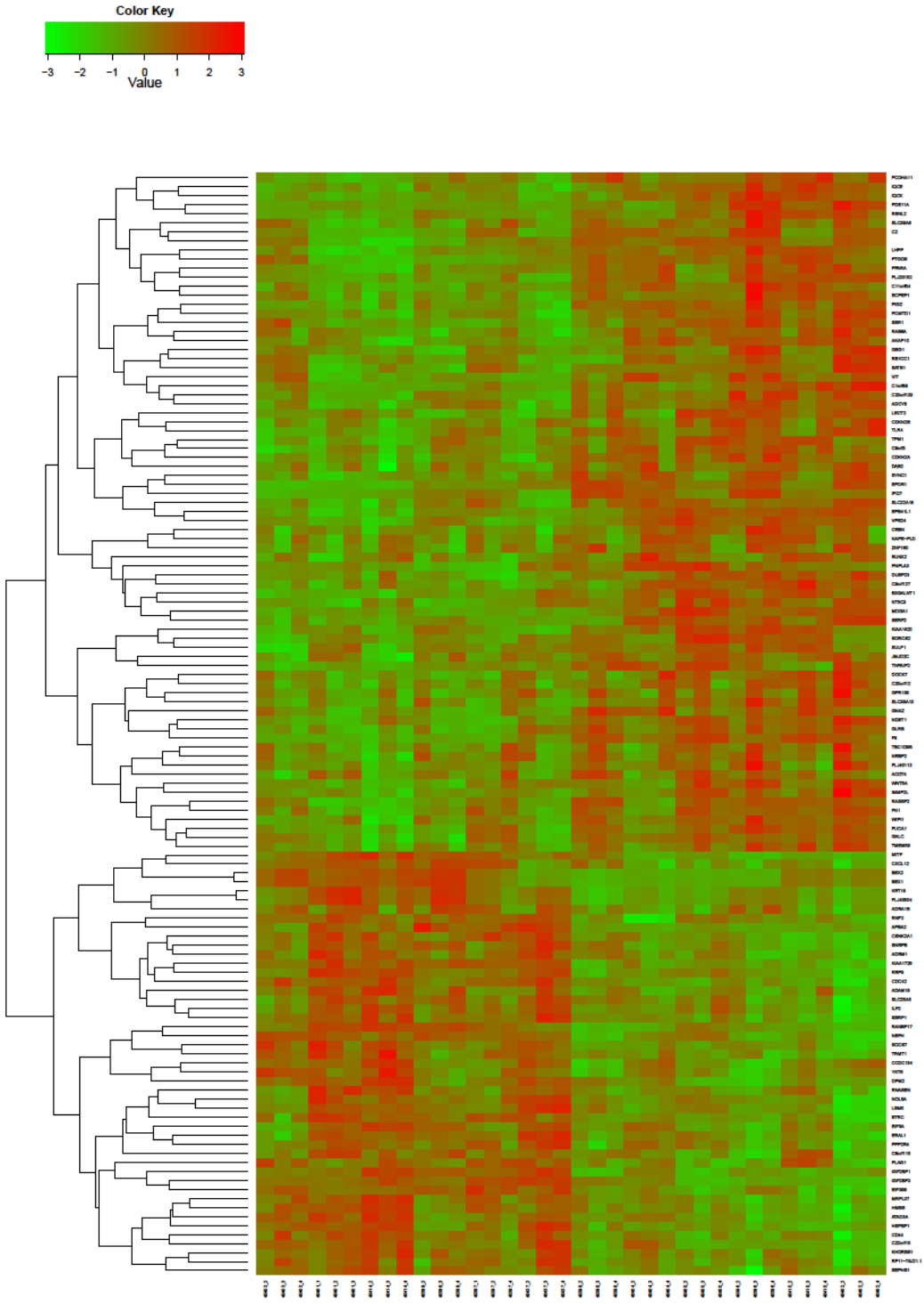

Chapter 7

Human *in vivo* longevity is reflected *in vitro* by differential metabolism as measured by ^{1}H-NMR profiling of cell culture supernatants

Pim Dekker, Axel Meissner, Roeland W. Dirks, P.E. Slagboom, Diana van Heemst, André M. Deelder, Hans J. Tanke, Rudi G.J. Westendorp, Andrea B. Maier

Mol Biosyst.. 2012 Jan [Epub ahead of print]

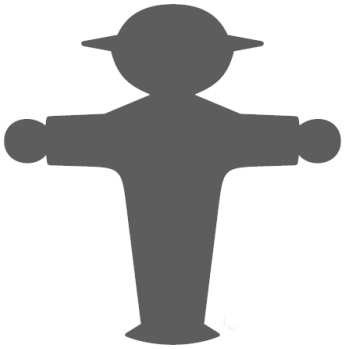

Summary

The offspring of nonagenarian siblings suffer less from age related conditions and have a lower risk of mortality compared with their partners. Fibroblast strains derived from such offspring in middle age show different *in vitro* responses to stress, more stress-induced apoptosis and less senescence when compared with strains of their partners. Aiming to find differences in cellular metabolism *in vitro* between these fibroblast strains, cell culture supernatants collected at 24-hours and five days were analyzed using ^{1}H nuclear magnetic resonance (NMR)-based metabolic footprinting. Between 24-hours and five days of incubation, supernatants of all fibroblast strains showed decreased levels of glucose, pyruvate, alanine-glutamine (ala-gln), valine, leucine, isoleucine, serine and lysine and increased levels of glutamine, alanine, lactate and pyroglutamic acid. Strains from offspring and their partners were compared using a partial least squares-discriminant analysis (PLS-DA) model based on the data of the five-day time point. The ala-gln and glucose consumption was higher for fibroblast strains derived from offspring when compared with strains of their partners. Also, production of glutamine, alanine, lactate and pyroglutamic acid was found to be higher for fibroblast strains derived from offspring. In conclusion, differences in NMR-based metabolic profiles of human cells *in vitro* reflect the propensity for human longevity of the subjects from whom these were derived.

Introduction

Life expectancy has dramatically increased in Western society, but there is much inter-individual variation in life expectancy (1). Healthy longevity has been shown to be a combination of genetic, environmental and chance factors. To study the phenotype and genetic component of healthy aging we designed the Leiden Longevity Study (LLS), in which families with exceptional longevity were recruited (2). Nonagenarian siblings and their offspring showed a lower risk of mortality than controls from their birth cohort. As compared with their partners, this offspring show a lower prevalence of myocardial infarction, hypertension and diabetes mellitus (3) and features such as preservation of insulin sensitivity with age and a beneficial glucose handling (4;5) and lipid metabolism (6). The contrast between offspring of nonagenarian siblings that express the propensity for longevity and their partners was also found to be reflected by cellular characteristics *in vitro*. In dermal fibroblast strains from offspring, oxidative stress induced less reactive oxygen species (ROS), less senescence, more apoptosis and slower growth speed when compared with strains from the partners of the offspring (7;8). Furthermore, cytotoxic T cell responses were more pronounced in offspring (9).

In accordance with other features of healthy metabolism we found that offspring had a lower thyroidal sensitivity to thyrotropin, affecting levels of the thyroid hormone, which is primarily responsible for regulation of protein, fat and carbohydrate metabolism (10). For model organisms it has been shown that caloric restriction extends life span, which has been suggested to be caused by a shift from carbohydrate to fatty acid metabolism. This is thought to result in decreased cellular damage, since fatty acid metabolism preferentially uses mitochondrial complex II, which is known to produce less damaging ROS than the other mitochondrial complexes I, III, IV and V (11). However, for humans not much is known about the relation between cellular metabolism and longevity.

We have already reported that skin fibroblast strains derived from offspring of nonagenarian siblings show a cellular phenotype *in vitro* that differs from their partners (7;8). We now aimed to investigate if these fibroblast strains also show differences in cellular metabolism *in*

vitro. To measure metabolic changes, we chose to measure the metabolites in the cell culture supernatants of the strains. Measurement of intracellular metabolites requires rapid quenching of metabolism and a time-consuming and often inadequate extraction and separation procedure (12). ^{1}H-NMR-based metabolic footprinting (13) of cell culture supernatants requires minimal sample preparation, thus introducing fewer artefacts (14). This methodology will therefore also allow better correlation with *in vivo* techniques. Here we describe the results of ^{1}H-NMR-based metabolic footprinting (13) of cell culture supernatants of human fibroblast strains *in vitro* from offspring and their partners.

Material and methods

Study design

The LLS was set up to investigate the contribution of genetic factors to healthy longevity by establishing a cohort enriched for familial longevity (2). From July 2002 to May 2006, 421 families were recruited consisting of 944 long-lived Caucasian siblings together with their 1671 of their offspring and 744 of the partners thereof. There were no selection criteria on health or demographic characteristics. Compared with their partners, the offspring were shown to have a 30% lower mortality rate and a lower prevalence of cardio-metabolic diseases (2;3). During the period November 2006 and May 2008, a biobank was established from fibroblasts cultivated from skin biopsies from 150 offspring-partner couples. Because it was expected that the difference in biological age between the offspring and partner groups would be relatively small, a relatively large sample size of 68 fibroblast strains from 34 couples was randomly chosen. In accordance with the Declaration of Helsinki we obtained informed consent from all participants prior to their entering the study. Good clinical practice guidelines were maintained. The study protocol was approved by the ethical committee of the Leiden University Medical Center before the start of the study.

Fibroblast Cultures

Four-mm skin biopsies were taken from the sun unexposed medial side of the upper arm. Fibroblasts were grown in D-MEM:F-12 (1:1) medium supplemented with 10% fetal calf serum (FCS, Bodinco, Alkmaar, the Netherlands, batch no. 162229), 1 mM MEM sodium pyruvate, 10 mM HEPES, 2 mM glutamax I, and antibiotics (100 Units/mL penicillin, 100 µg/mL streptomycin, and 0.25–2.5 µg/mL amphotericin B), all obtained from Gibco, Breda, the Netherlands. This medium will be referred to as standard medium. Fibroblasts were incubated at 37^{o}C with 5% CO_2 and 100% humidity. All cultures that are used in the present study were grown under predefined, highly standardized conditions and frozen at low passage as published earlier (7;15) Trypsin (Sigma, St Louis, MO, USA) was used to split fibroblasts using a 1:4 ratio each time they reached 80-100% confluence.

Experimental set-up

Experiments were set up in batches of maximally 10 fibroblast strains, which were thawed from frozen stocks on day zero. On day one, the medium was changed and on day four fibroblasts were passaged 1:4 and passaged further in equal numbers on days six and eight to have similar confluences for experiments. On day 11, 9x104 fibroblasts were seeded in 25 cm^2 tissue culture flasks for experiments and after overnight incubation with standard medium, fibroblasts were washed with serum-free medium and 3 ml serum-free medium per flask was added. Cell culture supernatants were collected at 24 hours and five days and stored at -70^{o}C. Cell-free/serum-free medium incubated at 37^{o}C with 5% CO_2 and 100% humidity for 24 hours and five days was used as control medium.

Plating efficiency

Plating efficiency could confound concentrations of metabolites in the cell culture supernatants. To test if plating efficiency between strains from offspring and partners was different, fibroblasts strains were also seeded in 96-well plates and fixed after four hours. Fibroblasts were washed with water and stained with 0.6 mg/ml Coomassie in 1:6 methanol/water overnight, washed again with water and air dried. Plates were then scanned with a high resolution Agfa XY-15 flatbed scanner (Agfa Gevaert, Mortsel, Belgium) and cells were counted automatically with the freely available image analysis software package

ImageJ 1.37v. No differences in plating efficiency were found (75±4% [mean±SD] and 76±4% for strains from offspring and partners, respectively, p=0.79).

NMR methodology

Preparation of cell culture supernatants for ^{1}H-NMR Spectroscopy

After thawing, cell culture supernatants were centrifuged with 3000g for 10 min at 4ºC for the removal of any cellular components. 540 µL supernatant was mixed with 60 µL of 1.5 M phosphate buffer (pH 7.4) in D2O containing 4.0 mM sodium 3-trimethylsilyl-tetradeuteriopropionate (TSP) and 2.0 mM NaN_3 (16). All reagents were purchased from Sigma-Aldrich, St Louis, MO, USA. The resulting samples were then centrifuged with 3000g for 10 min at 4ºC prior to manual transfer into 5 mm SampleJet sample tubes in 96 tube racks. Tubes were closed with polyoxymethylene (POM) balls and tube racks were placed on the sample changer where they were kept at 6ºC while queued for data acquisition.

NMR Data Acquisition and Processing

^{1}H-NMR data was obtained using a Bruker 600 MHz AVANCE II spectrometer equipped with a 5 mm TCI cryo probe and a z-gradient system; a Bruker SampleJet sample changer system was used for sample transfer. One-dimensional (1D) ^{1}H-NMR spectra were recorded at 300 K using the first increment of a NOESY pulse sequence (17) with presaturation (γB1 = 50 Hz) during a relaxation delay of 4 sec and a mixing time of 10 msec for efficient water suppression (18). Duration of 90 degree pulses were automatically calibrated for each individual sample using a homonuclear-gated nutation experiment (19) on the locked and shimmed samples after automatic tuning and matching of the probe head. 64 scans of 65,536 points covering 12,335 Hz were recorded and zero filled to 65,536 complex points prior to Fourier transformation, an exponential window function was applied with a line-broadening factor of 1.0 Hz. The spectra were manually phase and baseline corrected and automatically referenced to the internal standard (TSP = 0.0 ppm). Phase offset artefacts of the residual water resonance were manually corrected using a polynomial of degree 5 least square fit filtering of the free induction decay (FID) (20).

Multivariate Data Analysis of NMR Spectroscopic Data

A bucket table with a bucket size of 0.04 ppm was generated for the regions 10.0–5.1 and 4.5–0.2 ppm, respectively, using AMIX version 3.5 (Bruker Biospin, Germany). Buckets were normalized to a total area of 1.0 and metadata was included after import of the data into MS Excel (version 2003; Microsoft). For multivariate statistical analysis SIMCA-P+ (version 12.0, Umetrics, Sweden) software package was used. Since high abundant metabolites are generally the major source of the overall variability within the data, NMR variables were Pareto scaled and centred prior to PCA and PLS-DA analysis in order to emphasize variability of minor components. Variables were centred but not scaled for PLS-DA analysis after OSC filtering since the filtering step does remove variability not related to the classes investigated and hence already accentuate relevant minor components. Likewise, data for outlier detection was not scaled since outliers were defined as data with “abnormal” variability of specific variables on an absolute scale. For initial analysis and outlier detection PCA was performed using eight components. Outliers were identified based on scores (Hotelling’s T2 range) and distance of the observation in the training set to the X model plane values, as well as visual inspection of the individual NMR spectra during data processing. Spectra of insufficient quality due to poor water suppression or bad automated shim performance (broad lines) were excluded from the analysis. For OSC-filtering and PLS-DA analysis samples were categorized based on offspring/partner and time point, respectively. PLS-DA models were validated by random permutation of the response variable and comparison of the goodness of fit (R2Y and Q2Y) of 200 such models with the original model in a validation plot. R2Y and Q2Y of the original PLS models as well as intersects of the R2Y and Q2Y regression lines of the validation plots with the vertical axis were calculated as quality parameters. Relative changes in metabolites were identified based on coefficient plots and variable importance in the projection (VIP). The cutoff for changes to be considered significant was based on VIP and the confidence interval derived from jack knifing of the corresponding coefficients. Mean spectra were calculated from the original NMR data for individual classes of the obtained models in order to assist annotation of loadings and coefficient plots and to determine relative differences in metabolite concentrations between the classes and to determine relative differences in metabolite concentrations between the classes.

Results

Table 1 shows the characteristics of the randomly selected subset of subjects from whom fibroblast strains were tested. Partners and offspring were of similar age, height and weight.

Initial PCA model and metabolic footprinting of fibroblast strains dependent on incubation period

Principal component analysis (PCA) was applied to detect biochemical outliers and to identify variability within the data that correlates with offspring/partner status, time point and gender classification. After removal of spectroscopic outliers (Supplemental table 1), a PCA model

Table 1. Clinical characteristics of offspring and partners from the Leiden Longevity Study, representing a difference in biological age.

	Offspring n=34	Partners n=34
Demographic data		
Female	19	15
Age, years (mean±SD)	61.7 (6.7)	60.5 (7.5)
Anthropometric data		
Height, cm (mean±SD)	170 (8)	174 (9)
Weight, kg (mean±SD)	74 (13)	79 (14)
Current smoking – no./total known	3/27	8/29
Diseases		
Myocardial infarction – no./total known	0/33	0/33
Stroke – no./total known	1/33	0/33
Hypertension – no./total known	5/33	7/33
Diabetes mellitus – no./total known	1/32	2/32
Malignancies – no./total known	0/31	1/31
Chronic obstructive pulmonary disease – no./total known	1/32	1/33
Rheumatoid arthritis – no./total known	0/33	0/33

based on data from 134 of 144 samples (34 offspring strains, 34 partner strains, four cell-free controls, all taken at 24 hours and five days), was built using eight components with an explained variability of 97.9% and a predicted variation of 94.0%. Already in the scores plot of the first two principal components (PCs) two dominating clusters correlating with the incubation time of 24 hours and five days, respectively, can be identified as shown in Figure 1. A strong time-dependent discrimination was already found in the first components of the PCA model since depletion of the medium components and accumulation of waste products over time are expected as main source of variability due to cellular metabolism. Furthermore, cell-free/serum-free medium (from here on referred to as control medium) did not change over time and the corresponding data for these control samples were found in the scores plot as separate sub-cluster at one side of the 24-hour cluster. Hence, a time trajectory emerged as indicated in Figure 1, starting from the control medium on the left and progressing to the right within the scores plot showing the cell culture supernatants incubated for 24 hours and five days.

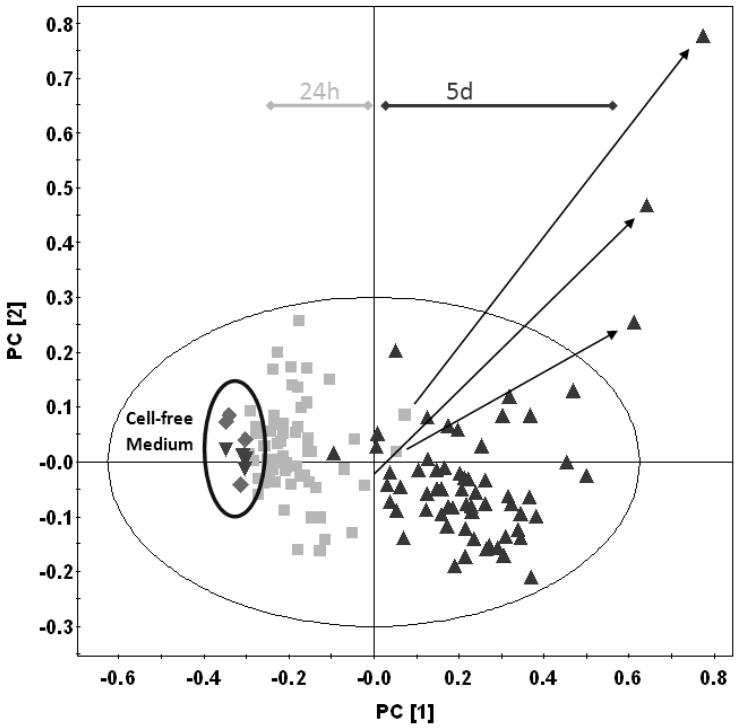

Figure 1. Scores plot of first two principal components from PCA model built from complete data set. Data points are labeled according to fibroblast culture incubation duration of 24 hours (■) and five days (▲) as well as cell-free medium incubated for 24 hours (◆) and five days (▼). Arrows indicate culture samples with accelerated metabolism (for details see text).

For detection of biological outliers, a separate PCA model based on centred but not scaled data was built using eight components. The scores (Hotellings T2 range) and distance of the observation in the training set to the X model plane values identified one outlier for the 24 hour incubation time point and three outliers for the five-day incubation time point (Supplemental figure 1). The three samples from the five-day time point, namely one male offspring, one female offspring and one female partner, respectively, already deviated from the other samples in the scores plot in Figure 1. The scores plot in Supplemental Figure 2 and closer investigation of the medium profiles for these three subjects showed deviations already for the 24h time point samples. The observed differences indicate accelerated metabolism for the fibroblasts of these three strains accompanied by increased lactate production. All identified biological outliers were excluded from further analysis.

The main metabolites responsible for the observed clustering in the initial PCA are shown in the loadings plot in Figure 2. In order to investigate the time dependent changes further, a separate PLS-DA two-class model was built with the time point as response variable. The scores plot of the first two components showed a clear discrimination between the two time points (Supplemental figure 3).

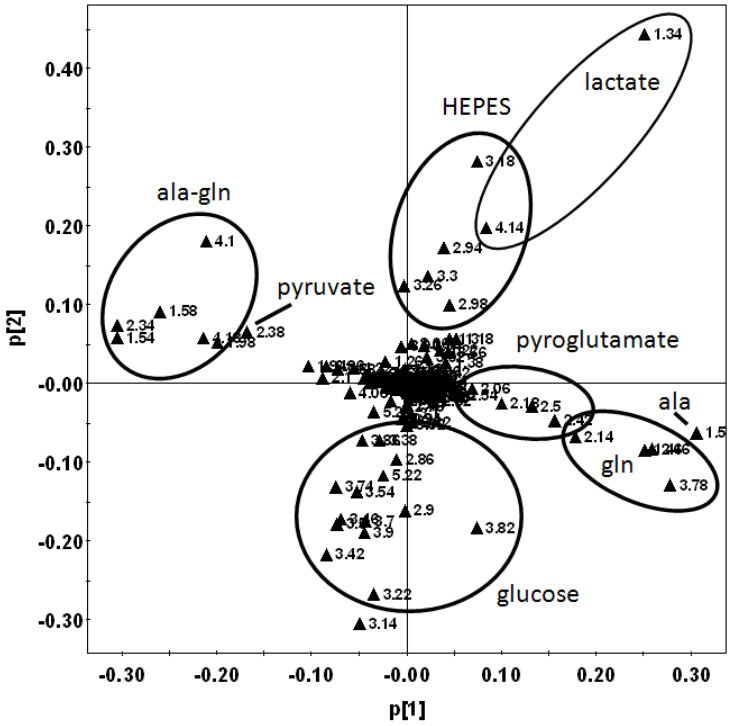

Figure 2. Loadings plot of first two principal components from PCA model built from complete data set. Main metabolites responsible for variability are annotated. Metabolites with negative p[1] loadings (left) are decreased in the five-day samples compared with the 24-hour samples, whereas metabolites with positive p[1] loadings (right) are increased in the cell culture supernatants of five days compared with those of 24 hours.

A cumulative R^2Y of 0.96 and Q^2Y of 0.94 were calculated for the model and the model validation plot showed intercepts of the R^2Y and Q^2Y regression lines with the vertical axis at 0.142 and -0.396, respectively, indicating a valid model. Based on coefficients (Supplemental figure 4) and loadings from this model the responsible metabolites for the discrimination of the two groups were identified. Decreased components in the five-day medium in comparison to 24-hour medium were grouped into energy metabolism compounds like glucose, pyruvate and the dipeptide ala-gln and amino acid building blocks like valine, leucine, isoleucine, serine and lysine. Increased metabolites in medium were lactate, alanine, glutamine, pyroglutamic acid, formic acid, glycine, 2-oxo-4-methyl pentanoic acid, 2-oxo-3-methyl pentanoic acid, 2-oxo-3-methyl butanoic acid and acetic acid. A direct link between ala-gln decrease and glutamine and pyroglutamic acid increase was established, suggesting ala-gln as an alternative energy source (Figure 3). An apparent increase of HEPES buffer was observed at the five-day time point when compared with the 24-hour time point. However, this increase can most likely be attributed to an inverse normalization effect, since consumption of major components will result in an apparent increase of invariant constituents after total area normalization. This is a well-known effect commonly observed in metabonomic analysis of normalized spectroscopic data (21;22).

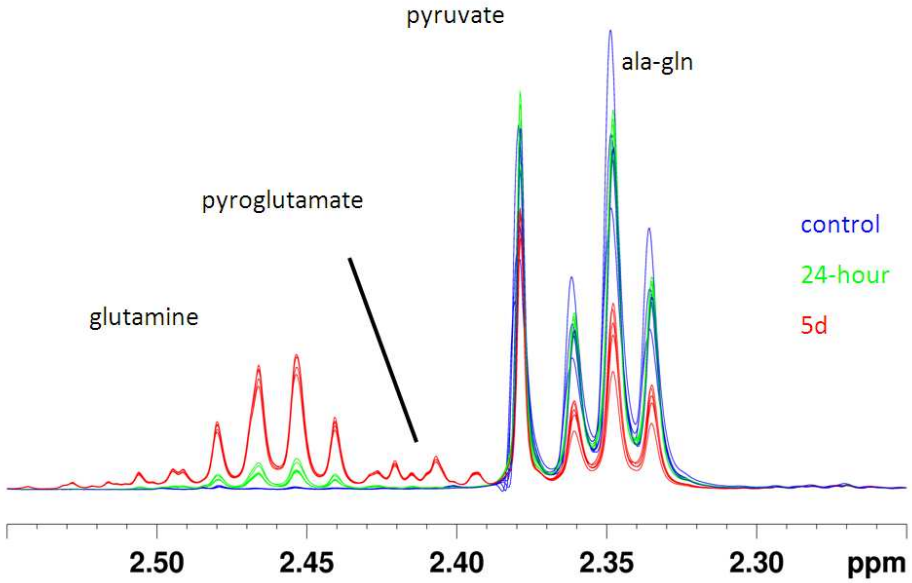

Figure 3. Excerpt of 1D NOESY spectra from representative traces (six each) of cell-free control medium (blue) and cell culture supernatant after 24 hours (green) and five days (red) incubation time, demonstrating link between ala-gln consumption and glutamine release.

PLS-DA model to detect differences in offspring/partner

Within the initial PCA model no additional clustering according to gender, age or offspring/partner classification was observed. To identify significant subtle differences between the metabolic profile of fibroblasts from offspring and partners, a PLS-DA model was built using data from the five-day time point. This time point was chosen to allow rather small differences to accumulate over time. However, the initial PLS-DA model did not discriminate between offspring and partner (data not shown). Therefore, a second PLS-DA two-class model after OSC-filtering using two components with a remaining sum of squares of 21.3% and an Eigenvalue of 11.1 was built. For two components, a cumulative R^2Y of 0.51 and Q^2Y of 0.32 were obtained and model validation showed intercepts of the R^2Y and Q^2Y regression lines with the vertical axis of the validation plot at 0.049 and -0.131, respectively, indicating a valid model. The OSC filtering step was independently validated using a leave-one-out cross validation procedure (see supplement material). Figure 4 shows the scores plot of the first and second components of this PLS-DA two-class model, indicating separation between offspring and partners with some degree of overlap between the two clusters. Based on coefficients and loadings from this model, molecular discriminators between metabolic footprint profiles of the fibroblast supernatants of offspring and partners were identified, as summarized in Table 2. The main differences were observed for metabolites involved in the energy metabolism.

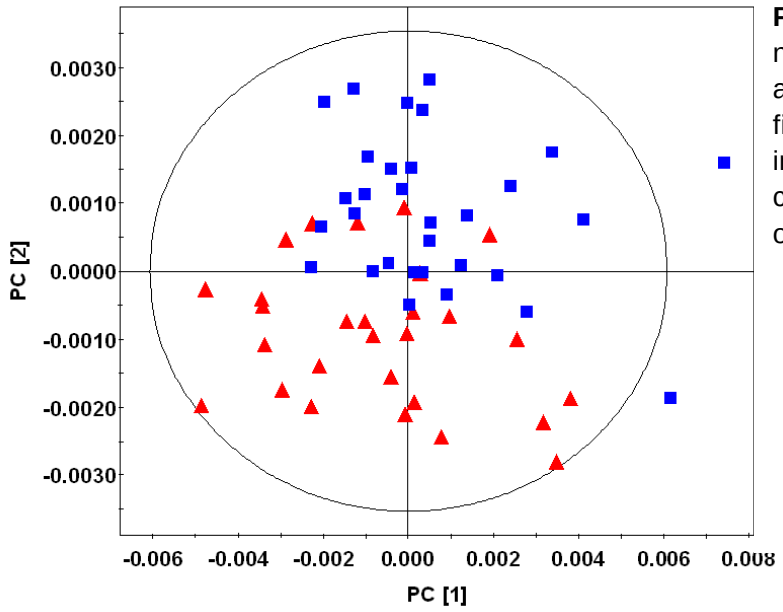

Figure 4. Scores plot of first two components from PLS-DA two-class model built after OSC filtering of NMR data from fibroblast cell culture supernatants after incubation for five days. Data points are coloured according to partner (■) and offspring (▲) classification, respectively.

Table 2. Metabolites in cell culture supernatants identified by PLS-DA model showing differences between offspring and partners from the LLS.

Metabolite	δ [ppm][a]	Relative difference offspring vs partner[b]	VIP[c]
Energy Metabolism			
Ala-gln	2.34, 1.54	0.95	1.30, 1.37
Alanine	1.50	1.02	2.67
Glucose	5.22, 3.90		1.51, 2.10
	3.78, 3.70	0.99	1.64, 2.65
	3.50, 3.42		1.62, 3.22
Glutamine	2.46	1.02	2.88
Pyroglutamate	4.18, 2.42	1.03	0.55, 0.15
Pyruvate	2.38	0.98	0.83
Lactate	4.10,1.34	1.03	1.52,10.62

[a] mean value of corresponding bucket

[b] as determined from mean spectra of corresponding classes

[c] Importance of contribution values of buckets generated from corresponding PLS-DA model

Discussion

Our main finding is that fibroblast strains derived from offspring of nonagenarian siblings show different levels of metabolites in their cell culture supernatants when compared with those of their partners. The ala-gln and glucose consumption was higher for fibroblast strains derived from offspring when compared with strains of their partners. Also, production of glutamine, alanine, lactate and pyroglutamic acid was found to be higher for fibroblast strains derived from offspring.

Changes in metabolic footprinting of fibroblast strains dependent on the incubation period

Between 24 hours and five days of incubation in serum-free medium, the cell culture supernatants of all fibroblast strains showed decreased levels of glucose, pyruvate and ala-gln. Furthermore, all supernatants showed decreased levels of the essential amino acids

valine, leucine, isoleucine, serine and lysine, consistent with the literature (23). After five days of incubation, levels of glutamine, alanine, lactate and pyroglutamic acid had increased in supernatants of all fibroblast strains.

The ala-gln dipeptide is an important additive in cell culture medium and an important source of glutamine and alanine (24). Increasing levels of glutamine and alanine in the cell culture supernatants could be the result of the intracellular enzymatic digestion of the ala-gln dipeptide (24), after which the excess of both amino acids (i.e. not needed for metabolism) is excreted back into the medium. This would also account for the decrease of ala-gln.
When available, glucose is the main source of energy of cells, explaining the decreasing levels of glucose in the cell culture supernatants of the fibroblast strains. Through the glucose-alanine cycle (25), alanine can be formed from glucose, possibly contributing to the increased levels of alanine observed in the cell culture supernatants. Indeed, it was reported earlier that in addition to the formation of lactic acid, alanine and glutamic acid are secreted into medium by murine fibroblasts (26). Furthermore, human fibroblasts were reported to convert a large proportion of glutamine in culture medium to lactate (27), dependent on cell density (23).

Different metabolic footprint profile of fibroblast strains from longevity family members

The ala-gln and glucose consumption was higher for fibroblast strains derived from offspring of nonagenarian siblings, when compared with fibroblast strains from their partners. Indeed, earlier we showed that serum glucose metabolism and insulin sensitivity is different for the long-living families (4;5). Indeed, earlier we showed that, *in vivo*, the offspring group showed lower levels of thyroid hormone (T3 and T4) (10). Since thyroid hormone stimulates lipid metabolism (28), these data suggest that fibroblast strains from offspring have a lower lipid metabolism. It is also important to realize that the fibroblast strains were cultured in serum-free medium. Serum is an important source of lipids in cell culture medium, so when it is removed, glucose will be the main energy substrate available. Since the fibroblast strains of offspring showed a higher glucose consumption, they might be better able to adapt to the serum free conditions when compared with the strains of the partners.

Production of glutamine, alanine, lactate and pyroglutamic acid was found to be higher for fibroblast strains derived from offspring, when compared with fibroblast strains from partners. The higher production of glutamine and alanine is consistent with the higher consumption of ala-gln and glucose since these are interconverted into each other by glycolysis and the glucose-alanine cycle.

Research into the disease lactiacidemia has implied the role of mitochondrial function in serum lactate levels (29;30). The higher glucose-consumption in strains from offspring is consistent with the finding that respiration-deficient fibroblasts show a higher constitutive rate of glucose transport (31), since we found earlier that strains from offspring are more sensitive to inhibition of the respiratory chain by rotenone, when compared with strains of partners (7;8). Fibroblast strains from offspring were more prone to go into rotenone-induced apoptosis, but showed less rotenone-induced senescence. Also, strains from offspring showed a stronger rotenone-induced decrease in growth rate.

Metabolites in energy metabolism have also been connected to cell damage, cell cycle, apoptosis and senescence. Lactate levels inhibit cell proliferation (32;33) and lactate dehydrogenase (LDH) mediates apoptosis in glucose-starved c-Myc transformed cells (34;35). High glucose levels have been shown to induce senescence in human fibroblasts (36). Fibroblast strains from offspring are more prone to go into stress-induced apoptosis but show less senescence when compared with strains from partners (7). This is consistent with the fact that we found lower levels of glucose for strains from offspring and could be explained by a process called hysteresis, described as metabolite-induced gene expression of the metabolic machinery, creating a molecular memory (11).

In vitro models to study metabolism

In vitro, the kinetics of metabolism are very much dependent on cell culture conditions. It has been suggested that treatments that induce cell proliferation activate enzymatic pathways leading to the formation of lactate (37). Removal of serum, as in our experiments, usually inhibits cell proliferation, implying decreased lactate production. Yet, fibroblast strains from offspring showed higher levels of lactate in the medium than those of their partners, possibly because strains from offspring are less sensitive to removal of factors which promote proliferation. Furthermore, serum starvation-induced quiescent cells are resistant to

becoming senescent (38). As already alluded to, we showed that fibroblasts strains from offspring are indeed less sensitive to (stress-induced) senescence (7).

Manipulation of single genes in model organisms has provided much insight in to the pathways regulating metabolism. Evidently, this genetic manipulation is limited in humans *in vivo* for ethical reasons. It is, however, possible to experiment with cells isolated from humans, providing a powerful tool to study the pathways regulating metabolism. Furthermore, it is difficult to measure metabolites at the cellular level in organisms *in vivo*, whereas this is much easier for cells *in vitro*. Care should be taken, though, in translating *in vitro* results to the *in vivo* situation, for two main reasons. First, *in vitro* characteristics of cells depend on culture conditions like the type of medium, batch and concentration of added serum, oxygen concentration and the number of PDs undergone *in vitro*, making it difficult to compare studies (39). Second, cells *in vitro* have been removed from their natural environment, being derived from many factors in the blood (e.g. cytokines and growth factors) and cell-cell and cell-matrix interactions (40). Despite these caveats, *in vitro* cultured cells derived from subjects of different populations reflect differences between these subjects, providing a powerful tool to study differences in metabolism between these subjects at the cellular level

An important strength of our study is the large number of fibroblast strains obtained from subjects of various biological ages, collected and stored in a highly standardized manner. An important limitation of this study is the fact that the observed differences were small and that, despite being valid, the predictive power of the model proved limited. This may be due to the fact that not all offspring carry the longevity traits and hence the observation in the fibroblasts of a random group of offspring dilutes the effects of longevity associated mechanisms that could be observed. In addition, compounds present at much lower concentrations could be responsible for metabolic differences between fibroblast strains from offspring and partners, but the methods applied here were not sensitive enough to detect differences in these compounds.

In conclusion, we report for the first time, that the NMR-based metabolic profiles of human cells *in vitro* reflect the propensity for human longevity of the subjects from whom these were

derived. Future work will have to elucidate the enzymes driving differences in metabolism and the pathways regulating these enzymes.

Reference List

(1) Oeppen J, Vaupel JW. Demography. Broken limits to life expectancy. Science 2002;296:1029-1031.

(2) Schoenmaker M, de Craen AJ, de Meijer PH, Beekman M, Blauw GJ, Slagboom PE, Westendorp RG. Evidence of genetic enrichment for exceptional survival using a family approach: the Leiden Longevity Study. Eur J Hum Genet 2006;14:79-84.

(3) Westendorp RG, van Heemst D, Rozing MP, Frolich M, Mooijaart SP, Blauw GJ, Beekman M, Heijmans BT, de Craen AJ, Slagboom PE. Nonagenarian siblings and their offspring display lower risk of mortality and morbidity than sporadic nonagenarians: The Leiden Longevity Study. J Am Ger Soc 2009;57:1634-1637.

(4) Rozing MP, Westendorp RG, de Craen AJ, Frolich M, de Goeij MC, Heijmans BT, Beekman M, Wijsman CA, Mooijaart SP, Blauw GJ, Slagboom PE, van HD. Favorable glucose tolerance and lower prevalence of metabolic syndrome in offspring without diabetes mellitus of nonagenarian siblings: the Leiden longevity study. J Am Geriatr Soc 2010;58:564-569.

(5) Wijsman CA, Rozing MP, Streefland TC, Le CS, Mooijaart SP, Slagboom PE, Westendorp RG, Pijl H, van HD. Familial longevity is marked by enhanced insulin sensitivity. Aging Cell 2010;10-9726.

(6) Vaarhorst AA, Beekman M, Suchiman EH, van HD, Houwing-Duistermaat JJ, Westendorp RG, Slagboom PE, Heijmans BT. Lipid metabolism in long-lived families: the Leiden Longevity Study. Age (Dordr) 2010.

(7) Dekker P, Maier AB, van HD, de Koning-Treurniet C, Blom J, Dirks RW, Tanke HJ, Westendorp RG. Stress-induced responses of human skin fibroblasts in vitro reflect human longevity. Aging Cell 2009;8:595-603.

(8) Dekker P, van Baalen LM, Dirks RW, Slagboom PE, van Heemst D, Tanke HJ, Westendorp RGJ, Maier AB. Chronic inhibition of the respiratory chain differentially affects fibroblast strains from young and old subjects. J Gerontol A Biol Sci Med Sci 2011 Nov 10 [Epub ahead of print].

(9) Derhovanessian E, Maier AB, Beck R, Jahn G, Hahnel K, Slagboom PE, de Craen AJ, Westendorp RG, Pawelec G. Hallmark features of immunosenescence are absent in familial longevity. J Immunol 2010;185:4618-4624.

(10) Rozing MP, Westendorp RG, de Craen AJ, Frolich M, Heijmans BT, Beekman M, Wijsman C, Mooijaart SP, Blauw GJ, Slagboom PE, van HD. Low serum free triiodothyronine levels mark familial longevity: the Leiden Longevity Study. J Gerontol A Biol Sci Med Sci 2010;65:365-368.

(11) Mobbs CV, Mastaitis JW, Zhang M, Isoda F, Cheng H, Yen K. Secrets of the lac operon. Glucose hysteresis as a mechanism in dietary restriction, aging and disease. Interdiscip Top Gerontol 2007;35:39-68.:39-68.

(12) Kell DB, Brown M, Davey HM, Dunn WB, Spasic I, Oliver SG. Metabolic footprinting and systems biology: the medium is the message. Nat Rev Microbiol 2005;3:557-565.

(13) MacIntyre DA, Melguizo SD, Jimenez B, Moreno R, Stojkovic M, Pineda-Lucena A. Characterisation of human embryonic stem cells conditioning media by 1H-nuclear magnetic resonance spectroscopy. PLoS One 2011;6:e16732.

(14) Bradley SA, Ouyang A, Purdie J, Smitka TA, Wang T, Kaerner A. Fermentanomics: monitoring mammalian cell cultures with NMR spectroscopy. J Am Chem Soc 2010;132:9531-9533.

(15) Maier AB, le Cessie S, Koning-Treurniet C, Blom J, Westendorp RG, van Heemst D. Persistence of high-replicative capacity in cultured fibroblasts from nonagenarians. Aging Cell 2007;6:27-33.

(16) Keun HC, Ebbels TM, Antti H, Bollard ME, Beckonert O, Schlotterbeck G, Senn H, Niederhauser U, Holmes E, Lindon JC, Nicholson JK. Analytical reproducibility in (1)H NMR-based metabonomic urinalysis. Chem Res Toxicol 2002;15:1380-1386.

(17) Kumar A, Ernst RR, Wuthrich K. A two-dimensional nuclear Overhauser enhancement (2D NOE) experiment for the elucidation of complete proton-proton cross-relaxation networks in biological macromolecules. Biochem Biophys Res Commun 1980;95:1-6.

(18) Price WS. Water signal suppression in NMR spectroscopy. 1999: 289-354. Ref Type: Book, Whole.

(19) Wu PS, Otting G. Rapid pulse length determination in high-resolution NMR. J Magn Reson 2005;176:115-119.

(20) Coron A, Vanhamme L, Antoine JP, Van HP, Van HS. The filtering approach to solvent peak suppression in MRS: a critical review. J Magn Reson 2001;152:26-40.

(21) Torgrip RJO, Aberg KM, Alm E, Schuppe-Koistinen I, Lindberg J. A note on normalization of biofluid 1D H-1-NMR data. Metabolomics 2008;4:114-121.

(22) Dieterle F, Ross A, Schlotterbeck G, Senn H. Probabilistic quotient normalization as robust method to account for dilution of complex biological mixtures. Application in 1H NMR metabonomics. Anal Chem 2006;78:4281-4290.

(23) Lemonnier F, Gautier M, Moatti N, Lemonnier A. Comparative study of extracellular amino acids in culture of human liver and fibroblastic cells. In Vitro 1976;12:460-466.

(24) Yagasaki M, Hashimoto S. Synthesis and application of dipeptides; current status and perspectives. Appl Microbiol Biotechnol 2008;81:13-22.

(25) Felig P. The glucose-alanine cycle. Metabolism 1973;22:179-207.

(26) Lanks KW. End products of glucose and glutamine metabolism by L929 cells. J Biol Chem 1987;262:10093-10097.

(27) Zielke HR, Sumbilla CM, Sevdalian DA, Hawkins RL, Ozand PT. Lactate: a major product of glutamine metabolism by human diploid fibroblasts. J Cell Physiol 1980;104:433-441.

(28) Pucci E, Chiovato L, Pinchera A. Thyroid and lipid metabolism. Int J Obes Relat Metab Disord 2000;24 Suppl 2:S109-12.:S109-S112.

(29) Robinson BH. Cell culture studies on patients with mitochondrial diseases: molecular defects in pyruvate dehydrogenase. J Bioenerg Biomembr 1988;20:313-323.

(30) Robinson BH, McKay N, Goodyer P, Lancaster G. Defective intramitochondrial NADH oxidation in skin fibroblasts from an infant with fatal neonatal lacticacidemia. Am J Hum Genet 1985;37:938-946.

(31) Andrejchyshyn S, Continelli L, Germinario RJ. Permanent hexose transport upregulation in a respiration-deficient human fibroblast cell strain. Am J Physiol 1991;261:C973-C979.

(32) Hehenberger K, Heilborn JD, Brismar K, Hansson A. Inhibited proliferation of fibroblasts derived from chronic diabetic wounds and normal dermal fibroblasts treated with high glucose is associated with increased formation of l-lactate. Wound Repair Regen 1998;6:135-141.

(33) Yevdokimova NY, Podpryatov SE. Hyaluronic acid production and CD44 expression in cultured dermal fibroblasts of patients with non-insulin-dependent diabetes mellitus with and without chronic ulcers on the lower extremity. Wound Repair Regen 2005;13:181-188.

(34) Shim H, Chun YS, Lewis BC, Dang CV. A unique glucose-dependent apoptotic pathway induced by c-Myc. P Natl Acad Sci USA 1998;95:1511-1516.

(35) Dorai H, Kyung YS, Ellis D, Kinney C, Lin C, Jan D, Moore G, Betenbaugh MJ. Expression of anti-apoptosis genes alters lactate metabolism of Chinese Hamster Ovary cells in culture. Biotechnol Bioeng 2009;103:592-608.

(36) Blazer S, Khankin E, Segev Y, Ofir R, Yalon-Hacohen M, Kra-Oz Z, Gottfried Y, Larisch S, Skorecki KL. High glucose-induced replicative senescence: point of no return and effect of telomerase. Biochem Biophys Res Commun 2002;296:93-101.

(37) Fodge DW, Rubin H. Stimulation of lactic acid production in chick embryo fibroblasts by serum and high pH in the absence of external glucose. J Cell Physiol 1975;86:453-457.

(38) Demidenko ZN, Blagosklonny MV. Growth stimulation leads to cellular senescence when the cell cycle is blocked. Cell Cycle 2008;7:3355-3361.

(39) Macieira-Coelho A. Relevance of in vitro studies for aging of the organism. A review. Z Gerontol Geriatr 2001;34:429-436.

(40) Horrobin DF. Modern biomedical research: an internally self-consistent universe with little contact with medical reality? Nat Rev Drug Discov 2003;2:151-154.

Supplemental material

Supplemental table 1. Outlier identification: Characteristics of Spectroscopic Outliers

#	Sample ID	TSP line width	Water Suppression
89	Sample missing	-	-
91	Sample missing	-	-
109	50-24h	Acquisition failed	-
169	111-24h	OK (1.03 Hz)	FAIL
195	117-5d	FAIL (4.06 Hz)	OK
197	118-24h	FAIL (6.56 Hz)	OK
199	118-5d	FAIL (3.44 Hz)	OK
203	119-5d	FAIL (3.19 Hz)	OK
207	120-5d	OK (1.15 Hz)	FAIL
235	127-5d	OK (0.82 Hz)	FAIL
287	121-128-control-5d	FAIL (7.43 Hz)	OK
289	129-136-control-24h	FAIL (1.56 Hz)	FAIL

Visual inspection of the individual spectra during data processing was used to remove spectroscopic outliers. As parameter for shim quality, the half width of the TSP line was evaluated after processing without apodization. Water suppression quality was assessed by total height of the remaining water resonance and presence of shoulders at the base of the signal. A total of 10 datasets were removed prior to further analysis as summarized in Supplemental table1. Biological outliers were identified based on Hotelling's T2 range (above 99% T2 critical value) and distance of the observation in the training set to the X model plane values (> 2) (These parameters describe how well the data is located within model space).

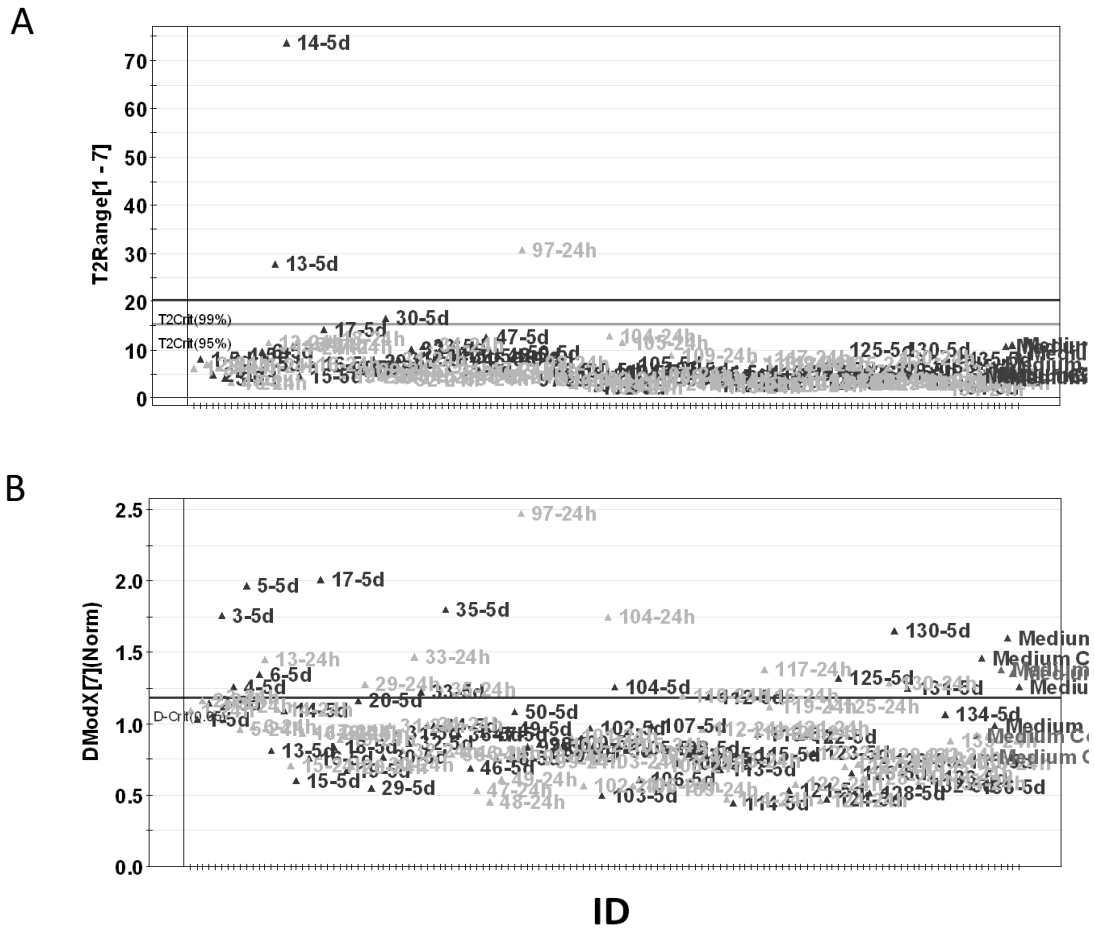

Supplemental figure 1. Hotelling's T2 plot (A) and DModX plot (B) for PCA model built using eight components from data without scaling of variables. Data points are labeled according to fibroblast culture incubation duration of 24 hours (▲) and five days (▲) as well as control medium incubated for 24 hours (▲) and five days (▲).

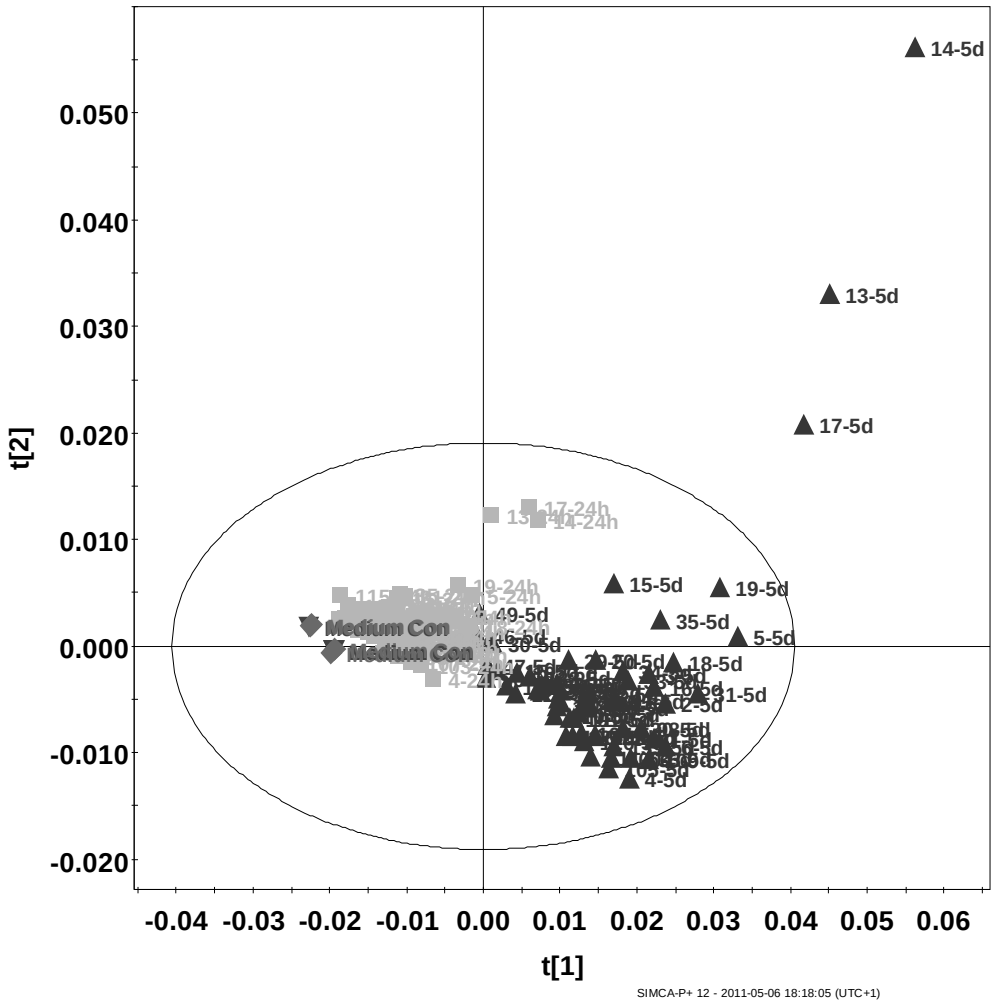

Supplemental figure 2. Scores plot of first two principal components from PCA model built from complete data set without scaling of variables. Data points are labeled according to fibroblast culture incubation duration of 24 hours (■) and five days (▲) as well as cell-free/serum-free medium (control medium) incubated for 24 hours (◆) and five days (▼).

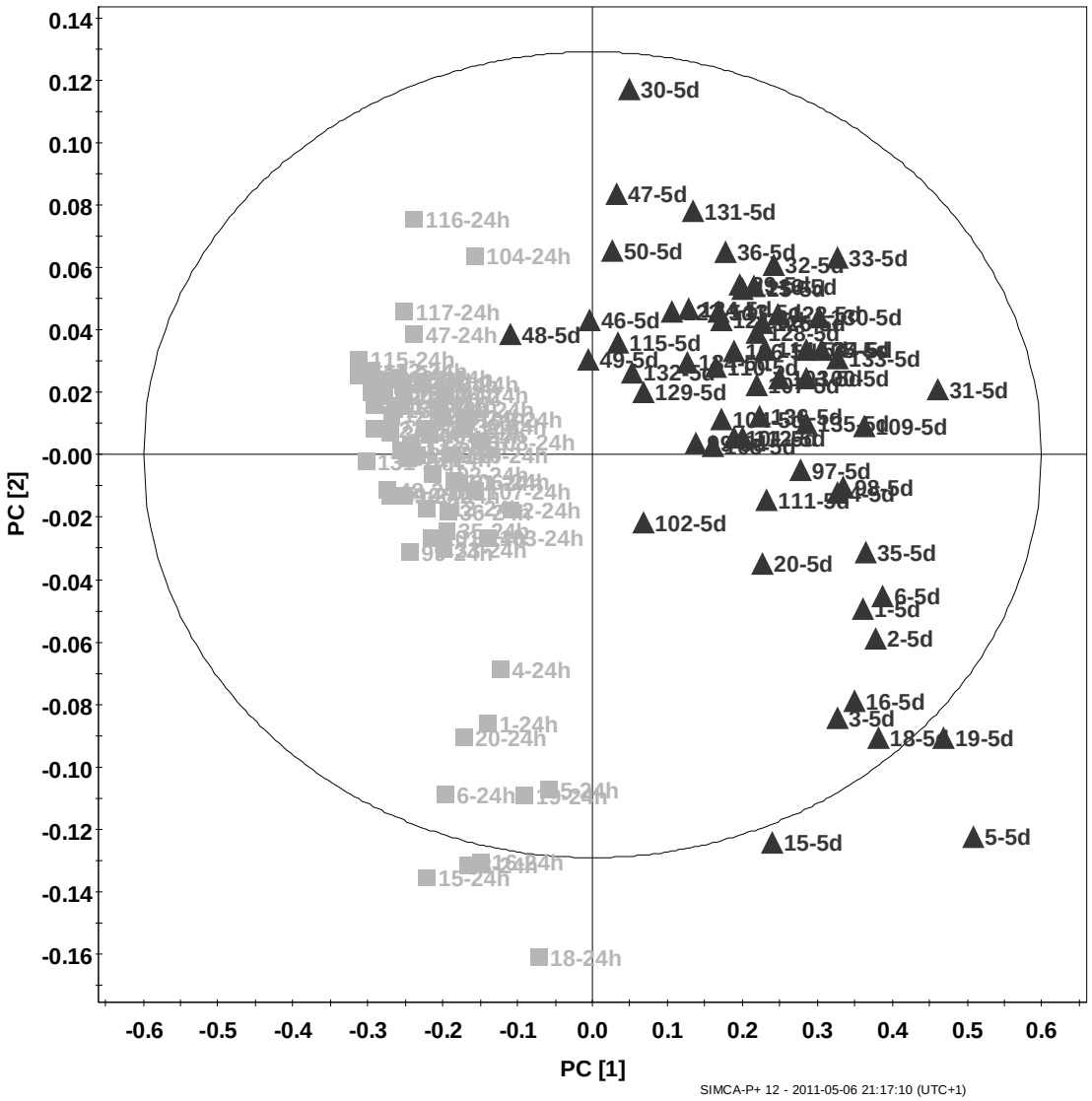

Supplemental figure 3. Scores plot of first two components from PLS-DA model built using time point as response variable. Data points are labeled according to fibroblast culture incubation duration of 24 hours (■) and five days (▲), respectively.

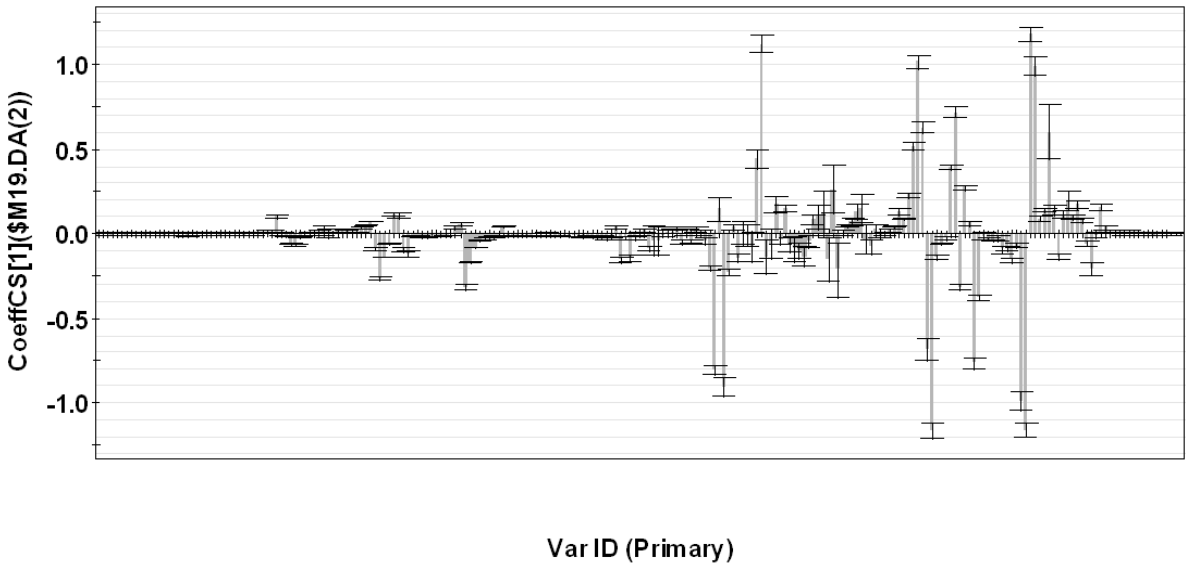

Supplemental figure 4. Coefficients plot for first component of PLS-DA model built using time point as response variable.

OSC Validation

For validation of the OSC filtering step, 59 datasets were generated using OSC filtering of the original data leaving out one of the 59 observations, such that each sample was omitted once (leave-one-out cross validation). For each dataset an independent PLS-DA two-class models was build using the 58 observations that were included in the filtering step followed by prediction of the response variable for the excluded observation using the respective model. The predicted values were then used for classification of the samples as summarized in Supplemental table 2. The overall correct classification of all samples was 62.7% with a 95% confidence interval for the proportion correctly identified of [0.5036, 0.7504] excluding the null hypothesis.

Supplemental table 2. Misclassification table for OSC leave-one-out cross validation

			predicted	
	Members	Correct	offspring	partner
offspring	28	60.7%	17	11
partner	31	64.5%	11	20
Total	**59**	**62.7%**	**28**	**31**

.

Chapter 8

General discussion

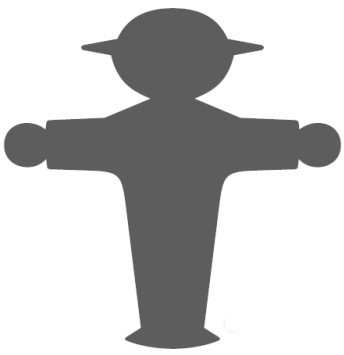

General discussion

This thesis aimed to investigate the cellular processes responsible for differences in human longevity. We studied *in vitro* stress responses of dermal fibroblast strains derived from offspring of nonagenarian siblings with the propensity for longevity and compared them with the responses of fibroblast strains derived from the partners of the offspring, representing the general population. As a proof-of-principle we also compared fibroblast strains from chronologically young and old subjects, hypothesizing that differences between offspring and partners should be similar, at least in terms of direction, to differences between fibroblast strains from chronologically young and old subjects.

Main findings

In **chapter 2** we describe the optimization of a flow cytometric method described earlier (1) to better differentiate between populations of fibroblasts in degrees of SA-β-gal activity. SA-β-gal activity is a widely used marker for cellular senenescence and is routinely detected cytochemically, manually discriminating negative from positive cells (2;3). This method is time-consuming, subjective and therefore prone to operator-error. Skin fibroblasts were isolated from young and very old participants of the Leiden 85-plus Study (4;5). To induce stress-induced senescence, fibroblasts were exposed to rotenone and senescence was assessed measuring SA-β-gal activity by cytochemistry and by flow cytometry. Under non-stressed conditions, fibroblasts from old subjects showed higher SA-β-gal activity than fibroblasts from young subjects and this difference was found for both the flow cytometric and cytochemical methods. However, under stress-induced conditions the flow cytometric method but not the cytochemical method revealed significantly higher SA-β-gal activity in fibroblasts from very old compared with young subjects. We concluded that the modified flow cytometric method for measuring SA-β-gal activity is superior in discriminating between degrees of senescence in different populations of fibroblasts.

Chapter 3 describes the cellular responses to stress in skin fibroblasts that were isolated from young and old participants of the Leiden 85-plus Study (4;5). These responses were compared with the responses of isolated fibroblast strains from participants of the Leiden Longevity Study, offspring of nonagenarian siblings, and their partners, representatives of the general population (6). Under non-stressed conditions SA-β-gal activity was lower and levels of apoptosis/cell death were higher in fibroblasts from young subjects when compared with fibroblasts from old subjects, as were stress-induced increases. Numbers and total size of colonies under non-stressed conditions were higher for fibroblasts from young subjects. Under non-stressed conditions there were no differences in levels of SA-β-gal activity and apoptosis/cell death between fibroblasts from offspring and partners. Stress-induced increases of SA-β-gal activity were smaller and levels of apoptosis/cell death higher in fibroblast strains of offspring when compared with strains of partners. Numbers and total size of colonies under non-stressed conditions were higher for fibroblasts from offspring whereas rotenone-induced decreases were lower. These results suggest that under stressed conditions, fibroblast strains from offspring resemble fibroblast strains from chronologically young subjects and provide support for the hypothesis that *in vitro* cellular responses to stress reflect the propensity for human longevity.

Cellular senescence, an important factor in aging phenotypes, can be induced by replicative exhaustion or by stress. **Chapter 4** reports on the relation between maximum replicative capacity, telomere length, stress-induced cellular senescence and apoptosis/cell death in human primary fibroblast strains obtained from nonagenarians of the Leiden 85-plus Study. Fibroblast strains cultured until replicative senescence (5) were stressed with rotenone at low passage. Fibroblast strains with a higher replicative capacity had longer telomeres. In non-stressed conditions replicative capacity was not associated with SA-β-gal activity and negatively associated with cell death. In rotenone-stressed conditions replicative capacity was negatively associated with senescence and positively associated with cell death. These data indicate that fibroblast strains with a higher maximum replicative capacity have longer telomeres, are less prone to go into stress-induced cellular senescence and more prone to die after stress.

The free radical theory of aging states that function of the respiratory chain becomes less efficient with age (7). The concomitant increased levels of ROS damage proteins and DNA. To model this process *in vitro*, we chronically exposed fibroblasts to a low dose of the mitochondrial complex I inhibitor rotenone. In **chapter 5** we describe the different responses between fibroblast strains from young and old subjects, and between offspring of nonagenarian siblings and their partners. Under non-stressed conditions, fibroblast strains from young subjects showed lower ROS levels and a higher growth speed when compared with old subjects, but telomere length and shortening rate were not different. Significantly increased ROS levels were observed after chronic exposure of fibroblasts to rotenone, whereas growth speed was inhibited and telomeres had shortened. Under stressed conditions, lower ROS levels and a larger decrease in growth speed were found for fibroblast strains from young subjects when compared with strains from old subjects. However, no differences in telomere shortening rate were observed. The stress-induced decrease in growth speed was larger in strains from offspring of nonagenarian siblings when compared with their age matched partners from the general population. Summarizing, fibroblast strains from young and old people are differentially affected by chronic inhibition of the respiratory chain and responses in fibroblast from offspring of nonagenarian siblings resemble the responses of strains from young subjects.

Not much is known about the complex interplay between upstream and downstream pathways leading to senescence. In **chapter** 6 we investigated the signaling pathways responsible for the different *in vitro* phenotypes between fibroblast strains from young and old subjects. We determined whole genome gene expression of non-stressed and rotenone-stressed human fibroblast strains from young and old subjects and identified gene sets involved in cell cycle, mitochondria and transcription. The gene whose expression differed most between fibroblast strains from young and old subjects was the cell cycle inhibitor p16, being higher in expression in fibroblast strains from old subjects. p16 is regarded as a robust marker for cellular aging (8) and increasing numbers of p16-positive cells can be found in mitotic aging of aging primates (9;10). Furthermore, p16 plays an important role in senescence (11). Unexpectedly p16 mRNA decreased after rotenone. To verify these results, we performed independent experiments and p16 was measured at both the mRNA level and

the protein level. Rotenone again resulted in decreased p16 mRNA expression, but this time p16 mRNA expression was lower in fibroblast strains from old subjects. This discrepancy might be explained by differences in seeding density and/or differences in incident diseases in the two different samples used for the microarray and replication experiments. No rotenone-induced changes or young-old differences in protein expression could be measured by Western blotting, whereas by immunocytochemistry fibroblast strains from old subjects showed higher percentages of p16-positive cells in both non-stressed and rotenone-stressed conditions.

When compared with the general population, nonagenarian siblings and their offspring showed a lower risk of diabetes mellitus (12), better insulin sensitivity and glucose handling (13;14) and a different lipid metabolism (15), indicating differences in metabolism in general. In **chapter 7** we investigated if fibroblast strains from offspring and partners also show differences in cellular metabolism *in vitro*. Ala-gln and glucose consumption were higher for fibroblast strains derived from offspring, when compared with fibroblast strains from their partners. Production of glutamine, alanine, lactate and pyroglutamic acid was found to be higher for fibroblast strains derived from offspring, when compared with fibroblast strains from their partners. In conclusion, the metabolic profiles of human fibroblasts *in vitro* reflect differences between offspring from families with the propensity for longevity when compared with fibroblasts from their partners.

Methodological issues

All the results described in this thesis were derived from *in vitro* experiments. As already alluded to in the introduction, translation of *in vitro* results to the *in vivo* situation requires much cautiousness (16). An important strength of our study is the fact that we can directly link the *in vitro* data to the *in vivo* data of the subjects the fibroblast strains were derived from. However, cells *in vitro* have been taken out of their natural context and are thus likely to display a very different cellular phenotype, making it difficult to interpret the relevance of *in vitro* results for the *in vivo* situation. Depending on the proliferative state of cells, they will be more or less responsive to stimuli and especially dermal fibroblasts are not as proliferative *in vivo* as they are *in vitro*.

Results can also be different depending on culture conditions. All cell types in the body experience oxygen tensions much lower than the oxygen tension of ambient air (17) under which cells are usually cultured. It is likely that ambient oxygen tension actually stresses cells and this background stress might make it difficult to measure stress responses induced by an experimental stressor (rotenone in our case). Cells can be handled and cultured under low oxygen tension conditions but the equipment necessary to do this is very costly and this is not feasible for many laboratories. Other culture conditions that will affect the results are the presence or absence of factors in the medium (e.g. growth factors, cytokines etc.), mostly derived from the foetal calf serum added to the medium but also often added separately. Different batches of foetal calf serum can yield different results so it is of paramount importance that when experiments are replicated, the same batch of serum is used and one batch of foetal calf serum will only allow for a limited number of experiments. We used the same batches of serum for our experiments, but the serum that was used for the Leiden 85-plus Study fibroblast strains was different than the batch used for the Leiden Longevity Study fibroblast strains, making one-on-one comparisons impossible. When comparing the results of the fibroblast strains of these studies, we could only look at the direction of differences. Furthermore, the sizes of the biopsies the fibroblasts were isolated from were different for the Leiden 85-plus Study (3 mm) and the Leiden Longevity Study (4 mm).

Another factor which should be taken into account when interpreting *in vitro* data is the cell type. The dermal fibroblast has been a popular *in vitro* model since this cell type is easily accessible and grows readily *in vitro*, providing ample (yet finite) experimental material. However, results generated with this model are not necessarily valid for other cell types. In the experiments described in this thesis we aimed to oxidatively stress the fibroblasts. One of the most commonly used oxidative stressors is hydrogen peroxide, but due to its reactive properties it is very unstable and it will readily react with other components in the culture medium, making it difficult to determine what final concentration is applied. Since one of the theories of aging states that a decreasing efficiency in oxidative phosphorylation results in mitochondria-derived increased ROS levels, we decided to use rotenone which inhibits complex I in the oxidative phosphorylation chain in the mitochondria. Although rotenone is extensively used in mitochondrial research, it is not used much in the field of aging, senescence and apoptosis, complicating comparison of our results with other workers.

Implications and future research

We have now shown that fibroblasts *in vitro* do reflect the population of subjects from which they were derived. More specifically, we have shown differences in *in vitro* stress responses dependent on chronological and biological age *in vivo*. Fibroblast strains of offspring with the propensity for longevity showed stress-induced responses that tended to be more like the responses from chronologically young subjects. Fibroblast strains from offspring of nonagenarian siblings showed less senescence and more apoptosis/cell death. The latter could be interpreted as being a tumor suppressive mechanism, removing damaged cells from the proliferative pool of cells before they become tumorigenic. Removed cells should then be replaced with healthy cells from a pool of replenishing stem cells. This could be a topic for further research.

Although there was much interindividual variation, *in vitro* stress responses might be regarded as a marker for biological age. Having found these *in vitro* differences, we performed initial experiments using a transcriptomics approach on the comparison of fibroblast strains of chronological young versus old subjects, to gain more insight in the pathway driving these differences. This approach should now be extended to the comparison of fibroblast strains of biologically young (offspring) with old (partners) subjects to determine if the pathways driving the differences in chronological age are similar to those driving biological age and to identify (combinations) of candidate genes as possible markers for biological age. Once pathways and key regulators in these pathways are defined, genetic variation in the responsible genes should be studied to see to what extent this variation can explain differences in responses to stress that ultimately lead to increased longevity. Ideally this approach should also be applied to cell types and stressors other than those described in this thesis. Once common pathways and genes responsible for the differences in chronological and biological age are identified, these pathways might be modulated by compounds resulting in biologically old cells becoming biologically younger, i.e. resemble chronologically younger cells.

Reference List

(1) Kurz DJ, Decary S, Hong Y, Erusalimsky JD. Senescence-associated beta-galactosidase reflects an increase in lysosomal mass during replicative ageing of human endothelial cells. J Cell Sci 2000;113:3613-3622.

(2) Dimri GP, Lee XH, Basile G, Acosta M, Scott C, Roskelley C, Medrano EE, Linskens M, Rubelj I, Pereirasmith O, Peacocke M, Campisi J. A Biomarker That Identifies Senescent Human-Cells in Culture and in Aging Skin In-Vivo. P Natl Acad Sci USA 1995;92:9363-93674.

(3) Toussaint O, Medrano EE, von Zglinicki T. Cellular and molecular mechanisms of stress-induced premature senescence (SIPS) of human diploid fibroblasts and melanocytes. Exp Gerontol 2000;35:927-945.

(4) Bootsma-van der Wiel A, Gussekloo J, de Craen AJM, van Exel E, Bloem BR, Westendorp RGJ. Common chronic diseases and general impairments as determinants of walking disability in the oldest-old population. J Am Geriatr Soc 2002;50:1405-1410.

(5) Maier AB, le Cessie S, Koning-Treurniet C, Blom J, Westendorp RG, van Heemst D. Persistence of high-replicative capacity in cultured fibroblasts from nonagenarians. Aging Cell 2007;6:27-33.

(6) Schoenmaker M, de Craen AJ, de Meijer PH, Beekman M, Blauw GJ, Slagboom PE, Westendorp RG. Evidence of genetic enrichment for exceptional survival using a family approach: the Leiden Longevity Study. Eur J Hum Genet 2006;14:79-84.

(7) Harman D. Aging: a theory based on free radical and radiation chemistry. J Gerontol 1956;11:298-300.

(8) Harman D. Aging: a theory based on free radical and radiation chemistry. J Gerontol 1956;11:298-300.

(9) Jeyapalan JC, Ferreira M, Sedivy JA, Herbig U. Accumulation of senescent cells in mitotic tissue of aging primates. Mech Ageing Dev 2007;128:36-44.

(10) Ressler S, Bartkova J, Niederegger H, Bartek J, Scharffetter-Kochanek K, Jansen-Durr P, Wlaschek M. p16INK4A is a robust in vivo biomarker of cellular aging in human skin. Aging Cell 2006;5:379-389.

(11) Ben-Porath I, Weinberg RA. The signals and pathways activating cellular senescence. Int J Biochem Cell Biol 2005;37:961-976.

(12) Westendorp RG, van Heemst D, Rozing MP, Frolich M, Mooijaart SP, Blauw GJ, Beekman M, Heijmans BT, de Craen AJ, Slagboom PE. Nonagenarian siblings and their offspring display lower risk of mortality and morbidity than sporadic nonagenarians: The Leiden Longevity Study. J Am Geriatr Soc 2009;57:1634-1637.

(13) Rozing MP, Westendorp RG, de Craen AJ, Frolich M, de Goeij MC, Heijmans BT, Beekman M, Wijsman CA, Mooijaart SP, Blauw GJ, Slagboom PE, van HD. Favorable glucose tolerance and lower prevalence of metabolic syndrome in offspring without diabetes mellitus of nonagenarian siblings: the Leiden longevity study. J Am Geriatr Soc 2010;58:564-569.

(14) Wijsman CA, Rozing MP, Streefland TC, Le CS, Mooijaart SP, Slagboom PE, Westendorp RG, Pijl H, van HD. Familial longevity is marked by enhanced insulin sensitivity. Aging Cell 2010;10-9726.

(15) Vaarhorst AA, Beekman M, Suchiman EH, van HD, Houwing-Duistermaat JJ, Westendorp RG, Slagboom PE, Heijmans BT. Lipid metabolism in long-lived families: the Leiden Longevity Study. Age (Dordr) 2010.

(16) Horrobin DF. Modern biomedical research: an internally self-consistent universe with little contact with medical reality? Nat Rev Drug Discov 2003;2:151-154.

(17) Balin AK, Fisher AJ, Anzelone M, Leong I, Allen RG. Effects of establishing cell cultures and cell culture conditions on the proliferative life span of human fibroblasts isolated from different tissues and donors of different ages. Exp Cell Res 2002;274:275-287.

Nederlandse samenvatting

Uit de Leiden Lang Leven Studie is gebleken dat negentigjarige broers en zussen uit families met een aanleg voor langlevendheid 41% minder kans hebben om te overlijden vergeleken met negentigjarigen die zonder broer of zus die leeftijd hebben weten te behalen (de zogenaamde sporadisch negentigjarigen). Ook de kinderen (± 60 jaar oud) van de negentigjarige broers en zussen uit de langlevende families vertonen een significant lagere prevalentie van hartinfarcten, hoge bloeddruk en suikerziekte vergeleken met de partners van de kinderen. Met andere woorden, de leden van de langlevende families lijken biologisch jonger te zijn dan leeftijdgenoten uit andere families. Het doel van dit proefschrift is het bestuderen van de cellulaire processen die ten grondslag liggen aan deze familiair aangelegde langlevendheid, gebruik makend van huidcellen, de zogenaamde fibroblasten. Het doel was om eerst aan te tonen dat de fibroblasten van de kinderen uit de langlevende families *in vitro* (kunstmatig gekweekt in het laboratorium) anders reageren, waarbij we fibroblasten van de kinderen vergeleken met de fibroblasten van hun partners. Zij delen immers dezelfde leefomgeving en (eet-) gewoontes en vertegenwoordigen de algemene bevolking. Om de kans te vergroten verschillen tussen deze twee groepen te zien, bestudeerden we de fibroblasten onder niet-gestimuleerde omstandigheden en na het toedienen van oxidatieve stress. Om deze processen ook te kunnen vergelijken voor kalenderleeftijd, vergeleken we verder fibroblasten afkomstig van jonge mensen (± 23 jaar oud) met fibroblasten van heel oude mensen (> 90 jaar oud) uit de Leiden 85-plus Studie. We hebben ons vooral gericht op de cellulaire processen apoptose (gereguleerde celdood) en cellulaire senescence (een staat waarin cellen stoppen met delen en heel andere eigenschappen krijgen), omdat deze processen een grote rol spelen in de reactie van cellen op stress en in ouderdomsgerelateerde ziekten. Verder waren we geïnteresseerd in de vraag welke signaaltransductieroutes verantwoordelijk zijn voor de verschillen tussen de fibroblasten afkomstig van de verschillende groepen mensen. Met signaaltransductieroutes bedoelen we de communicatie tussen de verschillende processen op celniveau.

In **hoofdstuk 2** wordt de optimalisatie beschreven van een flow-cytometriemethode waarmee beter onderscheid gemaakt kan worden tussen fibroblastpopulaties die een verschillende

mate van Senescence Associated-β-galactosidase (SA-β-gal) activiteit vertonen. SA-β-gal activiteit is een veelgebruikte marker voor cellulaire senescence die oorspronkelijk op een cytochemische (het kleuren van cellen) manier gebruikt wordt, waarbij cellen handmatig geteld worden. Deze methode is tijdrovend, subjectief en daarom gevoelig voor fouten. Uit de resultaten trokken wij de conclusie dat de flow-cytometriemethode om SA-β-gal activiteit te meten superieur is in het onderscheiden van de mate van senescence van verschillende populaties van fibroblasten.

Hoofdstuk 3 beschrijft de cellulaire reacties op stress in fibroblasten geïsoleerd uit jonge en oude mensen die deelnamen aan de Leiden 85-plus Studie. Deze reacties werden vergeleken met de reacties van fibroblasten geïsoleerd uit kinderen uit de langlevende families en uit hun partners, als deel van de Leiden Lang Leven Studie. Wanneer senescence, apoptose/celdood en het vermogen van fibroblasten om te delen gemeten werden, leken de reacties van de fibroblasten uit de mensen uit de langlevende families meer op de reacties van de fibroblasten uit de jonge mensen, met andere woorden, deze fibroblasten leken biologisch jonger te zijn. Hieruit concludeerden wij dat de uitzonderlijke langlevendheid van de mensen uit de langlevende families ook tot uiting komt in de cellulaire reacties van hun fibroblasten *in vitro*.

Cellulaire senescence wordt beschouwd als een belangrijke factor in het verouderingsproces en kan opgewekt worden door cellen net zo lang *in vitro* te laten groeien totdat zij stoppen met delen. Echter, senescence kan ook optreden in cellen als zij worden blootgesteld aan stress. In beide processen spelen telomeren een belangrijke rol. Telomeren zijn de uiteinden van de chromosomen en dienen als beschermende buffers tijdens het kopiëren van het DNA (vergelijkbaar met de uiteinden van veters om te voorkomen dat deze gaan rafelen). In **hoofdstuk 4** hebben we gekeken of er een relatie is tussen de verschillende oorzaken van senescence. We vonden dat fibroblasten waarvan bekend is dat zij een grotere replicatiecapaciteit hebben (ofwel langer door kunnen groeien *in vitro*) ook langere telomeren hadden, minder gevoelig waren voor stress-geïnduceerde senescence en juist sneller doodgingen als gevolg van stress.

Eén van de bekendste theorieën van veroudering is gebaseerd op de veronderstelling dat het omzetten van brandstof en zuurstof in cellen minder efficiënt wordt met toenemende leeftijd. Dit leidt tot het vrijkomen van meer reactieve zuurstofradicalen die eiwitten en DNA kunnen beschadigen. In **hoofdstuk 5** beschrijven we experimenten waarmee we dit proces hebben willen simuleren. Rotenon is een chemische stof die het verbrandingsproces in de mitochondriën (de energiecentrales van de cel) verstoort en zo leidt tot toegenomen hoeveelheden zuurstofradicalen. Zowel in niet-gestresste en rotenon-behandelde toestand vonden we dat fibroblasten van mensen uit langlevende families leken op fibroblasten van jonge mensen. We vonden echter geen verschillen in telomeerlengte of mate van telomeerverkorting.

Er is nog niet veel bekend over de complexe samenwerking tussen de signaaltransductie-routes die leiden tot senescence en de routes die als gevolg van senescence actief worden. **Hoofdstuk 6** beschrijft de experimenten waarmee we deze signaaltransductieroutes hebben willen identificeren, gebruik makend van een techniek waarmee de expressie van vele duizenden genen tegelijk kan worden bestudeerd. We vergeleken fibroblasten van jonge en oude mensen en vonden verschillen in de signaaltransductieroutes die betrokken zijn bij de celcyclus, mitochondriale processen en transcriptie. In het bijzonder het eiwit p16, een celcyclusremmer, kwam in verschillend mate tot expressie in fibroblasten van jonge mensen vergeleken met de expressie in oude mensen. Het is bekend dat p16 een belangrijke rol speelt in senescence.

Vergeleken met de algemene bevolking hebben de mensen uit langlevende families minder kans op suikerziekte, betere insulinegevoeligheid, betere glucoseverwerking en een verschillend lipidemetabolisme. Deze verschillen duiden op verschillen in metabolisme tussen de normale bevolking en de langlevende families. In **hoofdstuk 7** hebben we gekeken of de fibroblasten van deze groepen mensen *in vitro* ook verschillen in metabolisme vertonen door met NMR-spectroscopie metabolieten in het celkweekmedium te meten. We vonden een hogere opname van glucose door fibroblasten uit mensen uit langlevende families. Ook andere metabolieten werden in verschillende mate uit het medium opgenomen

of in het medium uitgescheiden, wanneer fibroblasten uit mensen uit langlevende families vergeleken werden met fibroblasten uit hun partners.

Conclusie

We hebben laten zien dat de fibroblasten van verschillende populaties van mensen zich *in vitro* ook verschillend gedragen. In het bijzonder hebben we aangetoond dat de *in vitro* reacties op stress afhankelijk zijn van de kalenderleeftijd en de biologische leeftijd van de mensen waaruit de fibroblasten geïsoleerd zijn. Zo neigen de reacties van fibroblasten uit de mensen uit langlevende families meer naar reacties van de fibroblasten uit jonge mensen: de fibroblasten van jonge mensen en van de mensen uit de langlevende families vertonen minder senescence en gaan sneller dood als reactie op stress. Dit laatse lijkt een negatief effect, maar als cellen beschadigd raken lopen ze het risico de controle over de celcyclus te verliezen en ongecontroleerd te gaan delen. Dit verschijnsel is beter bekend onder de term kanker. Het verwijderen van deze cellen door ze gecontroleerd te verwijderen (apoptose) kan dus als beschermingsmechanisme tegen kanker gezien worden. De voorwaarde is dan wel dat de verwijderde cel vervangen kan worden door een gezonde cel. Vervolgonderzoek zal duidelijk moeten maken of dit inderdaad het geval is, welke genen en signaaltransductie-routes deze verschillen kunnen verklaren en hoe deze routes zodanig gemanipuleerd kunnen worden dat biologisch oudere fibroblasten (van de partners van mensen uit langlevende families) meer op biologisch jongere fibroblasten (van de mensen uit langlevende families) gaan lijken. Vervolgens zou dit principe voor andere celtypen *in vitro* aangetoond moeten en ten slotte *in vivo* (op het niveau van het organisme).

List of publications

Dekker P, Meissner A, Dirks RW, Slagboom PE, van Heemst D, Deelder AM, Tanke HJ, RGJ Westendorp, AB Maier. Human *in vivo* longevity is reflected *in vitro* by differential metabolism as measured by 1H-NMR profiling of cell culture supernatant. Accepted in *Molecular Biosystems*

Dekker P, Gunn D, McBryan T, Dirks RW, van Heemst D, Lim FL, Jochemsen AG, Verlaan-de Vries M, Nagel J, Adams PD, Tanke HJ, Westendorp RGJ, Maier AB. Microarray-based identification of age-dependent differences in gene expression of human dermal fibroblasts. Submitted for publication

Dekker P, van Baalen LM, Dirks RW, Slagboom PE , van Heemst D, Tanke HJ, Westendorp RGJ, Maier AB. Chronic inhibition of the respiratory chain in human fibroblast cultures: Differential responses related to subject chronological and biological age. Gerontol A Biol Sci Med Sci 2011 Nov 10 [Epub ahead of print].

Dekker P, de Lange MJ, Dirks RW, van Heemst D, Tanke HJ, Westendorp RG, Maier AB. Relation Between Maximum Replicative Capacity and Oxidative Stress-Induced Responses in Human Skin Fibroblasts *In Vitro*. *J Gerontol A Biol Sci Med Sci* 2011;66(1):45-50.

Dekker P, Maier AB, van Heemst D, de Koning-Treurniet C, Blom J, Dirks RW, Tanke HJ, Westendorp RG. Stress-induced responses of human skin fibroblasts *in vitro* reflect human longevity. *Aging Cell* 2009;8:595-603.

Noppe G*, **Dekker P***, Koning-Treurniet C, Blom J, van Heemst D, Dirks RJ, Tanke HJ, Westendorp RG, Maier AB. Rapid flow cytometric method for measuring Senescence Associated β-galactosidase activity in human fibroblasts. *Cytometry A* 2009;75:910-916.

Dekker P, Parish WE, Green MR. Protection by food-derived antioxidants from UV-A1-induced photodamage, measured using living skin equivalents. Photochem Photobiol. 2005 Jul-Aug;81(4):837-42.

*Both authors contributed equally to the studies

Dankwoord

Het soort onderzoek waaraan ik de laatste vier jaar heb deelgenomen staat of valt bij de gratie van vrijwillige proefpersonen. De huidcellen waarmee ik gewerkt heb zijn afkomstig van een groot aantal mensen en het is gemakkelijk uit het oog te verliezen dat achter de cellen in plastic flessen mensen van vlees en bloed schuilgaan. Dit proefschrift had niet tot stand kunnen komen zonder de medewerking van de deelnemers van de Leiden 85-Plus Studie en van de Leiden Langleven Studie. Ik ben hen zeer dankbaar en ik ben blij het voorrecht gehad te hebben een aantal van hen in levenden lijve te kunnen ontmoeten.
Verder ben ik veel verschuldigd aan iedereen - collega's (zowel van de afdeling Ouderen-geneeskunde als van andere afdelingen), ex-collega's van Unilever, studenten, familie en vrienden - die mij hierin heeft bijgestaan, op welke manier dan ook. Jullie weten wie je bent...
Tenslotte wil ik dit proefschrift postuum opdragen aan Dr. Bill Parish wiens passie voor de wetenschap mij er toe aangezet heeft alsnog te gaan promoveren.

Acknowledgements

The type of research I have participated in during the last four years is possible only thanks to voluntary test subjects. The skin cells I have worked with were derived from a large number of people and it is all too easy to forget the people of flesh and blood that these cells were part of. This thesis would not have seen the light of day without the cooperation of the participants of the Leiden 85-Plus Study and of the Leiden Longevity Study. I am very grateful to them and I am glad that I had the privilege to meet a number of them.
Furthermore I owe much to everyone – colleagues (both from the department of Gerontology and Geriatrics and from other departments), ex-colleagues from Unilever, students, family and friends – who has supported me, in whatever way. You know who you are…
Finally I wish to posthumously dedicate this thesis to Dr. Bill Parish whose passion for science stimulated me to go for a PhD degree after all.

Curriculum Vitae

Pim Dekker werd op 26 november 1973 geboren te Rotterdam en groeide op in het dorp Oude Tonge op het eiland Goeree-Overflakkee. Hij behaalde in 1992 zijn VWO-diploma aan de Rijksscholengemeenschap Goeree-Overflakkee (RGO) te Middelharnis en ging daarna biologie studeren aan de Universiteit Utrecht. Eén van zijn stages deed hij bij Unilever op de afdeling Corporate Research in Sharnbrook, Engeland, met als onderwerp oxidatieve stress in huidcellen. Na het afstuderen in 1999 ging hij in 2000 bij dezelfde afdeling van Unilever als onderzoeksassistent werken aan een vergelijkbaar onderwerp. Door samenwerking tussen de Unilever en de afdeling Ouderengeneeskunde van het Leids Universitair Medisch Centrum (LUMC) begon hij in 2007 zijn promotieonderzoek onder begeleiding van Professor Rudi Westendorp, Professor Hans Tanke, Dr. Diana van Heemst, Dr. Andrea Maier en Dr. Roeland Dirks. De resultaten van dit onderzoek worden beschreven in dit proefschrift.

Pim Dekker was born in Rotterdam on the 26th of November 1973 and was raised in the village of Oude Tonge on the island of Goeree-Overflakkee. In 1992 he got his high school diploma at the Rijksscholengemeenschap Goeree-Overflakkee, Middelharnis, The Netherlands and went on to study biology at Utrecht University. He did one of his traineeships in the department of Corporate Research at Unilever, Sharnbrook, England. The subject of this project was oxidative stress in skin cells. After finishing his study in 1999 he started working on a similar subject as a research assistant for the same department at Unilever. Through a cooperation between Unilever and the department of Gerontology and Geriatrics at the Leiden University Medical Center (LUMC) he started his PhD project in 2007, supervised by Professor Rudi Westendorp, Professor Hans Tanke, Dr. Diana van Heemst, Dr. Andrea Maier en Dr. Roeland Dirks. The results of this project are described in this thesis.